

Acid Catalysts in Industrial Hydrocarbon Chemistry

Guido Busca[†]

Laboratorio di Chimica delle Superfici e Catalisi Industriale, Dipartimento di Ingegneria Chimica e di Processo "G.B. Bonino", Università di Genova, P.le Kennedy, I-16129 Genova, Italy

Received January 22, 2007

Contents

1. Introduction	5366
2. Concepts and Measures of Acidity	5367
3. Hydrocarbons as Basic Molecules	5368
4. Thermodynamic Instability of Hydrocarbons in a Reducing Environment: Coking and Pollution of Acid Catalysts	5369
5. Liquid-Phase Brønsted Acid Catalysts in Industry	5370
5.1. Sulfuric Acid	5370
5.2. Hydrofluoric Acid	5371
5.3. Friedel–Crafts Type Catalysts: HCl/AlCl ₃ and Acidic Ionic Liquid Catalysts	5372
5.4. Diffusion of Organics in Liquid Acid Media	5373
6. Solid Acid Catalysts	5374
6.1. Surface Acidity of Solids	5374
6.1.1. Characterization Techniques	5374
6.1.2. Strength, Amount, and Distribution of Surface Acid Sites on the Ideal Surface of a Solid	5376
6.1.3. Practical Aspects on the Use of Solid Acid Catalysts	5376
6.1.4. Deactivation and Reactivation of Solid Acid Catalysts	5377
6.2. Oxide Solids	5378
6.2.1. Acidity and Basicity on the Ideal Surface of a Solid Oxide	5378
6.2.2. Pure Oxides	5379
6.2.3. "Mixed Oxides" of Silicon and Aluminum: H-Zeolites and Silica-aluminas	5382
6.2.4. SAPO-34	5395
6.2.5. Acid Catalysts from Clays	5395
6.2.6. Pure and Mixed or Supported Transition Metal Oxides: Titania, Zirconia, Tungsta, and Their Combinations	5397
6.2.7. Sulfated Zirconia	5399
6.3. Solid Acids	5399
6.3.1. Sulfonic Acid Resins	5399
6.3.2. "Solid Phosphoric Acid"	5400
6.3.3. Niobic Acid and Niobium Phosphate	5401
6.3.4. Heteropolyacids	5402
6.3.5. Friedel–Crafts Type Solids	5403
7. Conclusions	5404
8. References	5404



Prof. Guido Busca was born in Milan, Italy, in 1953. He received his Laurea degree in chemistry at the University of Milan in 1977. Next he joined the group of Prof. V. Lorenzelli at the University of Genova (Italy) working in the field of infrared spectroscopy of materials. He was assistant professor of organic and industrial chemistry at the Engineering Faculty of the University of Bologna from 1983 to 1988. In the 1980s he collaborated with Prof. J. C. Lavalley at the University of Caen (France) in the field of spectroscopy of catalyst surfaces. He also worked in collaboration with Prof. F. Trifirò (University of Bologna) in the field of heterogeneous oxidation catalysis. In 1988 he was made an associate professor of chemistry at the Engineering Faculty of the University of Genova, and since 2000 he has been a full professor of chemistry, and later of industrial and technological chemistry, at the Chemical and Process Engineering Department of the University of Genova. He has been the Coordinator of the Italian Group of Catalysis, 2000–2002. His research interests continue to be in the field of surface chemistry of oxide materials including heterogeneous catalysis.

1. Introduction

The hydrocarbon era¹ began at the end of the 19th century, as a result of the discovery of oil fields in the United States and together with the development of internal combustion engines. The refinery industry started to grow in the 1920s of the 20th century, following the increased demand for antiknocking power of gasoline for cars as well as for aviation. During the World War II, oil-refining technology and capacity were boosted worldwide to support the war effort. After the war, the petrochemical industry developed very rapidly, one of the main driving forces being the necessity to lower the production costs of monomers supplying the plastics and rubber industries. At the end of the 20th century environmental issues became dominant, and the need for less polluting fuels and materials, as well as for safer processes, caused further improvements of products and technologies.

At the beginning of the 21st century the hydrocarbon era may appear to be at its end, because the oil resources are expected to drain quite rapidly. This expectation, however,

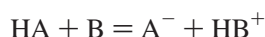
[†] Telephone int-39-010-3536024; fax int-39-010-3536028; e-mail Guido.Busca@unige.it.

pushes for more efficient and clean processes for a better use of the fossil resources. Moreover, liquid hydrocarbons can now be produced quite efficiently from natural gas as well as from coal and even from biomasses, via syngas, with processes such as the Fischer Tropsch, MTG, and MTO technologies. Biorefineries, where large-scale conversion of biomasses to intermediates, with chemical and biotechnological processes, will be performed, are designed to promote the growth of an industrial organic chemistry based on renewables. Clearly, the organic chemistry of biofuels and renewables is strictly related to the hydrocarbon chemistry based on fossil resources, developed in the 20th century.

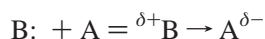
The development of more efficient, safer, and more environmentally friendly chemical technologies is consequently a major need for humanity. A large part of the industrial organic and hydrocarbon chemistry is based on catalysis. The nature of the catalyst used determines part of the features of the process and influences its efficiency, safety, and environmental friendliness. In this review, a particular subject in this field is considered. We will focus on the characteristics of the acid catalysts largely used in the industrial hydrocarbon chemistry. We will not enter the subject of reaction mechanisms, already discussed in many studies and reviewed recently.² Our contribution is intended to underscore the link of chemical knowledge of the catalyst with the engineering of the process and its environmental impact.

2. Concepts and Measures of Acidity

S. A. Arrhenius,³ Nobel prize winner for chemistry in 1903 and an early pioneer in physical chemistry, defined an acid as any hydrogen-containing species able to release protons and a base as any species able to release hydroxide ions. J. M. Brønsted⁴ and, simultaneously and independently but less precisely, T. M. Lowry⁵ in 1923 modified the definition of bases: a base is any species capable of combining with protons. In this view acid–base interactions consist in the equilibrium exchange of a proton from an acid HA to a base B (which may be the solvent, e.g., water) generating the conjugated base of HA, A[−], plus the conjugated acid of B, HB⁺ (e.g., the hydroxonium ion H₃O⁺):

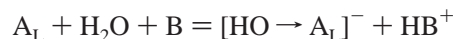


In the same year, 1923, G. N. Lewis⁶ proposed a different approach. In his view, an acid is any species that, because of the presence of an incomplete electronic grouping, can accept an electron pair, thus forming a dative or coordination bond. Conversely, a base is any species possessing a nonbonding electron pair, which can be donated to form a dative or coordination bond. The Lewis-type acid–base interaction can be consequently denoted as follows:

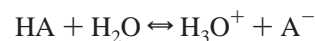


This definition is completely independent from water as the reaction medium and is more general than the previous ones. According to the above definitions, Lewis basic species are also Brønsted bases. Instead, Lewis-type acids (such as coordinatively unsaturated cations) do not correspond to Brønsted-type acids (typically species with acidic hydroxy groups): the Brønsted-type acid HA is the result of the interaction of the Lewis-type acid species H⁺ with the base A[−]. However, a Lewis-type acid converts into a Brønsted-

type acid in the presence of water (even in traces), actually enhancing the acidity of water:



The acid strengths in diluted water solutions may be described by the dissociation equilibrium⁷



$$K_a = [\text{H}_3\text{O}^+][\text{A}^-]/[\text{HA}] \quad \text{p}K_a = -\log K_a$$

where the molar concentration of the species is used as an approximation of their activity, the activity of water being approximated to 1.

The acid strength in water solution is determined by the dissociation of the acid, which is actually promoted by the solvation of protons by water molecules, generally believed to form the hydroxonium ion H₃O⁺. However, the energy of proton hydration by liquid water, 1091 kJ/mol, is so high as to suggest that the real state of solvated proton in water is [H(H₂O)₆]⁺ rather than H₃O⁺.⁸ Interestingly, the formation of such a complex (or of even more hydrated species) is possible only when the amount of available water is sufficient, that is, only for sufficiently diluted acid solution with an acid concentration not higher than 5–10 mol/L.⁸

The solvation of the anion A[−] by water also has a relevant effect in the stabilization of the anion and in determining, as a consequence, the scale of the acid strengths. The acid strength for oxoacids has been correlated to the number of oxygen atoms, where the negative charge of the anion resulting by dissociation may be delocalized. For this reason, the anions SO₄^{2−} and ClO₄[−] are the (very weak) conjugated bases of very strong acids, sulfuric and perchloric acids, whereas SO₃^{2−} and ClO₃[−] are the conjugated bases of less strong acids, sulfurous and chloric acids. Actually, the four oxygen atoms of SO₄^{2−} and ClO₄[−] anions also allow more extensive H-bonding solvation by water molecules than SO₃^{2−} and ClO₃[−] anions.

In any case, it is evident that the acidity of acids in water solutions is buffered by the basicity of water itself. Bases that are definitely weaker than water are not protonated in water solutions. To protonate very weak bases very highly concentrated or anhydrous acids are required.

The extent of dissociation of pure anhydrous acids is by far lower than for the corresponding water solutions, just because the ability of the acid molecule to solvate the proton is far lower than that of water. The K_a values of sulfuric and hydrofluoric acids in water are >10² and ~10^{−3}, respectively, but they decrease to ~10^{−4} and ~10^{−10}, respectively, in the absence of water (100% acids).⁸ Obviously, an intermediate case occurs when the concentration of the acid in water solution is very high, not allowing the stoichiometric formation of the highly solvated proton species [H(H₂O)₆]⁺.

The acid strength of anhydrous or highly concentrated acids is mostly described in terms of the so-called Hammett acidity function, proposed by L. P. Hammett in the 1930s⁹

$$H_0 = \text{p}K_{\text{BH}^+} + \log [\text{B}]/[\text{BH}^+]$$

where B is a basic indicator and pK_{BH⁺} is the pK_a of its conjugated acid. The obtained value of H₀ is almost independent of the indicator base B. The H₀ values for fully anhydrous H₂SO₄ and HF are near −12 and −15, respec-

tively, the strongest liquid acid known being the $\text{SbF}_5/\text{HSO}_3\text{F}$ solution, called “magic acid”, characterized by $H_0 = -23/-26.5$ and the 1:1 complex HF/SbF_5 with $H_0 = -28$. Both are combinations of a Brønsted acid with a Lewis acid. Acidity strength scales for very strongly acidic liquids may also be derived from spectroscopic measurements, such as the ^{13}C NMR $\Delta\delta$ scale proposed by Fărcașiu and Ghenciu¹⁰ (where $\Delta\delta$ is the difference between the chemical shifts of the α and β carbons of mesityl oxide upon O-protonation) and the IR $\Delta\nu\text{NH}$ scale proposed by Stoyanov et al.¹¹ (where $\Delta\nu\text{NH}$ is the shift of νNH of protonated trioctylamine, measuring the very weak basicity of the anion).

The term “superacidity”, first used in 1927 by Conant¹² to describe very strong acids, has been reclaimed by Gillespie in the 1960s to indicate acids stronger than 100% H_2SO_4 .¹³ This field has been mostly investigated by Olah, the Nobel prize in chemistry in 1994, and his co-workers.^{14–16} A list of liquid superacids is reported in Table 1.

Table 1. Some Relevant Liquid Superacids and Their Hammett Constants (from References 14–16)

HF/SbF_5	$H_0 = -28$
$\text{SbF}_5/\text{HSO}_3\text{F}$ “magic acid”	$H_0 = -23/-26.5$
HF (fully anhydrous)	$H_0 = -15$
HSO_3F	$H_0 = -15$
$\text{H}_2\text{S}_2\text{O}_7$	$H_0 = -15$
HCl/AlCl_3	$H_0 = -15/-14$
HF/BF_3	$H_0 = -15/-14$
$\text{H}_2\text{O}/\text{BF}_3$	$H_0 = -15/-14$
$\text{CF}_3\text{SO}_3\text{H}$ “triflic acid”	$H_0 = -14.1$
100% H_2SO_4	$H_0 = -11.9$

Reed and co-workers recently developed carborane superacids^{17,18} ($\text{HCB}_{11}\text{H}_{11-x}\text{X}_x$, where X may be Cl, Br, or I), which are solid materials able to protonate extensively weakly basic molecules such as olefins, aromatics, and fullerenes without the addition of Lewis acids. The application of the above cited ^{13}C NMR $\Delta\delta$ and IR $\Delta\nu\text{NH}$ scales, in SO_2 solution, shows that carborane acids are even stronger than “traditional” neat superacids, such as HSO_3F .

In 1963, Pearson^{19,20} introduced the concept of hard and soft acid and bases (HSAB): hard acids (defined as small-sized, highly positively charged, and not easily polarizable electron acceptors) prefer to associate with hard bases (i.e., substances that hold their electrons tightly as a consequence of large electronegativities, low polarizabilities, and difficulty of oxidation of their donor atoms), whereas soft acids prefer to associate with soft bases, giving thermodynamically more stable complexes; these hard–hard and soft–soft associations also occur more rapidly. According to this theory, the proton is a hard acid, whereas metal cations may have different hardnesses.

The acidic and basic properties may also be evaluated experimentally or estimated by theory. The enthalpy of deprotonation of the (conjugated) acid in the gas phase²¹ leads to an acidity/basicity scale based on “proton affinity” (PA):

$$\text{PA} = -\Delta H_{\text{protonation}}$$

3. Hydrocarbons as Basic Molecules

Typical basic species have electron pairs in nonbonding (n-) orbitals. These “doublets” can be used to produce a dative bond with species having empty orbitals, such as protons or coordinatively unsaturated cations. They are consequently denoted n-bases.

The ability of hydrocarbons (which do not have n-orbitals) to interact with protic acids has been recognized long ago and is evident from very simple experiments. In Figure 1

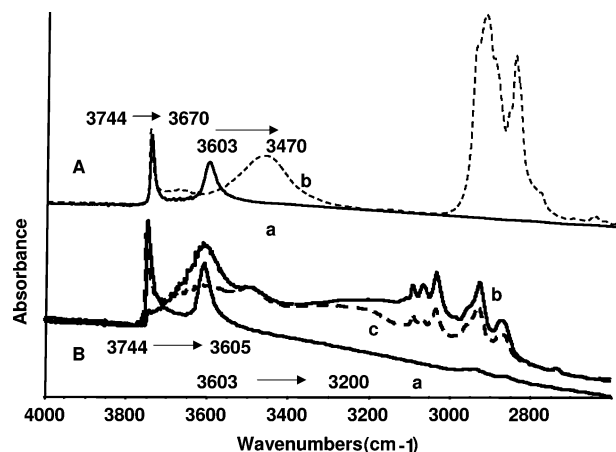


Figure 1. FT-IR spectra of H-MFI zeolite (Si/Al atomic ratio 45) activated at 723 K (a) and put in contact with methylcyclohexane (A) at room temperature (b), put in contact with toluene vapor (B) at room temperature (b), and after outgassing at room temperature (c).

the infrared spectra of a solid acid, H-MFI zeolite, are reported after outgassing at 450 °C (spectra a) and after contact with methylcyclohexane (A) and toluene (B). The OH stretching band due to the “zeolitic” hydroxy groups is observed at 3603 cm^{-1} on the pure sample (spectra a), but it shifts down to 3470 cm^{-1} ($\Delta\nu \sim 135 \text{ cm}^{-1}$) in contact with methylcyclohexane (spectrum A,b) and down to near 3200 cm^{-1} ($\Delta\nu \sim 400 \text{ cm}^{-1}$) with toluene (spectra B,b and c). Instead, the OH stretching band due to the silanol groups is observed at 3744 cm^{-1} in the pure sample (spectra a), but it shifts down to 3670 cm^{-1} ($\Delta\nu \sim 75 \text{ cm}^{-1}$) in contact with methylcyclohexane (spectrum A,b) and down to near 3605 cm^{-1} ($\Delta\nu \sim 100 \text{ cm}^{-1}$) with toluene (spectra B,b and c). The stronger shifts observed with toluene with respect to methylcyclohexane point to the stronger basicity of toluene, whereas the stronger vibrational shifts undergone by the zeolitic OH groups with respect to silanol groups point to the stronger acidity of the zeolitic OH groups. The enthalpies associated with the interactions between hydrocarbons and acids can be evaluated calorimetrically, and the heat of interaction trend agrees with the perturbation evidenced by IR.

At higher temperature or in the presence of very strong acidity these interactions can produce a true proton transfer, thus, hydrocarbons acting as Brønsted bases. In Table 2 the proton affinity scale of some hydrocarbons is reported.²² The PA data follow again the trend π -orbital containing compounds (olefins and aromatics) > isoalkanes > n-alkanes > methane.

Table 2. Proton Affinities (kJ/mol) of Hydrocarbons and of Ammonia for Comparison (from NIST Database, Reference 22)

ammonia	846.0	n-bases
isobutylene	802.1	π -bases
toluene	784.0	
1,3-butadiene	783.4	
propylene	751.6	
benzene	750.4	
ethylene	680.5	
isobutane	677.8	σ -bases
propane	625.7	
ethane	596.3	
methane	543.5	

Olefins can react with protic acids and can produce the so-called trivalent “classical” carbocations (carbenium ions) as intermediates of electrophilic addition reactions. The history of carbocations, which are intermediates also in nucleophilic substitution reactions ($\text{S}_{\text{N}}1$) and in elimination reactions (E_1), begins at the end of the 19th century¹⁶ and involves very distinguished organic chemists such as Meerwein, Ingold, Whitmore, and many others. The reactivity of olefins, through their π -type orbitals, toward protons is evidence of the so-called π -basicity of these compounds, probably first proposed by M. J. Dewar.²³ The result of this interaction, with the intermediacy of protonated π -bonded transition state, is the formation of carbenium ions,²⁴ when the π -type orbitals disappear and one of the carbon atoms rehybridizes from sp_2 to sp_3 , the hydrogen becoming covalently bonded to the carbon atom via a σ -bond. The carbenium ions are more stable and more easily formed on tertiary carbon atoms, whereas their formation on primary carbon atoms is very difficult. This is associated with the electron-donating properties of alkyl groups that allow the cationic charge to be delocalized, thus stabilizing the cation. Olah and co-workers¹⁶ isolated several carbenium ions as stable species by using very weak nucleophiles as balancing anions.

The π -basicity of aromatic hydrocarbons was also observed long ago,²³ and the existence of quite stable protonated forms of benzenes and the methyl substituent effects on them were determined.²⁵ Protonation of aromatic rings generates arenium ions for which the cationic charge is delocalized on the ring and in particular in the ortho and para position with respect to the position where the attack of the electrophile (the proton in this case) occurred.

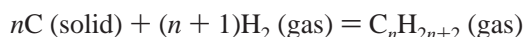
More recently, Olah and Schlosberg²⁶ and Hogeveen et al.²⁷ for the first time observed the protonation of alkanes by superacids, thus suggesting that alkanes may behave as σ -bases. The basicity scale for σ -bonds of hydrocarbons is reported to be $\text{tert-C-H} > \text{C-C} > \text{sec-C-H} > \text{prim-C-H} > \text{CH}_4$, although this depends also on the protonating agent and the steric hindrance of the hydrocarbons.²⁸ In fact, protonation at the C–C bond may be significantly affected by steric hindrance.²⁹ Protonation of alkanes generates the so-called “nonclassical” pentacoordinated carbonium ions, which contain five-coordinated (or higher) carbon atoms.

According to the HSAB^{19,20} theory olefinic and aromatic hydrocarbons are softer bases than alkanes.

The carbocations, which may be stabilized by solvation, are more or less stable species and may act as intermediate species or as transition states in the conversion of hydrocarbons.^{2,30} In this case the acid is regenerated after the completion of the reaction and acts consequently as a catalyst. Many of the hydrocarbon conversion industrial processes are acid catalyzed, and the formation of carbocations is one of the steps in the reaction mechanism.

4. Thermodynamic Instability of Hydrocarbons in a Reducing Environment: Coking and Pollution of Acid Catalysts

The formation reaction of alkanes



is associated with a significant decrease of the number of moles of gaseous compounds. This diminution is lower for

olefins and even less for acetylenes and aromatics having the same carbon atom number, due to their smaller hydrogen content. Consequently, the hydrocarbon formation reactions are characterized (except for acetylene) by a decrease in entropy ($\Delta S_{\text{form}} < 0$): the higher the hydrogen content in the hydrocarbon molecule, the stronger is the decrease of S_{form} . Thus, ΔG_{form} versus T curves have a positive slope but, due to the different ΔS_{form} values for different hydrocarbon groups, the slope is higher for alkanes, lower for olefins, and even lower for aromatics. Only for acetylene itself is there no diminution of gaseous moles, and the slope of the ΔG_{form} versus T curve is weakly negative. This is shown in the so-called Francis diagram,³¹ reported in Figure 2.

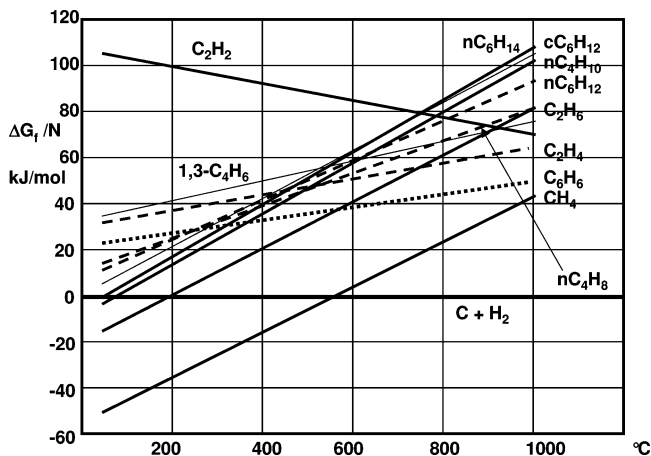


Figure 2. Dependence of the free energy of formation per C atom ($\Delta G_f/N$) versus T for some hydrocarbons (ref 31).

Due to the negative ΔS_{form} , the hydrocarbons (except acetylene) are less stable with increasing temperature, with respect to the elements, that is, hydrogen and carbon. Coking may be considered as the reverse reaction of the formation of hydrocarbons and is consequently thermodynamically favored at $T > 200$ °C for all hydrocarbons except methane. Petroleum coke, or “petcoke”, is formed by thermal coking of heavy hydrocarbons in a refinery process. Carbonaceous materials, also denoted “coke”, form on the surface of acidic catalysts upon high-temperature contact with hydrocarbons. This phenomenon results in catalyst deactivation. Most solid acid-catalyzed processes for hydrocarbon conversion are influenced by the occurrence of catalyst coking and the need for frequent catalyst regeneration.

For the same reason, that is, the different slopes of the ΔG_{form} versus T (due to the different ΔS_{form}) of alkanes, alkenes, and aromatics, dehydrogenation of alkanes to alkenes and dehydrocyclization to aromatics also become favored above a relatively low temperature (300–600 °C). Also, the cracking of high paraffins and olefins to light hydrocarbons is favored in this temperature range. These reactions tend to decrease selectivities in acid catalysis on solid acids, performed at relatively high temperatures. Coking and cracking are competitive reactions. In general, the activation energy of catalyst coking is lower than that of cracking. For this reason, the amount of coke formed may have a maximum at an intermediate temperature, decreasing when cracking becomes predominant.

These problems are definitely less important in liquid acids mainly because they are used at lower temperatures, when

Table 3. Characteristics of Some Industrial Hydrocarbon Conversion Processes Involving Sulfuric Acid Catalysts

process	protonated species	H ₂ SO ₄ concn (%)	T (°C)	P (MPa)	reactor type
ethylene glycol synthesis	ethylene oxide	1	50–70	0.1	tank reactor
phenol and acetone synthesis	cumene hydroperoxide	few	45–65	0.2–0.3	backmixed reactor
isobutylene hydration	isobutylene	50	50	0.4–0.5	wash towers
propylene indirect hydration	propylene	60	75–85	0.6–1	wash towers
isobutylene oligomerization	isobutylene	60–65	20–25		
benzene alkylation to cumene	propylene	<90	35–40	1.15	stirred tank
ethylene indirect hydration	ethylene	94–98	65–85	1–3.5	wash towers
isobutane/butylene alkylation	isobutylene	90–98	20–40	0.3–0.5	horizontal stirred tank contactor or cascade reactor
benzene alkylation to LABs	linear higher olefins	96–98	10–30		stirred tank

Table 4. Characteristics of Processes for the Production of Cumene by Alkylation of Benzene with Propene

time of development	company	catalyst	phase	P (bar)	T (°C)
		AlCl ₃ /EtCl	liquid/liquid	3–7	40
		H ₂ SO ₄ < 90%	liquid/liquid	11.5	35–40
1940s	UOP	solid phosphoric acid	vapor/solid	15–35	200–250
	Hüls	HF	liquid/liquid	7	50–70
1986–1988	Monsanto	AlCl ₃ /EtCl	single liquid phase	10	110
1980s	Unocal	Y-zeolite	gas/solid		
1992	UOP Q-Max	H-BEA	liquid/solid		
1992	Dow-Kellogg 3-DDM	dealuminated H-MOR	liquid/solid		170
1994	Mobil-Raytheon	MCM-22 (H-MWW)	liquid/solid		180–220
	CDTech	zeolite	catalytic distillation		
1996	Enichem-Polimeri Europa	H-BEA	liquid/solid	25–40	150–200

coking, dehydrogenation, dehydrocyclization, and cracking are less or not favored and also much slower. On the other hand, at low temperature (and high pressures) the oligomerization and polymerization (which is the reverse of cracking) as well as addition reactions are favored. The performances of liquid acid catalysts with reactive hydrocarbons (such as olefins and dienes) may be strongly influenced by these reactions. Oligomeric species may form and cause loss of reactants and pollution of the acid catalyst. Moreover, addition reactions may also cause the formation of acid-soluble oils (ASOs), that is, functionalized organic compounds mixing in the acid phase and diluting and polluting it.

5. Liquid-Phase Brønsted Acid Catalysts in Industry

A very large number of liquids and solutions have been tested as acid catalysts for hydrocarbon conversion in academic research. Clearly, only a few of them have found a real industrial application, due to their superior properties as well as for economic reasons. Liquid acid catalysts may offer some advantages with respect solid acids, such as high activity and selectivity at low temperature, low investment costs, and better flexibility. Eventual drawbacks are related to difficult and expensive product/catalyst separation and loss of the catalyst, as well as safety and environmental concerns.

5.1. Sulfuric Acid

Sulfuric acid is a strong diprotic acid in diluted water solutions ($K_{a1} \sim 10^2$, $K_{a2} = 1.2 \times 10^{-2}$). The Hammett acidity function of concentrated sulfuric acid water solutions increases from near -3.5 for 50% H₂SO₄ (7 M) to -7.5 for 80% H₂SO₄³² up to $H_0 = -11.9$ for 100% H₂SO₄. H₂SO₄ is an intermediate compound in the SO₃–H₂O system. This system presents a maximum azeotrope boiling at 339 °C with a composition of 98.3 wt % H₂SO₄–1.7% H₂O. Pure H₂SO₄ is a dense liquid ($d = 1.8356$) reported to boil at 279.6 °C. SO₃ is soluble in H₂SO₄, producing “oleum”, the

solutions of SO₃ in H₂SO₄. By reaction of SO₃ with H₂SO₄ disulfuric acid H₂S₂O₇ is formed, which corresponds to 44.9 wt % oleum and is a superacid, with H_0 of -15 .

Industrial processes for hydrocarbon conversion may employ highly concentrated H₂SO₄ solutions (>40 wt %) up to azeotropic or pure H₂SO₄. Oleums are mostly used for sulfonations. Concentrated sulfuric acid, with compositions generally close to the azeotrope or a little less (90–99%), is a stable solution with high density ($d \sim 1.8$ depending on the concentration and temperature) and low volatility (vapor pressure = 10^{-1} – 10^{-3} mbar, mostly due to water vapor).

Typical reaction condition for processes employing H₂SO₄ as the catalyst are summarized in Table 3. Although for some reactions the processes based on sulfuric acid have been substituted by better performing and more environmentally friendly processes based on other catalysts (see, for example, Table 4, for cumene synthesis by benzene alkylation with propene), several processes based on sulfuric acid are still used worldwide. In Figure 3 the schematics of reactors used for H₂SO₄-catalyzed reactions are reported. For isobutane/butylene alkylation³³ (i.e., the reaction between isobutylene and isobutane, which produces “alkylate”, a very good gasoline fraction mainly composed of isooctane) horizontal contactors (several in the plant) with indirect internal refrigeration by heat exchange with the effluent and an internal impeller are used in the STRATCO process.³⁴ The EXXON-Mobil process instead uses cascade reactors with autorefrigeration by evaporation of reactants.³⁵ Both are variants of continuous stirred tank reactors (CSTR). CDTech³⁶ alternatively proposes for the same reaction reactive distillation towers. Distillation towers are also used, for example, for esterifications such as the methyl acetate synthesis from methanol and acetic acid.³⁷ Washing towers are used for the reaction of C3–C4 olefins with ~50% sulfuric acid in the processes of indirect hydration to give alcohols and ethers. The intermediate alkylsulfates are hydrolyzed in a second reactor.

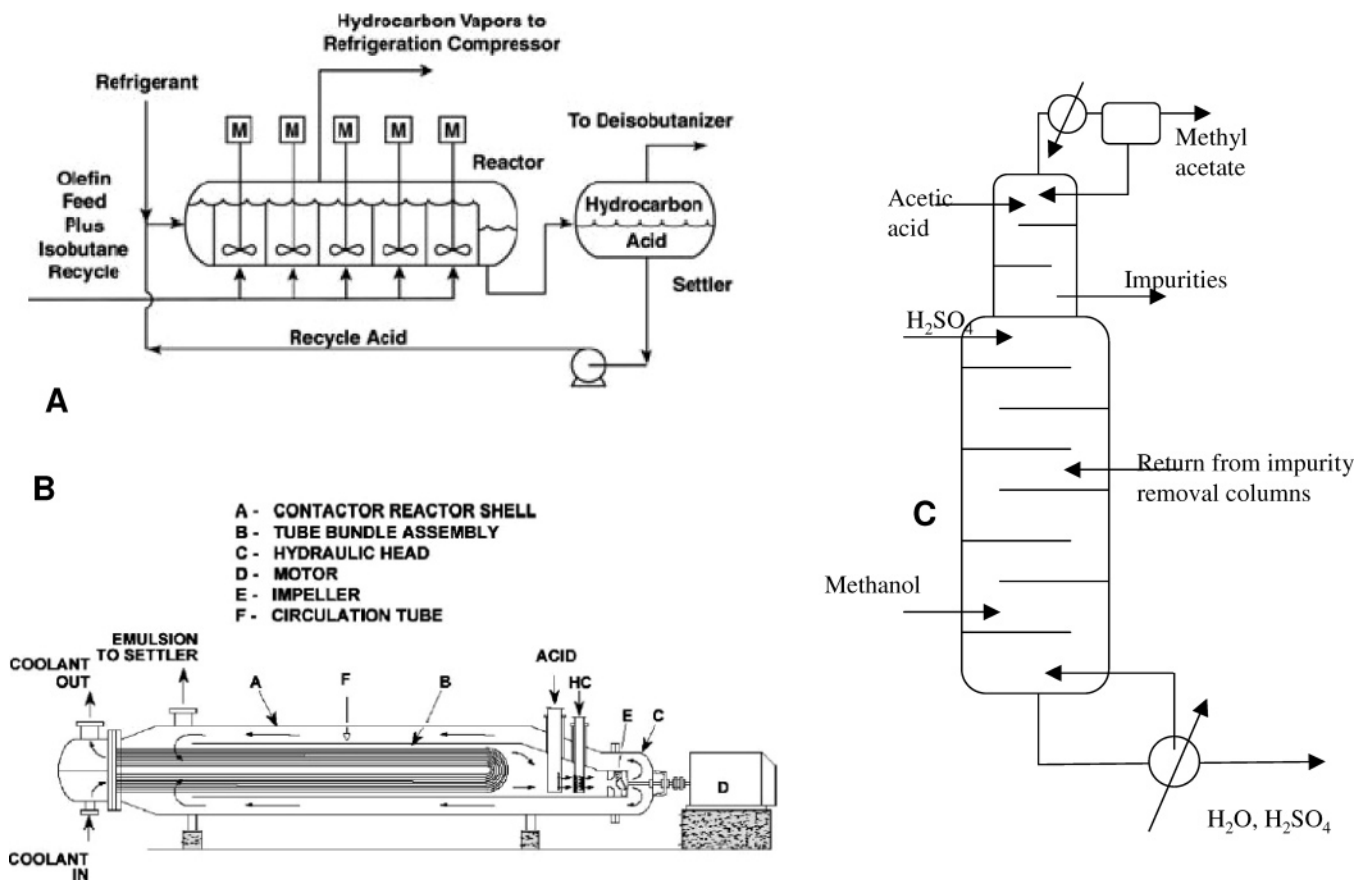


Figure 3. Schematics of some industrial reactors for H₂SO₄-catalyzed processes: A, EXXON-Mobil autorefrigeration cascade alkylation reactor (ref 35); B, STRATCO horizontal contactor for alkylation (ref 34); C, reactive distillation tower for esterification (ref 37).

The hydrocarbon–sulfuric acid system is biphasic: for isobutane/butylene alkylation an excess of sulfuric acid is used to produce an acid continuous emulsion with the hydrocarbon dispersed in the acid. After reaction, sulfuric acid is highly impure and diluted by water. Acid-soluble oils (ASOs) are formed as byproducts, and the acid also dries the hydrocarbon feed, so diluting itself. An additional problem typical of sulfuric acid is its capability to oxidize paraffins, forming water, SO₂, and alkenes, with an important contribution to its own degradation. Sulfones, sulfonic acids, and alcohols may also be produced. In the processes of ethylene indirect hydration 98% sulfuric acid is used as the reactant, and 45–55% sulfuric acid is recovered after hydrolysis. Also esterification produces water that dilutes the acid.

A main drawback of the use of concentrated sulfuric acid is related to the difficulty in its regeneration, purification, and concentration. For this reason, spent acid may be disposed of and stored in spent acid tanks: its consumption can be as high as 70–100 kg of acid/ton of alkylates in the case of isobutane/butylene alkylation.³⁸ Reconciliation of sulfuric acid is very demanding due to the very high boiling points of the acid and azeotrope. Sulfuric acid regeneration processes by decomposition to SO₂ and reoxidation and hydration find commercial application³⁹ for H₂SO₄-based alkylation processes, but they are also very demanding in terms of energy. The schematic of the Topsøe regeneration plant proposed for alkylation in a refinery is shown in Figure 4.

Additional difficulties are associated with the corrosive behavior of sulfuric acid, which imposes the use of lead,

tantalum, and aluminum alloys for reactors and distillation towers, as well as the potentially unsafe disposal of the spent acid.

5.2. Hydrofluoric Acid

Hydrofluoric acid is a weak acid in water solution [$K_{aq} = (2-7) \times 10^{-4}$]. Its acidity increases as a function of its concentration because of the increased stabilization of the F⁻ anion when its surroundings become more ionic.⁴⁰ The HF–water system presents a maximum azeotrope at 38.26% volume of HF. The solution has a maximum density around 70% HF ($d \sim 1.27$ at 0 °C). At increasing HF concentration, density decreases and vapor pressure increases. Pure anhydrous hydrofluoric acid HF, characterized by a density of 0.97, condensates at 1 atm at 19.5 °C, forming H-bonded “polymeric” chains (HF)_{*n*}. The extent of H-bonding at the liquid–vapor equilibrium at 1 atm is limited to $n = 3.75$, corresponding to a molecular mass of 74.9. As a pure liquid it is a superacid, with $H_0 = -15$ when fully anhydrous and $H_0 = -11$ in the presence of traces of water.

The acidity of HF is further enhanced by its combination with Lewis acids such as SbF₅. The system HF/SbF₅ is considered to be the strongest known, allowing H_0 values as low as -28. In this system the formation of solvated H₂F⁺ ions [H₂F⁺(HF)_{*n*}] and of solvated anions such as Sb₂F₁₁⁻ and Sb₃F₁₅⁻ tends to increase the acidity.⁴¹

For decades HF has largely been used in the refinery industry as the catalyst of the isobutane/butylene alkylation process³³ and in the petrochemical industry for benzene alkylation processes such as the synthesis of linear alkylbenzenes (LABs)⁴² and of cumene (Table 4). For the

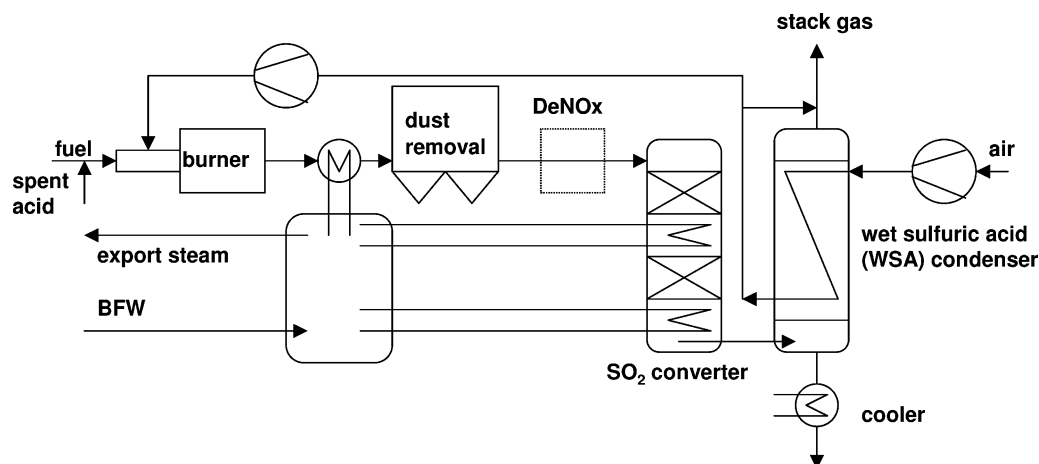


Figure 4. Schematics of the Topsøe sulfuric acid regeneration plant (ref 39).

synthesis of LABs, the liquid feed contains about 79% HF. The reaction temperature is very low, 0–10 °C, at ambient pressure with a large excess of benzene (4–10 mol of benzene/olefin).⁴³ For isobutane/butylene alkylation with the ConocoPhillips process, the reaction temperature is 25 °C, molar isobutane/alkene ratios are about 14–15, and acid concentrations are 86–92 wt %.⁴⁴ After reaction, occurring in a riser (Figure 5), the HF phase is separated from the

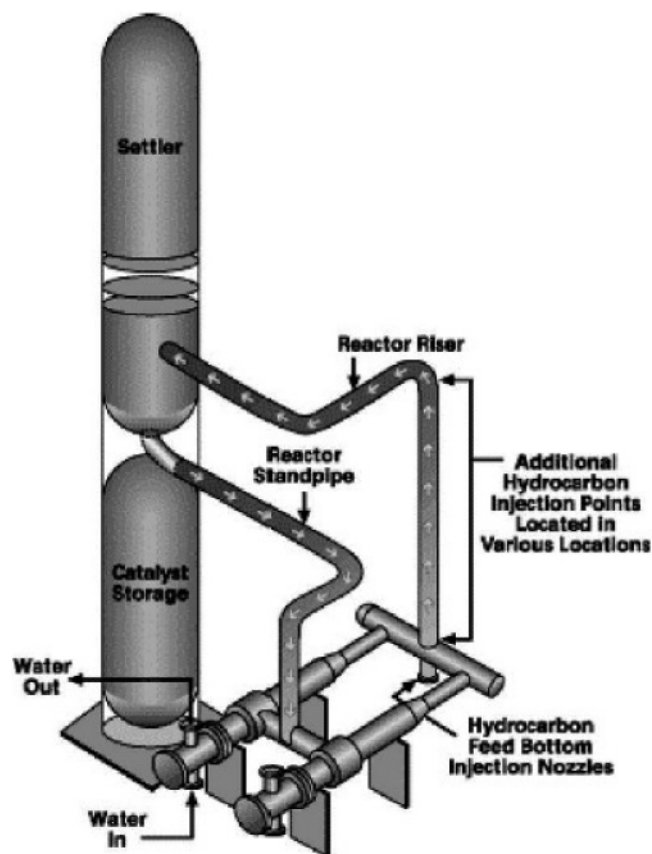


Figure 5. Schematics of the Conoco-Phillips HF alkylation reactor (ref 44).

hydrocarbon phase in a settler, cooled by heat exchange with water, and recycled to the reactor. However, acid-soluble oils are formed and dilute the catalyst. A strong advantage of HF with respect to H₂SO₄ is its easy separation and purification by distillation, due to its very high volatility. Accordingly, the acid loss is very small.

The main drawback in its use is related to safety concerns, due to its toxicity coupled with its volatility, with the possible formation of toxic aerosol clouds. A strategy to limit this drawback consists of the use of a vapor suppression additive. HF makes less volatile complexes with n-donor bases, such as the pyridinium poly(hydrogen fluoride) reagent, also called Olah's reagent, first described in 1973.⁴⁵ It has been found that several amine–poly(hydrogen fluoride) complexes are effective catalysts and are associated with lowered HF vapor pressure.⁴⁶ In the UOP Alkad process⁴⁷ it is claimed that the use of a vapor suppression additive can effectively mitigate as much as 90% of the risk of an HF release. In Figure 6

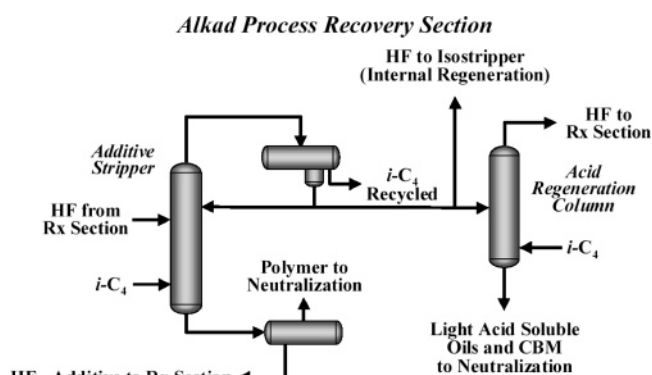


Figure 6. Schematics of the HF and additive recovery section of the UOP HF-alkylation technology (from ref 47).

the plant for HF recovery in the UOP Alkad process is shown. However, also in this case the loss of the acid is relevant. Organic fluorides are formed and may contaminate hydrocarbon products and byproducts. Similarly, ConocoPhillips together with Mobil developed an HF modified technology named ReVape. According to Feller and Lercher,³³ in the latter case the additive is most likely based on sulfones.

5.3. Friedel–Crafts Type Catalysts: HCl/AlCl₃ and Acidic Ionic Liquid Catalysts

Aluminum trichloride, AlCl₃, was proposed as a catalyst for aromatic alkylation and acylation reactions by C. Friedel and J. M. Crafts at the end of the 19th century. It melts at 193 °C, producing a typical molecular liquid mostly composed by the dimer Al₂Cl₆, although higher polymers may also exist.⁴⁸ It also produces several low-temperature eutectics with other metal chlorides and gives rise to liquid complexes

with hydrocarbons⁴⁹ and ionic liquids with organohalide precursors.⁵⁰ In the solutions, ionic species such as AlCl_4^- , Al_2Cl_7^- , or $\text{Al}_3\text{Cl}_{10}^-$ are formed. AlCl_3 is considered to be a very typical Lewis acid, according to the coordinative unsaturation of Al in the formal AlCl_3 monomeric molecule, which is saturated in the polymeric anions by a very weak nucleophile, the Cl^- anion. When activated with proton donor species, such as water or HCl , or its precursors such as alkyl halides, alkyl amine salts, imidazolium halides, pyridinium halides, or phosphonium halides, AlCl_3 gives rise to the formation of ionic liquids with very strong Brønsted superacidity, the strength of which have been evaluated to be similar to that of dry HF ($H_0 \sim -15$). These are very active as aromatic alkylation catalysts.^{51,52} The strong Brønsted acidity of this system, which allows olefin protonation, can be cooperatively enhanced by the Lewis acidity of AlCl_3 , able to interact with and activate aromatic rings.⁵³ The electrophilic character of the carbenium ion is enhanced by complexation of the halide to a Lewis acid such as Al_2Cl_6 , allowing it to leave as a less nucleophilic anion such as Al_2Cl_7^- .

Systems based on AlCl_3 and HCl have been used since the 1940s in the industry for liquid phase aromatic alkylations such as ethylbenzene synthesis from ethylene and benzene,⁵⁴ several plants being still in operation. In the original process, the reaction temperature is 130 °C and the pressure 2–4 bar in the presence of excess benzene and cocatalysts such as other metal chlorides and in the presence of small amounts of ethyl chloride as the source of HCl . That catalyst also catalyzes transalkylation that may be performed in the same reactor by recycling of polyalkylated benzenes. Bubble-tiled column reactors are used (see Figure 7⁵⁵) where the

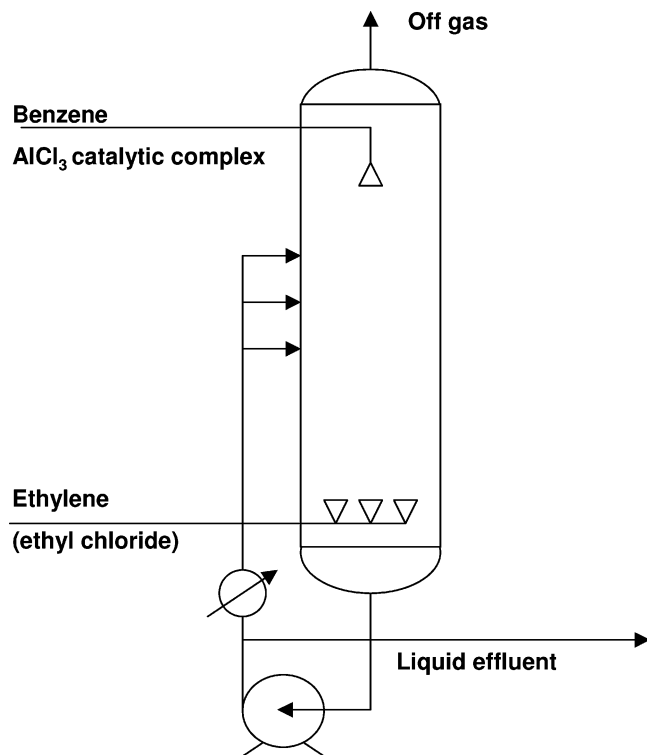


Figure 7. Schematics of a bubble column for benzene alkylation in the presence of HCl/AlCl_3 catalyst (from refs 54 and 55).

reaction mixture is formed by two liquid phases. The catalytic complex formed by aromatics complexed by HCl/AlCl_3 is a separate phase from the hydrocarbon solution. The catalytic

complex phase is separated from the reaction products and recycled to the reactor, but cannot be regenerated. The product must be washed with caustic to hydrolyze and separate catalyst residuals. These procedures result in relevant catalyst consumption (1–3% of the ethylbenzene product in benzene ethylation⁵⁴). An improved process was commercialized by Monsanto in the 1970s: a slight increase in reaction pressure (up to 10 bar) and temperature (160 °C) and a careful drying of the reactants allow the use of less catalyst and improve the process in terms of energy and acid consumptions. Also, the transalkylation step may be performed in a different reactor. With the same catalyst, cumene and higher LABs for the detergents industry may be produced through benzene alkylation by propene (110 °C; Table 4) and by linear higher olefins (55–60 °C). Several other reactions are catalyzed by similar systems such as the Gattermann–Koch carbonylation of toluene, producing *p*-tolualdehyde (Mitsubishi process) using either HF/BF_3 or an aluminum halide alkyl pyridinium halide ionic liquid catalyst.⁵⁶ The system HF/BF_3 is also used in the Mitsubishi process for the separation of *m*-xylene from C8 aromatic mixture.⁴² The acid forms the complex preferentially with the more basic *m*-xylene isomer. The complex is separated from the other C8 mixture and decomposed thermally, and the acid is recycled.

The main problems with these processes are represented by the requirement of reactors made in anticorrosion materials (ceramics, enamels, glasses), corrosion of piping, non-regenerability of the catalysts, and problems in disposal of the spent catalyst. Classical Friedel–Crafts catalysts present problems in their separation from the products,⁵⁷ performed by hydrolysis with the production of corrosive wastes.

The complexes produced by the reaction of alkyl halides (e.g., ethyl chloride) with AlCl_3 , and those obtained by an amine and HF belong to the family of acidic ionic liquids, which are currently the object of much investigation as liquid acidic catalysts.⁵⁰ Ionic liquids are low-melting-point salts ($T_m < 100$ °C) constituted by monovalent organic cations and inorganic anions such as Cl^- , CuCl_2^- , ZnCl_3^- , SnCl_3^- , BF_4^- , Al_2Cl_7^- , PF_6^- , AsF_6^- , SbF_6^- , and $\text{F}(\text{HF})_n^-$. When the cation is a protonated base, they are carriers of hydrogen halides (HCl , HF) and may act as Brønsted acid catalysts. These materials are certainly interesting as alternatives to liquid acids because of their lower volatilities and fewer corrosion problems, as well as the very large variety of applications and conditions they offer. However, they do not radically resolve the drawbacks of liquid acids. They appear to be very interesting catalysts for fine chemicals, where the small dimension of the plants can limit the safety and environmental drawbacks of these compounds. Less interesting seems to be their future application in the refinery and petrochemical industry.

5.4. Diffusion of Organics in Liquid Acid Media

The reciprocal solubility of hydrocarbons and polar solvents such as liquid acids is generally low. The system is consequently normally biphasic. The reaction occurs either in the acid phase, where active protons are, or at the phase interface. Isobutane/butylene alkylation is performed on a sulfuric acid continuous phase in which the hydrocarbon phase is dispersed with vigorous stirring. The larger the interfacial area, the faster the reaction.⁵⁸ Consequently, the rate of protonation reaction of hydrocarbons by Brønsted acids, which is rate determining,⁵⁹ depends on the acid

Table 5. Summary of Industrial Solid Acid Catalysts

	formula/example	acid group/ catalytic active species	reaction (ex)	phase	typical <i>T</i> range (°C)	deactivation	reactivation
alumina (silicated)	Al ₂ O ₃ Al _{2-x} Si _x O _{3+x/2}	AlOH or Al-OH-Al (SiOH) Al ³⁺	olefin skeletal isomerization alcohol dehydration	gas/solid	> 400	coking	burning
silicalite-1	SiO ₂	SiOH	Beckmann rearrangement of cyclohexanone-oxime	gas/solid	300	coking tar formation	burning
chlorided alumina	Al ₂ O _{3-x} Cl _{2x}	Cl _x AlOH Al ³⁺	paraffin isomerization aliphatic alkylation	gas/solid liquid/solid	120–200	chlorine loss coking coking/poisoning	difficult washing
acid-treated montmorillonite clays	Na _x [Al _{2-x} Mg _x Si ₄₋ O ₁₀ (OH) ₂] <i>n</i> H ₂ O	SiOH Al ³⁺	cracking	gas/solid (liquid/solid)	200–550	coking structural damage	burning
silica–alumina/ aluminated silica	H _y Si _{1-x} Al _x O _{2-x/2+2y}	SiOH	cracking dehydrochlorination alkylation	gas/solid liquid/solid	200–550 200	coking	burning
H-zeolites	H _x Si _{1-x} Al _x O ₂	Si-OH-Al	aromatics alkylation paraffin and olefin isomerization cracking aromatics alkylation	gas/solid liquid/solid	200–550 150–250	coking structural collapse poisoning	burning hydrogenation burning
SAPO	H _{x-y} Si _{1-x-y} P _y Al _x O ₂	Si-OH-Al	methanol to olefins	gas/solid	400–450	coking	burning
sulfated zirconia	H ₂ SO ₄ -ZrO ₂	SOH	paraffin isomerization	gas/solid	170–230	coking	difficult
tungstated zirconia	WO ₃ -ZrO ₂	WOH	paraffin isomerization	gas/solid	200–270	coking	burning
solid phosphoric acid	H ₃ PO ₄ /SiO ₂ (kiselghur)	POH [H(H ₂ O) _n] ⁺	olefin oligomerization and hydration aromatics alkylation	gas/solid	150–300	leaching coking	difficult
heteropolyacid	C _s H _{3-x} PW ₁₂ O ₄₀	W-OH-W [H(H ₂ O) _n] ⁺	ethyl acetate synthesis	gas/solid liquid/solid	140–250 60		difficult
niobic acid	Nb ₂ O ₅ · <i>n</i> H ₂ O	NbOH [H(H ₂ O) _n] ⁺	ethylene hydration fructose dehydration	gas/solid water/solid	200 100	coking	burning
sulfonated polystyrene– polydivinylbenzene resins		-SO ₃ H [H(H ₂ O) _n] ⁺ [H(ROH)] ⁺	ether synthesis olefin oligomerization	liquid/solid	40–100	poisoning	washing

strength of the acid, measured as the H_0 Hammet function,⁶⁰ on the concentration of the hydrocarbon in the acid phase, and on the extent of stirring. In the case of isobutane/butylene alkylation reaction, the solubility of the olefin in the acid is higher (2–4 times) than the solubility of isobutane.⁶¹ Additionally, olefin oligomerization competes with alkylation. Thus, a large excess of isobutane is needed to obtain alkylation, and the kinetics is limited by mass transfer.

The higher solubility of isobutane in HF (2.7 wt % at 27 °C in 100% HF) and its lower viscosity allow higher isobutane consumption rates to be obtained in alkylation with HF than with H₂SO₄. Therefore, HF can be operated at higher temperatures, resulting in higher reaction rates.

The solubility of benzene in HF is also limited to 2.25 wt % at 0 °C. Aromatic alkylation in the presence of AlCl₃ also occurs in biphasic systems, where the hydrocarbon–AlCl₃ complex does not mix with the hydrocarbon phase.^{54,55} Here, however, the hydrocarbons are supposed to form the continuous phase where the catalytic complex is dispersed.⁵⁵ Data on the diffusivity of hydrocarbons in ionic liquids are becoming available now, showing larger solubilities of olefins and aromatics than of alkanes.^{62,63}

6. Solid Acid Catalysts

In Table 5 a summary of the families of solid acid catalysts that find industrial application is reported. Some data are also reported concerning the practical conditions of their application, which will be discussed later.

6.1. Surface Acidity of Solids

6.1.1. Characterization Techniques

Several techniques allow the study of the surface acidity and basicity of solids at the gas–solid interface^{64–66} or at

the solid–water solution interface.⁶⁷ Most of the techniques performed at the gas–solid interface involve the use of molecular probes (see Table 6) and allow the determination of the amount of adsorbed probe molecules (such as gravimetry and volumetry), the differential and integral heat evolved during adsorption (adsorption microcalorimetry⁶⁸), and the amount of molecules that are desorbed at increasing temperature, so allowing the calculation of the desorption energies (temperature-programmed desorption⁶⁹). These techniques allow a characterization of the strength and amount of adsorbed species per unit of surface area and/or weight and, consequently, allow the measure of the number of the adsorption sites of different quality. However, to have a more direct idea of what happens upon adsorption, spectroscopic techniques are necessary.

Among these characterization methods, IR spectroscopic techniques^{65,70,71} find today wide application due to moderate cost of the FT-IR instruments and the well-established principles of the technique. The analysis of the IR spectrum of pressed disks of the pure catalyst powder (by using the transmission/absorption technique) or of the powder deposited as such (using the diffuse reflectance technique, DRIFTS) allows the detection of the vibrational modes of the surface hydroxy groups (OH stretchings in the region of 3800–2500 cm⁻¹) and, in some cases, also of metal–oxygen surface bonds. The spectra of adsorbed molecules can also be investigated, showing, for example, protonation of quite strong bases (such as pyridine or ammonia) over Brønsted acidic OH groups or the formation of H-bondings with weaker bases (such as nitriles and carbon monoxide) and the perturbation of the spectrum of the probes over Lewis acid sites. The use of probes characterized by different steric hindrance can also give information on the location of active sites in or out of micropores. Coupled with volumetry, IR

Table 6. Molecular Probes Applied for Surface Acidity Characterization

family	base		basic strength		mostly applied techniques
	example	formula	pK _a	PA	
cyclic amines	piperidine	C ₅ H ₁₀ NH	11.1	933	IR, ¹⁵ N NMR, calorimetry, TPD
alkylamines	n-butylamine	n-C ₄ H ₉ -NH ₂	10.9	916	calorimetry, TPD, ¹⁵ N NMR, IR
ammonia		NH ₃	9.2	857	calorimetry, TPD, ¹⁵ N NMR, IR
phosphines	trimethylphosphine	(CH ₃) ₃ P	8.65	957	³¹ P NMR, IR
phosphine oxides	trimethylphosphine oxide	(CH ₃) ₃ P=O		907	³¹ P NMR
heterocyclic amines	pyridine	C ₅ H ₅ N	5.2	928	IR, ¹⁵ N NMR, calorimetry, TPD
ketones	acetone	(CH ₃) ₂ C=O	-7.2	824	¹³ C NMR, IR
nitriles	acetonitrile	CH ₃ -CN	-10.4	783	IR, ¹⁵ N NMR
hydrocarbons	benzene	C ₆ H ₆		750	IR
	ethylene	H ₂ C=CH ₂		680	IR
carbon monoxide		CO		598	IR, calorimetry
nitrogen		N ₂		477	IR
argon		Ar		369	TPD

Table 7. Evaluation of the Lewis Acid Strength of the Surface Cationic Sites on Catalytic Materials by IR Spectroscopy of Adsorbed Probe Molecules. Position (cm⁻¹) of the Sensitive IR Bands of the Basic Probes (Lewis Acid Strength Roughly Decreases from Top to Bottom, See References 66, 70, and 71)

catalyst	adsorbate/IR mode				adsorbing site type
	CO νCO	pivalonitrile νCN	pyridine ring stretch (8a)	ammonia δ _{sym} NH ₃	
AlF ₃		2309, 2305	1627		ivAl ³⁺
zeolites (external surface)	2230	2300	1625	masked	ivAl ³⁺
silica-alumina	2235	2296	1625	masked	ivAl ³⁺
γ-Al ₂ O ₃	2235	2296	1625	1295	ivAl ³⁺
	2210–2190		1615	1265	ivAl ³⁺
	2170		1595	1220	viAl ³⁺
alumina-pillared montmorillonite		2290	1625	masked	ivAl ³⁺
acid-treated montmorillonite		2295	1625	masked	ivAl ³⁺
SiO ₂ -TiO ₂	2226 w	2308 w	1610	masked	Ti ⁴⁺
	2208	2285			
WO ₃ , unsupported	=	2290	1613	1275, 1222	viWO ⁴⁺
ZrO ₂	2195		1606	1210, 1160	Zr ⁴⁺
	2170				
sulfated zirconia	2160		1606	1210, 1150	Zr ⁴⁺
TiO ₂ anatase	2208	2285	1610	1225	vTi ⁴⁺
	2182	2260		1185	viTi ⁴⁺
liquids	2143	2236	1583	1054	

techniques allow a quite complete quantitative/qualitative analysis of the adsorption phenomena.

In this review we will base part of the discussion on results arising from IR experiments. In Tables 7 and 8 data on the Lewis and Brønsted acidity, respectively, of solid materials, as deduced by IR experiments, are summarized. When possible, we will also cite data on the Brønsted acid sites arising from MAS NMR techniques.^{72,73} The ¹H MAS NMR technique, in fact, performed on the solid catalyst after activation and upon adsorption, allows the detection of the signals due to the magnetic resonance of the protons of the surface hydroxy groups, the position of which is indicative of their environment. The perturbation of protonic centers upon adsorption of probes may also be investigated.²⁹Si and ²⁷Al MAS NMR techniques are also very relevant in the characterization of zeolites and different silicoaluminates, whereas advanced MAS NMR techniques allow the analysis of interactions between Si, Al, and protons.⁷⁴ ¹³C, ¹¹B, ¹⁵N, ¹⁹F, ³¹P, and ⁵¹V NMR techniques also allow the study of the spectra of molecular probes upon adsorption and of solid acids based on borates, nitrides, fluorides, phosphates, and vanadates.

The measure of the strength of acid sites at the gas/solid interface is not an easy matter.⁷⁵ In the case of the surface hydroxy groups, which are potential Brønsted acid sites, deprotonation enthalpies can be estimated according to the Bellamy–Hallam–Williams relation⁷⁶ from the wavenumber

shift Δν̄ of the IR OH stretching band when a H-bonding interaction occurs with a reference basic probe molecule. In heterogeneous systems (in particular for zeolites^{77,78}) the proton affinity of strong Brønsted sites can be calculated by theory or evaluated from that of the silanol groups of silica, taken as a standard, from the equation

$$PA_{\text{Brønsted}} = PA_{\text{SiOH}} - A \log(\Delta\bar{\nu}_{\text{Brønsted}}/\Delta\bar{\nu}_{\text{SiOH}})$$

the ratio Δν̄_{Brønsted}/Δν̄_{SiOH} being independent from the base chosen and where PA_{SiOH} = 1390 kJ/mol and A = 442 kJ/mol.

Alternatively, deprotonation enthalpies can be evaluated from probe adsorption calorimetric data or from temperature-programmed desorption measurements. The strengths of surface Lewis acid sites can be also evaluated, in principle, by the heats of probe adsorption or desorption. In all cases, however, probe adsorption on solids can result in multiple interactions: for example, van der Waals interactions can be superimposed to true acid–base interactions, which can also be multiple and give finally rise to some kind of solvation effects, in particular in the zeolite cavities.^{79–81} Thus, the pure acidity/basicity data are difficult to extract from experimental results.

Titration methods,^{82,83} that is, the study of the interaction of indicator dyes with the solids from solutions, have been proposed as a technique for both qualitative and quantitative

Table 8. Evaluation of the Brønsted Acid Strengths of Surface Hydroxy Groups on Catalytic Materials by Different IR Techniques (Brønsted Acid Strengths Roughly Decrease from Top to Bottom, See References 66, 70, and 71)

catalyst	νOH (cm^{-1})	$\Delta\nu\text{OH}$ (cm^{-1})		behavior with n-C ₄ H ₈ PA ~ 750	polymerization of				protonation of				
		CO PA = 594	acetonitrile PA = 783		C ₂ H ₄ PA = 680	C ₃ H ₆ PA = 752	i-C ₄ H ₈ PA = 802	C ₄ H ₆ PA = 783	acetonitrile PA = 783	pyridine PA = 912	NH ₃ PA = 846	n-butyl- amine	piperidine PA = 933
H-zeolites	3650–3500	~300–340	ABC	polym + isom	yes	yes	yes	yes	yes ^s	yes	yes	yes	yes
SO ₄ ²⁻ /oxide	3650–3630	~140	ABC	polym	yes	yes	yes	yes	no	yes	yes	yes	yes
WO ₃ /oxide	broad		ABC	polym	tr	yes	yes	yes	no	yes	yes	yes	yes
SiO ₂ -Al ₂ O ₃	~3745	~70–150	ABC	polym	no	yes	yes	yes	no	yes	yes	yes	yes
		~300											
H ₃ PO ₄ /SiO ₂	~3660	~180–200	ABC	polym	no	no	yes	yes	no	yes	yes	yes	yes
Nb ₂ O ₅ ·H ₂ O	3740–3705		~500						no	yes	yes		
AlF ₃	3730 3655	~150	>500				yes	yes	no	tr	yes	yes	yes
SiO ₂ -TiO ₂	~3740	~70–150	~450	polym tr	no	no	tr		no	no	yes	yes	yes
Al ₂ O ₃ -B ₂ O ₃	3800–3650	~70–150	480–420 330–280	butoxide traces	no	no		yes	no	no	yes*	yes	yes
silicated γ -Al ₂ O ₃	~3740	~70–150	480–420 330–280	$\Delta\nu\text{OH}$ 200–300	no	no	no		no	no	yes*	yes	yes
γ -Al ₂ O ₃	3800–3650	~70–100	450–400 330–280	$\Delta\nu\text{OH}$ 200–300	no	no	no	yes	no	no	yes*	yes	yes
TiO ₂ -anatase	3750–3650	~110–150	<300		no	no	no	no	no	no	tr	tr	yes
am- SiO ₂	~3745	~70–150	400	$\Delta\nu\text{OH}$ 150–200	no	no	no	no	no	no	no	no	no

^a ABC, strong hydrogen bonding with formation of the ABC vibrational contour. ^b tr, traces.

* Possible ammonia disproportionation to NH₂-NH₄⁺.

characterization of solid surfaces and allow some comparison with liquid acids. If a basic indicator B is used, the proton acidity of the surface is expressed by the Hammett acidity function, as done for liquid acids. The amine titration method, described by Tanabe et al.,⁸³ consists of titrating a solid acid suspended in benzene with n-butylamine using an indicator. This technique has many limitations for the deduction of gas–solid phenomena, the surface Hammett acidity function having also doubtful physical meaning in this case.⁸⁴ Nevertheless, this technique is widely applied in the fields of colloids and soil sciences,⁶⁷ and many data are available also for solid catalysts.

6.1.2. Strength, Amount, and Distribution of Surface Acid Sites on the Ideal Surface of a Solid

In heterogeneous catalysis, the catalytic activity (reaction rate) depends on the amount of active sites (e.g., of acid sites having the appropriate strength) present on the catalyst as a whole. This means that the “density” of active sites (amount of sites per gram of the solid or per unit of surface area) is an important parameter. On solids, the amount and strength of acid or basic sites are quite independent parameters, so both of them must be analyzed independently for a complete characterization. Additionally, several different families of acid sites may occur in the same solid surface, so their “distribution” (density of sites of any site family) must be characterized.

Additionally, both acidic and basic sites can be present in different positions (but frequently near each other) on the same solid surface and can work synergistically. This provides evidence for the significant complexity of acid–base characterization of solids.

6.1.3. Practical Aspects on the Use of Solid Acid Catalysts

Solid catalysts have a great advantage over liquid catalysts. They are in fact generally almost fully recovered from reaction products without any operation (fixed beds) or with quite easy procedures (fluid and/or moving beds). They are frequently, but not always, quite easy and safe to dispose of. They can be applied to liquid-phase or to gas-phase reactions.

In the latter case, they mostly work at quite a high temperature, in a regimen where coking and cracking are thermodynamically favored and fast. This causes the main drawback of their use in that the field of hydrocarbon acid-catalyzed conversions consists in deactivation, mostly by coking. To recover catalyst activity, regeneration procedures might be required.

Solid catalysts generally consist of high surface area/small particle size powders. Most solid acid catalysis is performed in fixed bed reactors. If packed in fixed bed reactors, powders tend to form high-density layers opposing the reactants' flow, causing large pressure drops. Also, fine particles tend to be transported out of the reactor by the effluent flow. For these reasons, solid catalysts are shaped in pellets by extrusion procedures,⁸⁵ which resist the reactant pressure and leave a sufficient void fraction to limit pressure drops. In Figure 8

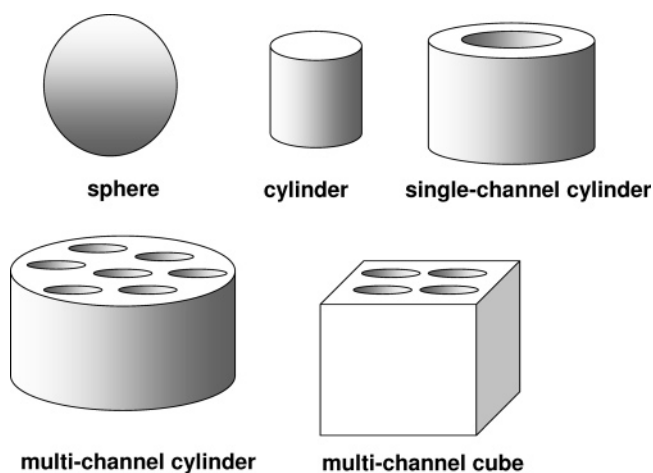


Figure 8. Shapes of commercial catalyst extrudates.

some usual shapes of commercial catalyst extrudates are shown. Extrudates are actually formed by mixtures of the real catalyst with additives such as binders and, possibly, stabilizers and activators. These materials may have a relevant role in the catalytic phenomena and, in particular, in the diffusion of reactants and products in the bed. In Figure

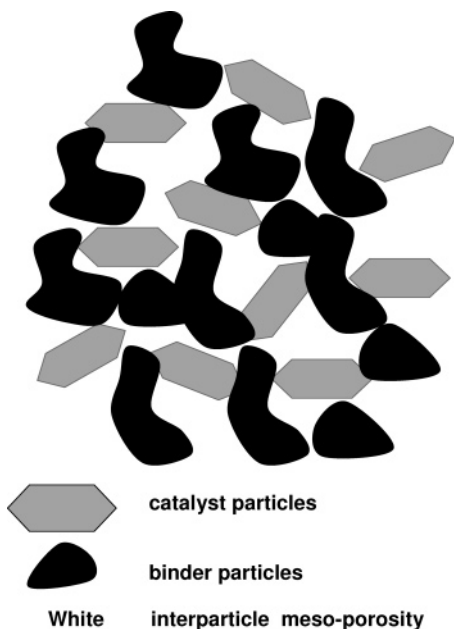


Figure 9. Schematics of the morphology of a real catalyst.

9 the morphology of an alumina-bound zeolite catalyst is schematized. Interparticle mesoporosity is formed between catalyst and binder particles and sums to catalyst and binder intraparticle micro- or mesoporosity.

In fixed bed tubular reactors, the catalyst extrudates are loaded above supporting grids and/or supporting inert ceramic materials in the form of balls. On top of the bed, layers of differently shaped catalysts, providing larger void sizes, and of inert materials may be deposited, to optimize fluidodynamics and to fix the bed. On top of the reactor, flow distributors allow limited preferential flow ways. A scheme of a single fixed bed axial downflow reactor is shown in Figure 10. When reactions are significantly exothermic,

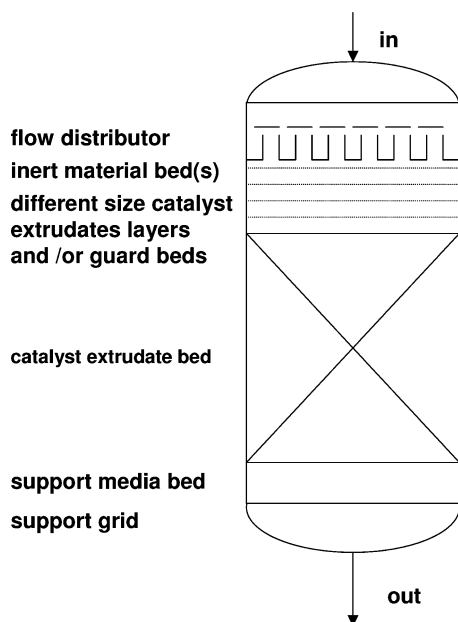


Figure 10. Possible arrangement for a fixed bed catalytic reactor.

several catalyst beds may be separated by quenching or heat exchange devices, to subtract the reaction heat. In the case of endothermic reactions, the effluents between each bed are directed through furnaces to recover heat.

Catalysts for moving or fluid bed reactors should resist the attrition due to the catalyst movement. To this purpose, particular agglomeration and extrusion procedures must be applied to form mechanically resistant microspheres

6.1.4. Deactivation and Reactivation of Solid Acid Catalysts

As already said, deactivation by coking is a very common phenomenon in heterogeneous catalysis by solids. Coking, associated with the thermodynamic instability of hydrocarbons at high temperature with respect to the elements, gives rise to the formation of carbonaceous deposits that kill the acid sites and cover the catalyst surface. Reactivation is mostly obtained by burning, with air or pure oxygen, the coke particles. Obviously, regeneration by burning is exothermic and causes temperature peaks at the catalyst surface. The catalyst must be consequently stabilized to stand this treatment, in particular, if repeated frequently, without relevant damage, sintering, and surface area loss. Other regeneration procedures are performed sometimes, such as hydrogenation, if noble metal particles are present and catalyze this reactivation reaction.

Coking occurs with variable rate, depending on several factors. In general, coking is faster the higher the temperature (at least until a maximum when cracking becomes predominant), the higher the hydrocarbon pressure, the higher the content of very reactive hydrocarbons in the feed (1,3-dienes > branched olefins > olefins > aromatics > paraffins, even at the impurity level), and the stronger is the catalyst acidity and the more microporous is the catalyst. According to these conditions, deep deactivation by coking may occur in years, months, weeks, days, or minutes.

Other reversible deactivation processes may occur in some cases, in particular due to adsorption of poisons (such as sulfur or amine bases). Also, these poisons may be burned off with air or oxygen, or, alternatively, may be desorbed by proper treatments.

Different reactivation procedures are possible, depending on the rate of catalyst deactivation.⁸⁶ The schematics of the plants, depending on the different regeneration procedures, are reported in Figure 11. When deactivation occurs in years, reactivation might not be necessary at all. The catalyst might be substituted after its cycle life. However, also depending on the cost of the catalyst, procedures of reactivation in situ, during a normal switch-off of the plant for maintenance, can be performed. Alternatively, during maintenance times, the catalyst may be removed, reactivated elsewhere, and reloaded in the reactor.

When deactivation occurs in months or weeks, swing-type regeneration may be performed. An additional reactor may be used (two instead of one or five instead of four), and the reactor beds may be regenerated alternatively, allowing a continuous operation of the plant. This is applied, for example, in the cyclic catalytic re-forming process,⁸⁶ as well as in several gas-phase acid-catalyzed processes. When deactivation is very fast, moving bed reactors with intermittent or continuous addition of active catalyst and withdrawal of deactivated catalyst may be applied. This is applied in the moving bed continuous regeneration catalytic re-forming processes as well as in hydrocracking in slurry ebullated beds. In the case of endothermic reaction occurring with fast coking, the burning of coke may supply the heat of reaction. This converts an endothermic process into an autothermic one or even into an exothermic one. The fluid bed catalyst

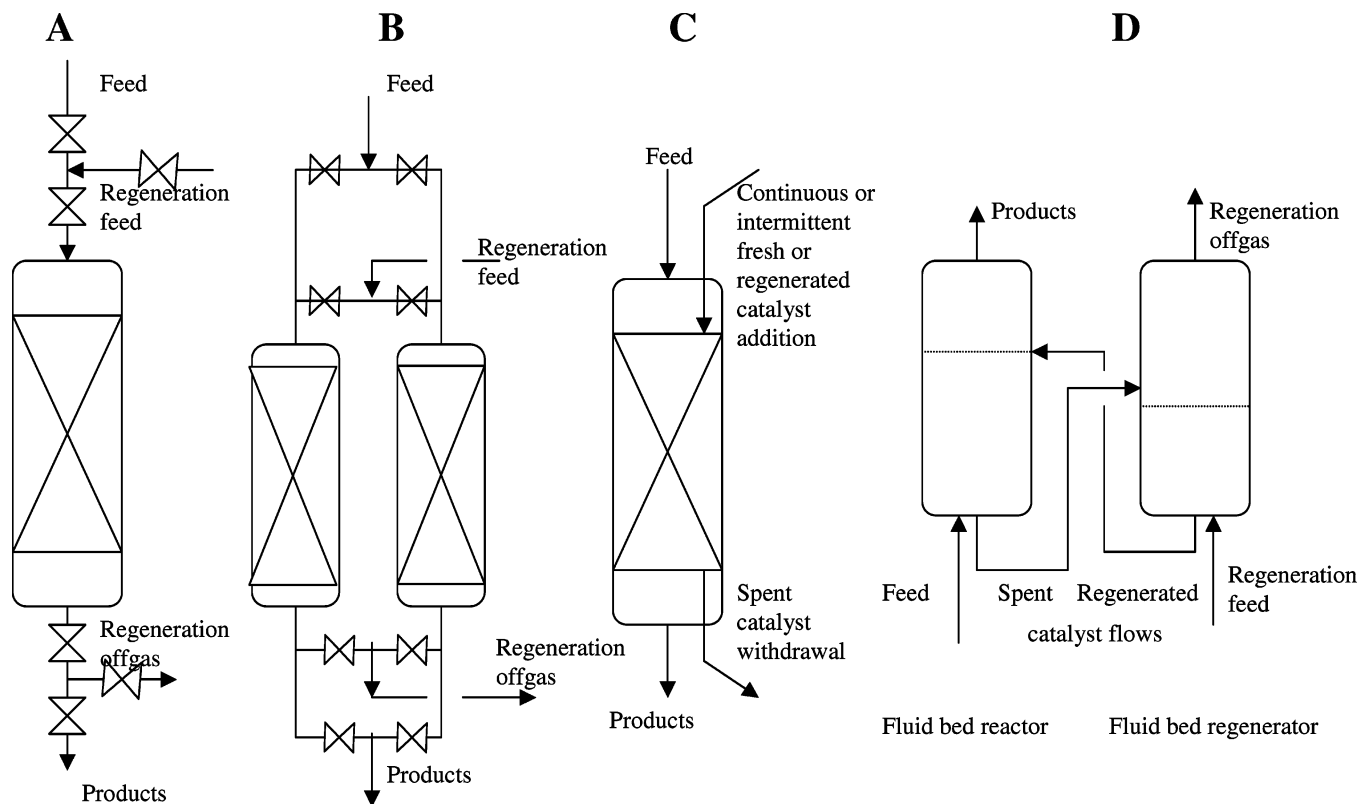


Figure 11. Schematics of catalytic reactors with different regeneration procedures: A, a single semiregenerative reactor; B, two swing reactors; C, moving bed reactor with intermittent or continuous catalyst addition/withdrawal; D, fluid bed reactor/regeneration system.

Table 9. Proposed Summary of the Acid–Base Properties of Binary Metal Oxides (References 66, 69, and 70)

element	oxidation state	cation size (radius, Å)	M–O bond nature	acidity type	acidity strength	basicity, nucleophilicity	examples
semi-metal	$\geq +5$	very small (≤ 0.2)	covalent molecular	Brønsted	medium-strong	none	P_2O_5 (SO_3)
	+4	small (≤ 0.4)	covalent network	Brønsted	medium-weak	none	SiO_2 , GeO_2
metal	high +5 to +7	small to medium (0.3–0.7)	largely covalent network \rightarrow layered \rightarrow polymeric	Brønsted	medium to strong	none	WO_3 , MoO_3 , CrO_3 , Ta_2O_5 , Nb_2O_5 , V_2O_5
		Lewis		strong		weak	
	medium +3 to +4	small (0.35–0.5)	ionic network	Lewis	medium	medium-weak	TiO_2 , Fe_2O_3 , Cr_2O_3
		medium (0.5–0.6)		Lewis	medium-weak	medium-strong	La_2O_3 , SnO_2 , ZrO_2 , CeO_2 , ThO_2 (Bi_2O_3 , Sb_2O_3)
low +1 to +2	large to very large (0.7–1.5)		Lewis	medium to very weak	strong to very strong	MgO , CaO , SrO , BaO , CoO , NiO , CuO , ZnO , (Cu_2O)	

may recycle from the reactor (frequently a riser tube) to the regeneration vessel where coke burning occurs, heating strongly the catalyst itself, and in this way it may provide the heat of reaction. This system has been developed for fluid catalytic cracking processes⁸⁷ (FCC) and has also been used in the paraffin dehydrogenation SNAMPROGETTI process.⁸⁸

6.2. Oxide Solids

6.2.1. Acidity and Basicity on the Ideal Surface of a Solid Oxide

As discussed elsewhere,^{66,70} typical metal oxides (such as titania, zirconia, and alumina) are essentially ionic network structures. Semimetal oxides, such as silicas and germania, are constituted by essentially covalent network structures. The nonmetal oxides and the oxides of transition metals in very high oxidation states may be molecular in nature (i.e., non-framework), formed either by relatively small molecules

(e.g., P_4O_{10}) or by macromolecular chains (e.g., CrO_3) or by layers (e.g., V_2O_5 and MoO_3). In Table 9 is reported a summary of the typical features of the surface chemistry, as a result of the structural features, of pure oxide solids.^{66,70}

In the case of ionic or covalent network materials, the surface is a defect situation where oxide species and metal or nonmetal centers remain exposed and coordinatively unsaturated at the surface. These sites should be associated with very high free energy and, consequently, should be very unstable. To stabilize the surface, reconstruction phenomena as well as reaction with molecules from the environment (e.g., water and CO_2) occur. This would limit the number of coordinatively unsaturated centers and cause the formation of new surface species such as hydroxy groups and surface carbonates. However, unsaturated centers at the surface can remain or be generated by desorption of adsorbed water (and CO_2) under heating. As a consequence of these phenomena, the surface of solid oxides can be constituted by surface oxide

species, acting as basic sites, and coordinatively unsaturated cations (mostly on ionic surfaces) or surface hydroxy groups (on both covalent and ionic surfaces), acting as Lewis and Brønsted acid sites, respectively. This actually may also occur with oxides formed by macromoles, linear or layered, at least on some surface planes.

6.2.2. Pure Oxides

6.2.2.1. Amorphous and Mesoporous Silicas and Siliceous Zeolites. Silica forms many different crystalline structures. All of the structures that are stable at ambient pressure present a tetrahedrally coordinated silicon atom, and the structure is associated with a covalent network.⁸⁹ On the other hand, silica is also the best known glass-forming material;⁹⁰ that is, it has very stable amorphous states, which also consist of a tetrahedral covalent network structure, although disordered.

Structurally, amorphous silica is quite a covalent oxide material;^{66,70} its surface behavior is dominated by the chemistry of the terminal silanol groups, characterized by a sharp and strong IR OH stretching band at 3748–3745 cm^{-1} (Figure 12) and by a ^1H MAS NMR signal centered at 1.7–2

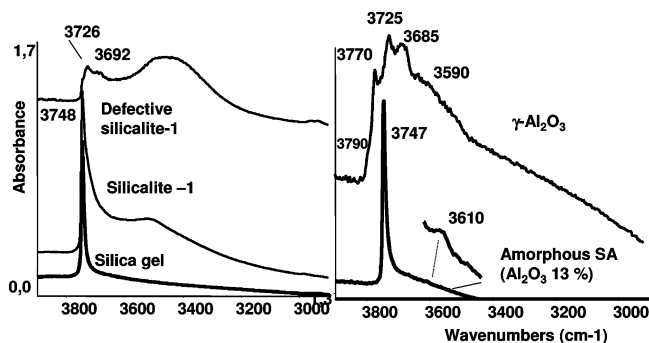


Figure 12. IR spectra of the surface hydroxy groups of silica, silicalite-1, defective silicalite-1, γ -alumina, and silica-alumina (outgassing at 450 °C).

ppm,⁹¹ generally multiple due to the coexistence of isolated or geminal silanols. These groups, although being weakly Brønsted acidic,⁹² are able to establish quite strong but easily reversible hydrogen bondings with polar molecules, which are the key phenomena occurring in adsorption–desorption cycles. Near-lying silanol groups also H-bond with each other, giving rise to chain-bonded hydroxyls. Recently, silsesquioxane compounds have been prepared as models of surface silica sites.⁹³ The relative amount of isolated and H-bonded silanols depends on porosity.⁹⁴ Evidence has also been found for the reactivity of surface siloxane bridges at high temperature.⁹⁵ The silanols make the surface of highly hydroxylated silicas strongly hydrophilic, and wet surfaces are even more active in adsorption. It is well-known that hydrogen bondings occur also between the silica's silanol groups and unpolar molecules such as hydrocarbons, allowing silicas to be also used for adsorption of these compounds. However, the Brønsted acidity of the silica's terminal silanol is generally found to be weak, no protonation occurring of basic molecules as, for example, pyridine. This is shown in Figure 13, where the strong bands at 1596 and 1446 cm^{-1} are the 8a and 19b ring stretching modes of py molecules weakly perturbed by H-bonding with silanols, no traces of pyridinium ions being found. Similarly also the reactivity toward hydrocarbons is weak, if found at all. In parallel, low-temperature CO adsorption⁹⁴ shifts down the silanol band of only $\Delta\nu \sim 75$ and ~ 155 cm^{-1} , two com-

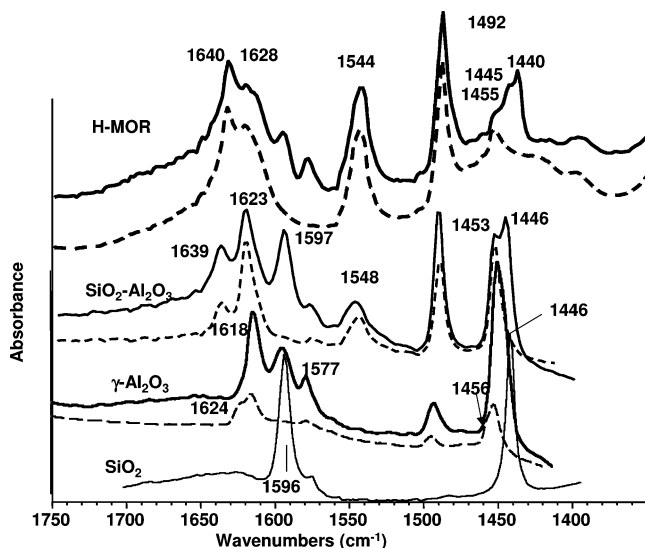


Figure 13. IR spectra of pyridine adsorbed on amorphous silica, γ - Al_2O_3 , silica-alumina, and HMOR zeolite: solid lines, outgassing at room temperature; broken lines, outgassing at 100 °C.

ponents possibly associated with two different families of silanol groups, the stretching of adsorbed CO being observed at 2155 cm^{-1} ($\Delta\nu \sim 17$ cm^{-1} with respect to liquid-like CO).

Amorphous silica, which has dozens of industrial applications as an adsorbent and a filler, does not seem to have application as a catalyst in hydrocarbon chemistry, but is very largely used as a support for catalysts and as a binder. Recently, mesoporous silicas have been prepared. Their basic chemistry is the same as for microporous silicas.

Silicalite-1 is a fully siliceous zeolite, with the MFI structure. Its crystalline framework, constituted by silicon oxide tetrahedra, has an essentially covalent and hydrophobic character. When well crystalline, hydrophilic silanols, having acidity comparable to that of silica,^{94,96} are present essentially at the external surface (Figure 12). However, when silicalite-1 is prepared in a “defective” form, nests of H-bonded silanol exist, giving rise to a quite complex IR spectrum in the OH stretching region (Figure 12): they are at least in part located in the channels⁹⁷ and make the structure more hydrophilic. This material has interesting application as an acid catalyst in an industrially important reaction, the vapor-phase Beckmann rearrangement of cyclohexanone oxime to ϵ -caprolactam with the Sumitomo process,^{98,99} occurring near 300 °C. The active sites for this reaction, which is also catalyzed by amorphous silica but less efficiently, are thought to be external and/or internal silanol nests.

Several other fully siliceous zeolites have been synthesized in recent times, such as ITQ-1, the siliceous form of zeolite MWW (MCM-22),¹⁰⁰ ITQ-29, the siliceous analog of zeolite A (LTA),¹⁰¹ and fully siliceous FER and BEA zeolites. However, published data on their acid sites are still very few. Fully siliceous zeolite BEA can be prepared in defective and nondefective forms and is also active in the Beckmann rearrangement.¹⁰² Nondefective fully siliceous BEA presents the strong band of silanol groups at 3740 cm^{-1} with a tail to lower frequencies, whereas the defective form also shows IR bands at 3735 and 3690 cm^{-1} .

6.2.2.2. Aluminas. **6.2.2.2.1. Structure-Related and Morphology-Related Surface Properties of Aluminas.** Aluminum oxide is a polymorphic material.^{103,104} The thermodynamically stable phase is α - Al_2O_3 (corundum), in which all Al ions are equivalent in octahedral coordination in a hcp oxide array. Corundum powders are applied in

catalysis as supports, for example, of silver catalysts for ethylene oxidation to ethylene oxide,¹⁰⁵ just because they have low Lewis acidity and low catalytic activity (so not producing undesired side reactions) while being mechanically and thermally very strong.

All other alumina polymorphs are metastable, and most of them have a structure which can be related to that of spinel, that is, cubic MgAl_2O_4 . $\gamma\text{-Al}_2\text{O}_3$, which is the most used form of alumina, is mostly obtained by decomposition of the boehmite oxyhydroxide $\gamma\text{-AlOOH}$ (giving medium surface area lamellar powders, $\sim 100\text{ m}^2/\text{g}$) or of a poorly crystallized hydrous oxyhydroxide called “pseudoboehmite” at 600–800 K, giving high surface area materials ($\sim 500\text{ m}^2/\text{g}$). The materials obtained with these precipitation methods are highly microporous. $\gamma\text{-Al}_2\text{O}_3$ powders with low porosity may be obtained by flame hydrolysis of AlCl_3 , but they show chlorine surface impurities.¹⁰⁶ Recently, high surface area mesoporous $\gamma\text{-Al}_2\text{O}_3$ ($200\text{--}400\text{ m}^2/\text{g}$) has been prepared by hydrolysis of an Al compound in the presence of ionic surfactants.¹⁰⁷

$\gamma\text{-Al}_2\text{O}_3$ is one of the most used materials in any field of technologies. However, the details of its structure are still a matter of controversy. It has a cubic structure described by Lippens and de Boer¹⁰⁸ to be a defective spinel, although it can be tetragonally distorted. The stoichiometry of the “normal” spinel MgAl_2O_4 having Al ions virtually in octahedral coordination and Mg ions in tetrahedral coordination, the presence of all trivalent cations in $\gamma\text{-Al}_2\text{O}_3$ implies the presence of vacancies in usually occupied tetrahedral or octahedral coordination sites.²⁷ Al NMR spectra show that tetrahedral Al is near 25% of all Al ions but also shows a small fraction of Al ions that are in coordination five,¹⁰⁹ or highly distorted tetrahedral. Soled¹¹⁰ proposed that the cation charge can be balanced, more than by vacancies, by hydroxy ions at the surface. In fact, $\gamma\text{-Al}_2\text{O}_3$ is always hydroxylated, dehydroxylation occurring only at a temperature at which conversion to other alumina forms is obtained. XRD studies using the Rietveld method, performed by Zhou and Snyder,¹¹¹ suggested that Al^{3+} cations can be in positions different from those of spinels, that is, in trigonal coordination. The possibility of a structure of $\gamma\text{-Al}_2\text{O}_3$, as a “hydrogen-spinel” has been proposed on the basis of IR spectroscopy.¹¹² Calculations based on the composition HAl_5O_4 have been performed, but this structure has been found to be very unstable.¹¹³ DFT calculations have been performed recently, but did not allow the problem to be completely solved. Sohlberg et al.^{114,115} arrived at a structure very similar to that proposed by Zhou and Snyder,¹¹¹ based on spinel but with occupation of extra-spinel sites. On the contrary, Digne and Sautet¹¹⁶ and Krokidis et al.¹¹⁷ proposed a structure based on ccp oxide lattice but different from that of a spinel, with 25% of Al ions in tetrahedral interstices and no structural vacancies. According to these authors, this structure, although unstable with respect to corundum, is more stable than the spinel-based structures.

Calcination at increasing temperatures gives rise to the sequence $\gamma\text{-Al}_2\text{O}_3 \rightarrow \delta\text{-Al}_2\text{O}_3 \rightarrow \theta\text{-Al}_2\text{O}_3 \rightarrow \alpha\text{-Al}_2\text{O}_3$.¹¹⁸ According to ²⁷Al MAS NMR the ratio between tetrahedrally coordinated and octahedrally coordinated aluminum ions increases upon the sequence $\gamma \rightarrow \delta \rightarrow \theta\text{-Al}_2\text{O}_3$. Tetrahedral Al^{3+} is near 25% in $\gamma\text{-Al}_2\text{O}_3$, 30–37% in $\delta\text{-Al}_2\text{O}_3$, and 50% (in principle) in $\theta\text{-Al}_2\text{O}_3$.

According to Lippens and de Boer¹⁰⁸ and Wilson et al.,¹¹⁸ $\delta\text{-Al}_2\text{O}_3$ is a tetragonal spinel superstructure having a unit

cell constituted by three spinel unit blocks with tetragonal deformation, likely with a partial ordering of Al ions into octahedral sites. It is formed continuously in the range of 800–900 K. $\theta\text{-Al}_2\text{O}_3$ is formed above 900 K with simultaneous decrease of the surface area to near $100\text{ m}^2/\text{g}$ or less. Its monoclinic structure, which is the same as that of $\beta\text{-gallia}$, can be derived from that of a spinel, with deformation and some ordering of the defects, with half tetrahedral and half octahedral Al ions.¹¹⁹ Within the sequence $\gamma\text{-Al}_2\text{O}_3 \rightarrow \delta\text{-Al}_2\text{O}_3 \rightarrow \theta\text{-Al}_2\text{O}_3 \rightarrow \alpha\text{-Al}_2\text{O}_3$ the lamellar morphology of boehmite is mostly retained but with progressive sintering of the lamellae and disappearance of the slit-shaped pores.

$\eta\text{-Al}_2\text{O}_3$ is also considered to be a spinel-derived structure but is obtained by decomposing bayerite $\text{Al}(\text{OH})_3$. Most authors conclude that $\eta\text{-Al}_2\text{O}_3$ corresponds to a defective spinel such as $\gamma\text{-Al}_2\text{O}_3$ but with a different distribution of vacancies, namely, with more tetrahedrally coordinated (35%) and less octahedrally coordinated Al ions.^{111,114,115,120,121} This results in stronger acidity of $\eta\text{-Al}_2\text{O}_3$ with respect to $\gamma\text{-Al}_2\text{O}_3$. Calcination gives rise to the sequence $\eta\text{-Al}_2\text{O}_3 \rightarrow \theta\text{-Al}_2\text{O}_3 \rightarrow \alpha\text{-Al}_2\text{O}_3$.

Other metastable forms of alumina, denoted $\rho\text{-Al}_2\text{O}_3$, $\chi\text{-Al}_2\text{O}_3$, and $\kappa\text{-Al}_2\text{O}_3$ ^{103,104}, also exist and can be obtained from the hydroxides gibbsite and tohdite, but they seem to have less interest in catalysis. Amorphous aluminas,^{122,123} possibly impure from organic reagents, have also been investigated. They tend to convert into $\gamma\text{-Al}_2\text{O}_3$ upon hydrothermal treatment. Amorphous alumina appears to be quite inactive as an acid catalyst, and Al ions there appear to be essentially in octahedral coordination.

6.2.2.2. Active Sites of Aluminas. The catalytic activity of transitional aluminas (γ -, η -, δ -, $\theta\text{-Al}_2\text{O}_3$) is undoubtedly mostly related to the Lewis acidity¹²⁴ of a small number of low coordination surface aluminum ions, as well as to the high ionicity of the surface Al–O bond.⁷⁰ The alumina’s Lewis sites have been well characterized by adsorption of probes such as pyridine, carbon monoxide, and several other bases followed by IR,¹²⁵ ammonia and amines followed by calorimetry,^{126,127} and triphenylphosphine followed by ³¹P NMR.¹²⁸ They are the strongest among binary metal oxides. Volumetric, TPD, and calorimetric experiments allowed also the determination of the amount of such very strong Lewis sites present on transitional alumina surfaces, which, however, depend on the dehydroxylation degree (depending on the activation temperature) and on the peculiar phase and preparation.

The density of the very strong adsorption sites responsible for ammonia adsorption heat of $>200\text{ kJ/mol}$ is reported to be near 0.1 site/nm^2 .^{126,127} Taking into account the bulk density of $\gamma\text{-Al}_2\text{O}_3$, it is easy to calculate that at most 1 site of every 50–100 acts as a strong Lewis site on γ -alumina outgassed at 400–550 °C, the large majority being still hydroxylated or not highly exposed at the surface.

It seems that, although the different alumina “spinel-type” phases react a little differently to outgassing, the density of the strongest Lewis acid sites tends to decrease a little by increasing the historical calcination temperature of the alumina (i.e., upon the sequence $\gamma \rightarrow \delta \rightarrow \theta$, which is also a sequence of decreasing surface area). As a result of this, the number of strongest acid sites per gram significantly decreases in this sequence, although catalyst stability increases.

Although it is clear that surface Lewis acid sites on alumina are due to coordinatively unsaturated Al^{3+} ions, it

is not fully clear what the coordination of such surface ions is. Most authors agree that at least three different types of Lewis acid sites (weak, medium, strong) exist on transitional aluminas,¹²⁵ arising in some way from the two or three coordinations of the ions in the bulk spinel-type structure, that is, octahedral and tetrahedral (normal spinel positions) and trigonal. Pyridine adsorption produces three components for the 8a ring vibrations at 1624, 1618, and 1597 cm^{-1} (Figure 13), attributed¹²⁵ to three different Lewis bonded species. According to Sohlberg et al.¹¹⁴ trigonal Al ions in the bulk relax into quasi-octahedral coordination at the surface of $\gamma\text{-Al}_2\text{O}_3$, whereas they relax into quasi-tetrahedral ions at the surface of $\eta\text{-Al}_2\text{O}_3$, and this would justify the higher acidity of $\eta\text{-Al}_2\text{O}_3$. This is, however, in contrast to the fact that the difference between the surface acidities of the two polymorphs is quantitative more than qualitative. Liu and Truitt¹²⁹ emphasized the close proximity of Lewis acid sites with surface OH groups, whereas Lundie et al.¹³⁰ identified four different Lewis acid sites arising from coordinatively unsaturated octahedral (the weakest) and tetrahedral sites (the three strongest), three of which are considered to be associated with three different types of hydroxy groups.

Actually, the true particular sites of aluminas for most catalytic reactions are very likely anion–cation couples, which have very high activity and work synergistically. The basic counterpart may be oxide anions or hydroxyl species. Alcohol adsorption experiments^{131,132} allow the characterization of such sites where dissociative adsorption occurs. Mechanistic studies suggest that such cation–anion couples are likely those active in alcohol dehydration,¹³³ in alkyl chloride dehydrochlorination,^{134,135} and in double bond isomerization of olefins^{136,137} over $\gamma\text{-Al}_2\text{O}_3$.

Many studies have been devoted to the multiplicity of the surface hydroxy groups of aluminas. After the work of Peri¹³⁸ and that of Tsyganenko and Filimonov,¹³⁹ Knözinger and Ratnasamy reported a very popular model of the different exposed planes of spinel-type aluminas.¹⁴⁰ This model has been later modified by Busca et al.^{141,142} These studies have been reviewed by Morterra and Magnacca.¹²⁵ More recently, additional investigations have been published by Tsyganenko and Mardilovich¹⁴³ and on the basis of theoretical calculations by Fripiat et al.¹⁴⁴ and Digne and Sautet,^{116,145} who also attempted to model the interaction of probe molecules. Lambert and Che¹⁴⁶ reviewed again these models and evidenced that the problem is still not solved. At least five components are usually present in the IR spectrum of the hydroxy groups of aluminas (Figure 12), that is, at ca. 3790, 3770, 3740–3720, 3700–3690, and 3580 cm^{-1} , although in many cases the observed peaks are multiple. Data arising from our laboratory, based on the comparison between the surface hydroxy group spectra of other spinel-type compounds (e.g., magnesium, zinc, nickel, and cobalt aluminate, ferrite, and chromite, and $\gamma\text{-Fe}_2\text{O}_3$) compared with corresponding corundum-type oxides ($\alpha\text{-Al}_2\text{O}_3$, $\alpha\text{-Fe}_2\text{O}_3$, and $\alpha\text{-Cr}_2\text{O}_3$)¹⁴² and, more recently, on the comparison with the hydroxy group spectra of $\alpha\text{-Ga}_2\text{O}_3$ and $\beta\text{-Ga}_2\text{O}_3$ ¹⁴⁷ strongly support the assignment of both components near 3790 and 3770 cm^{-1} to terminal AIOH groups with Al in a tetrahedral-like environment. The splitting, not present in stoichiometric spinels, of these bands is actually in relation to the presence of vacancies with respect to the full stoichiometry of the spinel structure MA_2O_4 in transitional aluminas, Al_2O_3 . The band located in the range of 3740–3720 cm^{-1} should belong

to AIOH groups with Al in an octahedral-like environment, very likely terminal, too. In contrast to data reported by other authors,⁶⁵ our results^{66,71,91,147} indicate that the OH's absorbing at 3790, 3770, and 3740–3720 cm^{-1} are all active in adsorption and present medium-weak acidity [no protonation of pyridine (Figure 13), protonation of *n*-butylamine and piperidine]. The hydroxy groups absorbing below 3700 cm^{-1} , supposed to be more acidic,¹⁴⁰ appear instead to be quite inactive¹⁴⁷ and could be weakly H-bonded or located in small pores. A complete investigation on the accessibility of these sites has still not been performed, to our knowledge. We consequently agree with Lambert and Che¹⁴⁷ that a definitive picture is still lacking.

Although most authors attribute essentially Lewis acid properties to transitional aluminas, several studies show that some of their multiple surface hydroxy groups also have medium-strong Brønsted acidity.¹⁴⁸ Actually, among the pure ionic oxides, aluminas are some of the strongest Brønsted acids. The activity of pure $\gamma\text{-Al}_2\text{O}_3$ as a good catalyst of skeletal *n*-butylene isomerization to isobutylene has been attributed to its medium-strong Brønsted acidity, sufficient to protonate *n*-butylenes at high temperature, producing carbenium ions, but too low to cause much cracking and coking.¹⁴⁹

The effect of surface impurities on the acidity of the surface as well as on the corresponding spectroscopic data has been frequently neglected. Sodium content on alumina strongly depends on the preparation method. Aluminas derived from aluminum metal via alkoxide have Na content (≤ 40 ppm as Na_2O) generally about 10 times lower than that derived from bauxite via the Bayer process. Sodium impurities decrease the number of active sites but also possibly decrease their strength, according to induction effects,¹⁵⁰ so finally decreasing the alumina activity in acid-catalyzed reactions. Sodium cations are so big that they are unable to enter the cavities of ccp oxide ions of spinel-type structures. For this reason, even when their total concentration is small, they concentrate at the surface and have a relevant poisoning effect.

Actually, the activity trend, that is, in *n*-butylene isomerization,⁶⁶ correlates well with the total integrated intensity of the νOH stretching band of the surface hydroxy groups and, inversely, with the sodium content derived by chemical analysis. This content is always very low, but differs significantly among the samples. It seems likely that sodium exchanges the protons of the surface hydroxy groups. It has been concluded that the amount of residual sodium, although always low, is determinant for decreasing the number of the active sites for *n*-butylene isomerization on $\gamma\text{-Al}_2\text{O}_3$, which is believed to be a proton-catalyzed reaction.^{66,149}

Transition aluminas, mostly denoted $\gamma\text{-Al}_2\text{O}_3$, but actually being frequently a mixture of $\gamma\text{-Al}_2\text{O}_3$, $\delta\text{-Al}_2\text{O}_3$, and $\theta\text{-Al}_2\text{O}_3$, or of $\eta\text{-Al}_2\text{O}_3$ and $\theta\text{-Al}_2\text{O}_3$, have wide application as the catalyst for the Claus process, the production of sulfur from H_2S and SO_2 in the refineries.

Aluminas are used as commercial catalysts of the alkylations of phenol with alcohols, such as the synthesis of *o*-cresol and 2,6-xyleneol using methanol at 300–400 °C.⁴² Aluminas are very active in the dehydration of alcohols to olefins and to ethers¹⁵¹ and have been used in the 1960s for producing ethylene from the dehydration of bioethanol.¹⁵² They are applied to produce dimethyl ether from methanol at 250–280 °C and 0.04–0.05 MPa, as a first step in the methanol to olefin (MTO) process.¹⁵³

Aluminas may be used for the dehydrofluorination of alkyl fluorides, which are byproducts of the HF-catalyzed isobutane/butylene alkylation process. Fluoroalkanes react at 170–220 °C, being converted to olefins. HF is adsorbed on the alumina to form aluminum fluoride, regeneration being needed every 6 months.¹⁵⁴

However, the main uses of aluminas in hydrocarbon conversions are as an adsorbent, as a support, as a catalyst binder, and as an additive (e.g., in FCC catalysis). They are also the precursor for fluorided and chlorided aluminas, which may be produced in situ upon halogenation, as well as for silicated aluminas (see below), borated aluminas, and other “modified aluminas” produced ex situ by chemical treatments.

6.2.3. “Mixed Oxides” of Silicon and Aluminum: H-Zeolites and Silica-aluminas

Several “mixed oxides” of silicon and aluminum have relevant roles in catalysis.¹²⁴ Three polymorphic forms of Al_2SiO_5 (kyanite, andalusite, and sillimanite) and mullite (the composition of which ranges between $3\text{Al}_2\text{O}_3 \cdot 2\text{SiO}_2$ and $2\text{Al}_2\text{O}_3 \cdot \text{SiO}_2$) are Al-rich crystalline aluminum silicates⁸⁹ generally obtained at high temperature as sintered ceramic materials. Silicon is always tetrahedral, whereas the Al ion is octahedral in kyanite, half-octahedral and half-tetrahedral in sillimanite, and half-octahedral and half-pentacoordinated in andalusite. In mullite Al is basically octahedral, but a variable amount of it occupies also tetrahedral sites. A spinel-type phase with the composition $6\text{Al}_2\text{O}_3 \cdot \text{SiO}_2$, where Si substitutes for Al in tetrahedral coordination, has also been reported as a metastable form.¹⁵⁵

The substitution of aluminum for silicon in a silica covalent network leads to a charge unbalance, which must be compensated by “extra-framework” cations, mostly alkaline. This occurs in the cases of the so-called “stuffed silicas”: these alkali aluminosilicate materials have structures strictly related to the crystalline forms of silica, but with cations in the interstices to counterbalance the presence of Al ions substituting for Si. This is the case, for example, of eucryptite (LiAlSiO_4 , a stuffed β -quartz) or nepheline (NaAlSiO_4 , a stuffed tridymite).

A similar mechanism also occurs in the amorphous networks of glasses,⁹⁰ as well as in the case of zeolites. They are natural framework silicoaluminates in which charge-balancing cations (usually alkali or alkali earth) are located in relatively large cavities formed by the $[\text{Si}_{1-x}\text{Al}_x\text{O}_2]^{x-}$ negatively charged framework. These cavities are connected by channels that give rise to a variety of microporous structures which can be penetrated only by sufficiently small molecules, so giving rise to the “molecular sieving” effect¹⁵⁶ as well as the “shape selectivity” effect in catalysis.^{157,158} The cations are exchangeable, so zeolites may also act as cationic exchangers. The exchange can be performed with ammonium ions, which can be later decomposed into gaseous ammonia and a proton. This allows the production of protonic zeolites, which are very strong solid Brønsted acids. Protonic zeolites are mostly synthesized directly, by using templating agents.¹⁵⁹ In this case the protons may be residual from the combustion or decomposition of the templating agents.

6.2.3.1. Protonic Zeolites: Acidity and Shape Selectivity. Protonic zeolites are formally crystalline Si–Al mixed oxides or solid solutions of alumina in crystalline microporous silica networks, in which the protons are necessary for stoichiometry. Their general formula is $\text{H}_x\text{Si}_{1-x}\text{Al}_x\text{O}_2$. The

value of x is generally quite low, the protonic structures becoming unstable when Al content is relatively high, although this depends from the particular zeolite structure. The totally siliceous materials ($x = 0$) not always can actually be synthesized. At least 133 zeolite-type structures exist that are denoted by a three capital letter code by the Commission of the International Zeolite Association (IZA). A detailed description of the structure of each zeolite type and their code can be found in the IZA website¹⁶⁰ as well as in the book by Baerlocher et al.¹⁶¹ edited by IZA and Elsevier. The schematics of the zeolite structures reported here have been taken from the IZA website.

Protonic zeolites find industrial applications as acid catalysts in several hydrocarbon conversion reactions.^{157,158,162} The excellent activity of these materials is due to two main properties: a strong Brønsted acidity of bridging Si–(OH)–Al sites generated by the presence of aluminum inside the silicate framework and shape selectivity effects due to the molecular sieving properties associated with the well-defined crystal pore sizes, where at least a part of the catalytic active sites are located.


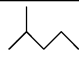
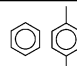

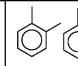
The main factor allowing molecular sieving and, consequently, shape selectivity is generally considered to be exclusively a steric effect; that is, only molecules having a critical kinetic diameter lower than the channel diameter are allowed to enter the pores (reactant shape selectivity) and to react on an active site or, in case, to exit them and be recovered as a product of the reaction (product shape selectivity). Alternatively, transition state shape selectivity effects limit the formation of bulky transition state intermediates inside the pores that may be formed and avoid the formation of some reaction products. The molecular sieve effect is actually a dynamic phenomenon that depends on the temperature. In fact, molecules that have moderately larger diameter than the cavities may manage to access them, in particular, at high temperature. However, a cutoff size exists. For example, the access at the supercages of Y-zeolites, limited by 7.4 Å rings, can occur with molecules having up to 10.2 Å diameter. In Table 10 some characteristics of protonic zeolites used in the industry as acid catalysts, including data on the diffusion of molecules in their cavities, as measured at room temperature using IR spectroscopy of molecular probes, are summarized.

Real zeolite catalysts are frequently pretreated in various ways such as steaming, and are not “perfect” structures: extra-framework species (EF) are frequently present and can also have a role either as active sites or as material hindering the molecular diffusion into the cavities. Additionally, different preparation methods of the same zeolite can give rise to quite different properties, due to several additional effects such as different particle sizes¹⁶³ and morphologies,¹⁶⁴ different active site densities, or different distribution of framework aluminum and, consequently, of protons from surface to bulk.¹⁶⁵ In most cases the roles of shape selectivity and of pretreatments such as dealumination are still imperfectly known or under debate.

Other important properties of zeolites are their sufficient thermal stability, their quite easy reactivation when coked, mostly by burning the coke, and finally their safe disposal when non-regenerable.

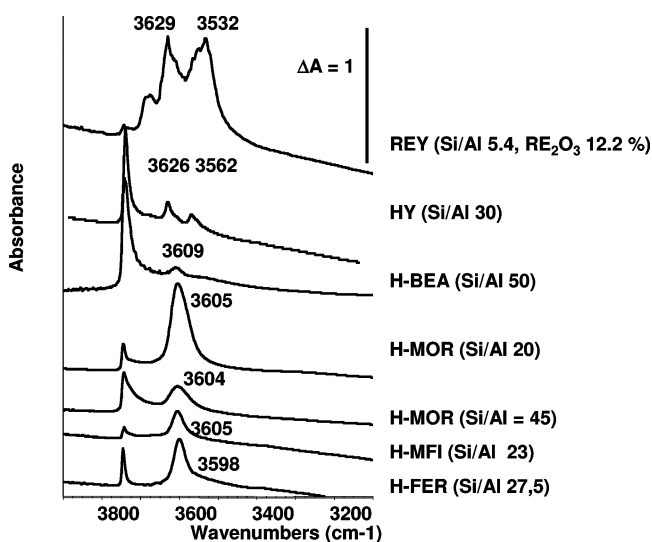
6.2.3.1.1. Acidity of Protonic Zeolites: Brønsted Sites in a Cavity. It is unanimously recognized that the bridging hydroxy groups Al–(OH)–Si, which are located in the walls of the zeolitic cavities, constitute the strong acidic sites of

Table 10. Summary of the Characteristics of Protonic Zeolites and the Diffusion of Hydrocarbons in Their Cavities (E, Easy; D, Difficult) As Measured by IR Spectroscopy at Room Temperature

Code	Channels - cages	Channel sizes	IR νOH (cm^{-1})	$^1\text{H NMR}$ δ_{H} (ppm)					
FER	8 ring channel [010]	3.5 Å x 4.8 Å	3598	4,4	E	D	D	D	D
	10 ring channel [001]	4.2 Å x 5.4 Å	3591		E	E	D	D	D
MFI	10-ring channel [100] (sinusoidal)	5.1 Å x 5.5 Å	~ 3610 channel	4,1-4,3	E	E	E	D	D
	10-ring channel [010] (straight)	5.3 Å x 5.6 Å	~ 3620 intersect.		E	E	E	D	D
BEA	12 ring channels [001]	5.6 Å x 5.6 Å	3609	3.8-5.6	E	E	E	D	D
	12 ring channels [100]	6.6 Å x 6.7 Å	3628, 3608, 3590		E	E	E	E	D
MOR	8-ring compressed channels [001]	2.6 Å x 5.7 Å	3588 side-pocket 3609 intersect. 3605 main chann.	4.0-4.2 4.6	D	D	D	D	D
	8-ring side pockets [010]	3.4 Å x 4.8 Å			D	D	D	D	D
	12-ring main channels [001]	6.5 Å x 7.0 Å			E	E	E	E	D
FAU	Hexagonal prisms accessed through 6-ring channels	ca 2.7 Å x 2.7	3501	4.7-4.8	D	D	D	D	D
	Sodalite cages accessed through 6-ring channels	ca 2.7 Å x 2.7	3553		D	D	D	D	D
	Supercages accessed through 12-ring main channels [111]	7.4 Å x 7.4 Å	3625	3.7-4.4	E	E	E	E	E

protonic zeolites. The proton balances the charge defect due to the Al for Si substitution in the framework. It has been recently underscored that the bridging OH groups are detected only in the interior of the zeolitic cavities, the corresponding spectroscopic features being absent in any non-zeolitic material based on silica and alumina⁹⁴ and also on the external surfaces of different zeolites (see below). Thus, the existence of the bridging hydroxy groups Al(OH)–Si should imply the existence of the cavity. In other words, the cavities are possibly involved in the generation and/or stabilization of the bridging OH sites.⁹⁴

The bridging hydroxy groups of zeolites are well characterized by the presence, in the IR spectrum, of quite definite and strong bands in the region between 3650 and 3500 cm^{-1} (Figure 14), which are present together with a band of weakly

**Figure 14.** IR spectra of the surface hydroxy groups of different zeolites (after outgassing at 450 °C).

acidic terminal silanol groups at 3745–3748 cm^{-1} . The position of the IR band due to bridging OH groups is somehow dependent on the size of the zeolite cavities, νOH

being generally lower the smaller the cavity. The OH stretching band position and width can be influenced by weak H-bondings through the cavities,¹⁶⁶ which provides evidence of their poor availability for steric hindrance and makes them unreactive toward weak basic molecules. In the case of zeolites with more than one type of quite different cavities, splitting of the band of the bridging hydroxy groups can be observed. Some authors suggested that a correlation exists between OH stretching frequency and the Si–O(H)–Al bond angle.¹⁶⁷

The strong Brønsted acid strength of the zeolites bridging OH groups is confirmed by adsorption of basic probes followed by different techniques. Quite strong bases such as pyridine are easily protonated, as shown in the upper spectra of Figure 13 where the bands of pyridinium ions (1640, 1628, 1544, 1492 cm^{-1}) are fully predominant after pyridine adsorption on H-MOR. Weak bases such as nitriles and CO hydrogen bond with these OH groups with a strong shift down of the νOH mode. In Figure 15 the spectra of two H-MFI samples upon low temperature adsorption of CO are reported. The band at 3622–3615 cm^{-1} , due to bridging OH groups, shifts down to near 3300 cm^{-1} , with a $\Delta\nu \sim 310$ –330 cm^{-1} , as evidence of the strong acidity of these groups. In parallel, the CO triple bond stretching shifts up from 2138 cm^{-1} for the liquid-like species to ~ 2175 cm^{-1} . For the same zeolite structure, the intensity of νOH strongly depends on the Al content (see Figure 14 for H-MOR and Figure 16 for H-FER), its position being also slightly affected by composition.

Interestingly, careful analysis of the IR spectra of zeolites sometimes provides evidence of very broad absorptions together with the sharp ones due to free surface OH groups. This is found in Figure 17 for a H-MFI and a H-MOR sample. Broad bands centered near 3400 and 3300 cm^{-1} , respectively, are evident. It is possible that these bands are associated with H-bonded OH groups in Al-rich portions of the structure. It seems that these groups are almost not reactive, because their absorption is not perturbed by the adsorption of bases. This is likely due to their inaccessibility.

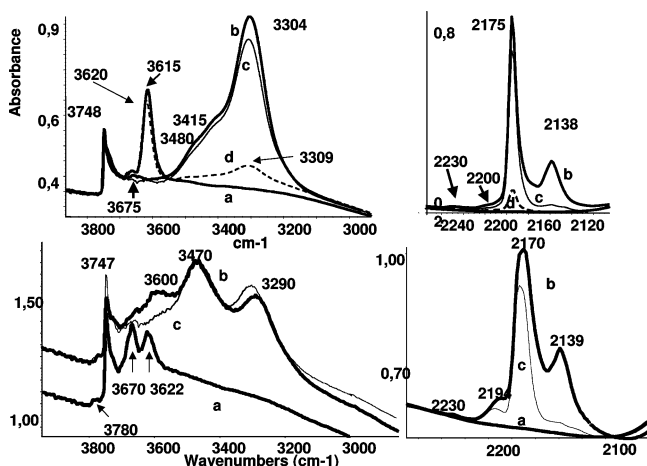


Figure 15. IR spectra of two H-MFI zeolites after outgassing at 450 °C and cooling to 130 K (a), subsequent contact with CO gas at 130 K (b) and outgassing at 130 K (c), and upon warming until 250 K (d).

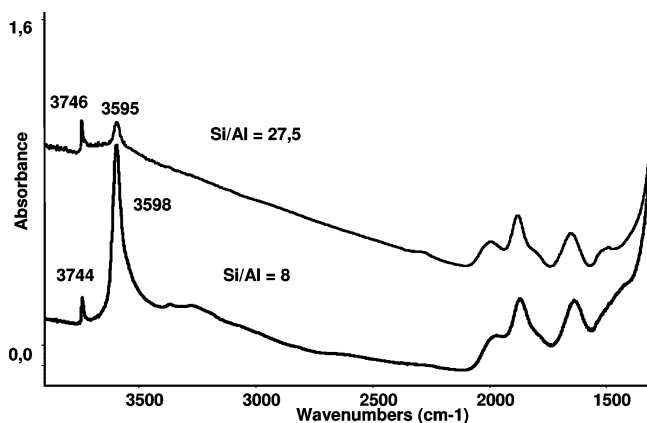


Figure 16. IR spectra of two H-FER zeolites after outgassing at 450 °C; spectra recorded at 130 K.

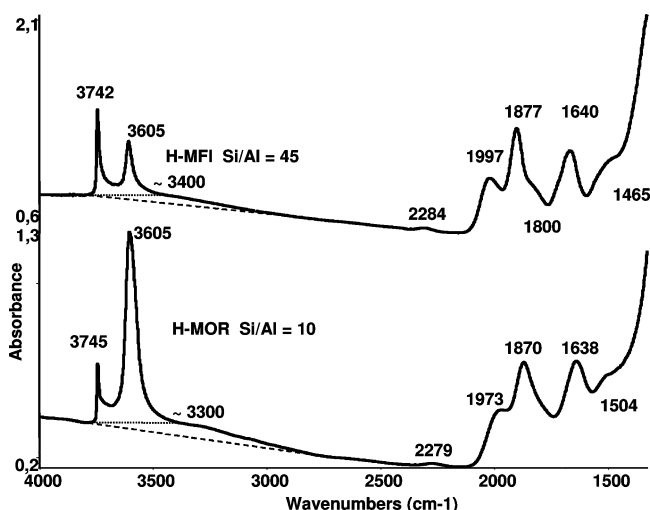


Figure 17. IR spectra of H-MFI and H-MOR zeolites after outgassing at 450 °C.

Broad bands of this type may be found mostly in the case of Al-rich zeolites, such as Al-rich H-FER¹⁶⁸ (see also Figure 16) and H-CHA with Si/Al atomic ratio of 2.¹⁶⁹

The bridging OH groups of zeolites is also characterized by evident ¹H MAS NMR narrow peaks in the region of 3.8–5.2 ppm,^{170,171} which are perturbed by adsorption of probes. In Figure 18 the ¹H MAS NMR spectra of dehydrated

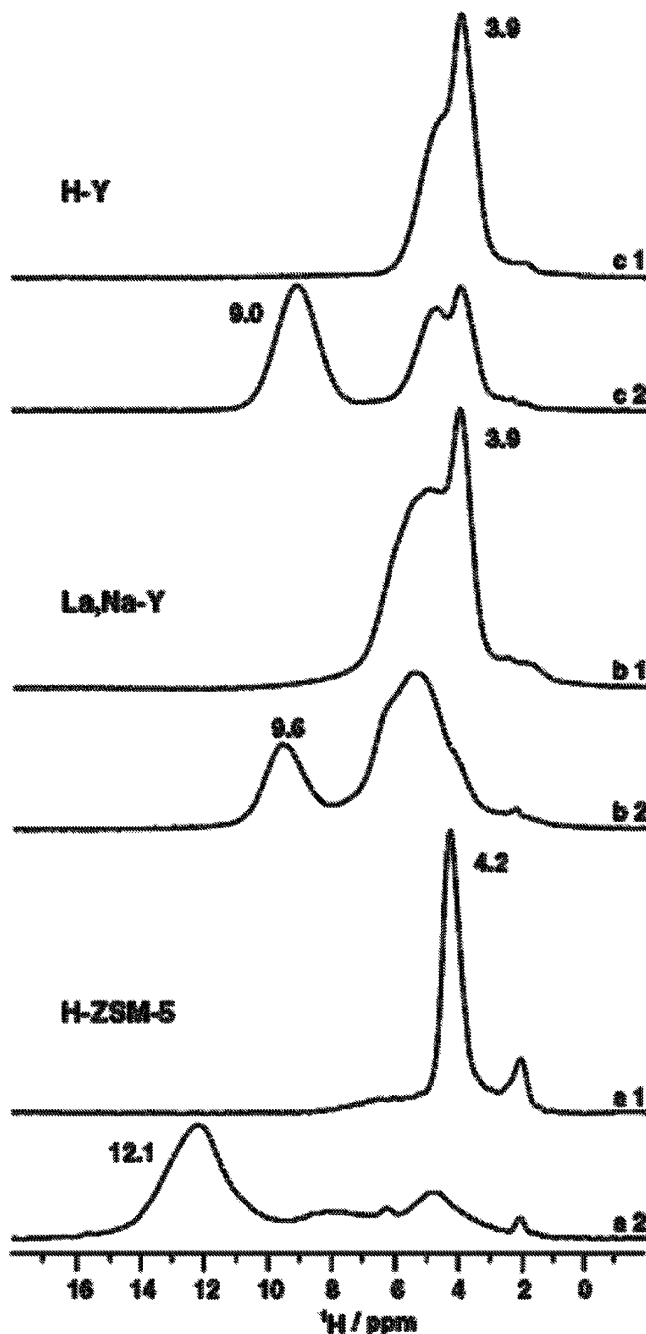


Figure 18. ¹H MAS NMR spectra of dehydrated zeolites H-ZSM-5 (Si/Al a.r. 26, a), La,Na-Y (Si/Al a.r. 2,7, b), and H-Y (Si/Al a.r. 2,7, c) before (1) and after (2) loading with one molecule of acetonitrile per acidic bridging OH group. (Reprinted with permission from ref 172. Copyright 2007 Elsevier.)

zeolites H-ZSM-5, La,Na-Y, and H-Y, published by Huang et al.,¹⁷² are reproduced (spectra denoted 1). The spectra are dominated by the signals at 3.9–4.2 ppm due to bridging OH groups located in the supercages of zeolites H-Y and La,Na-Y and in the 10-ring channels of zeolite H-ZSM-5. Low-field signals indicate the presence of nonaccessible bridging OH groups (4.8 ppm) and LaOH groups (6.3 ppm) in the small cages of zeolite H-Y and La,Na-Y, respectively. Weak signals at 1.8–2.2 ppm are caused by nonacidic SiOH groups. Upon adsorption of CD₃CN and formation of hydrogen bondings between Brønsted acid sites and probe molecules (spectra denoted 2), a strong low-field shift of the ¹H MAS NMR signals of accessible bridging OH groups occurs.

Simperler et al.,¹⁷³ who reviewed briefly the experimental data on ¹H MAS NMR spectra of protonic zeolites, emphasized some significant disagreement between the position of the peaks observed by different authors for the same zeolite. This is possibly associated with the high sensitivity of the modern instruments, relatively still under improvement. According to these authors, the trend among these studies is for increased chemical shift to correspond to an increase in the intrinsic acid strength (proton affinity); that is, protons are more deshielded in zeolites perceived to be acidic, such as MFI, and in small cages, whereas the shift can be much lower in FAU (e.g., H-Y) zeolites in which the protons in the more open supercages are reckoned to be less acidic.

Parallel ¹H NMR and IR studies show that the IR extinction coefficient of the zeolite's bridging OH groups is far higher than that for silanol groups, and this allowed Kazansky et al.¹⁷⁴ to propose the use of the intensity of the IR band to determine the surface acid strength.

Most data agree, suggesting that, when the Al content is relatively low, the amount of Brønsted sites in zeolites actually strictly depends on Al concentration, according to the theory. The ratio between catalytically active sites and Al ions ranges apparently from 80 to 100% for highly siliceous extra-framework-species-free zeolites.^{175,176} Corma et al.¹⁷⁷ reported data on the accessibility of protonic sites of different zeolites to 2,6-di-*tert*-butylpyridine (DTBP). This molecule has been considered to be "selective" for Brønsted sites, due to its impossible interaction with Lewis sites for steric hindrance. According to these authors, however, the interpretation of the data is not straightforward, for several reasons such as the presence of different cavities and the big size of the probe itself. Surprisingly, Corma et al. found a complete accessibility of the sites of H-BEA zeolite to DTBP. This contrasts with the data of Trombetta et al.,¹⁷⁸ who showed that protonic sites exist also on the smaller channels of H-BEA, the access of which to DTBP seems very unlikely. Fărcașiu et al.¹⁷⁹ reported an accessibility of 90% of the protons of H-BEA to DTBP, much higher than the 36% for H-MOR and 31% for H-USY.

Different opinions seem still to exist on whether the position of the OH stretching band and of the ¹H NMR peak can actually be correlated with the Brønsted acidity of the site. The effect of the zeolite structure on their acidity has been investigated by several authors with different techniques. Zecchina and co-workers have investigated the hydrogen bonding of different basic probes with different zeolites and other Brønsted acids such as HF and H-Nafion.^{78,180,181} They found protonic zeolites to be weaker acids than H-Nafion and stronger acids than HF. On the other hand, it seems that differentiation of the acid strength of protonic zeolites, such as H-MFI, H-MOR, and H-BEA, is difficult, although all of them seem to be slightly more acidic than H-FAU. A quite similar trend has been reported by Auroux,¹⁸² who summarized the microcalorimetric data concerning ammonia adsorption: according to these data the trend for the cited zeolites is H-MOR ($\Delta H_{\text{adsNH}_3} > 160$ kJ/mol) \geq H-ZSM5 \geq H-FER $>$ H-BEA \geq H-FAU ($\Delta H_{\text{adsNH}_3} \sim 130$ kJ/mol), although the secondary "solvation" effects in the cavities could be even more determinant in this measure. Also, ammonia TPD data reported by Niwa and co-workers gave a similar trend: H-MOR $>$ H-MFI $>$ H-BEA $>$ H-FAU.¹⁸³ Thibault-Starzyk et al.,¹⁸⁴ instead, deduced from the low-temperature CO adsorption the trend H-MOR $>$ H-FAU $>$ H-MFI $>$ H-FER, whereas, using the

high-temperature protonation of acetonitrile, obtained a trend that correlates better with n-hexane cracking, that is, H-MOR $>$ H-FER $>$ H-MFI $>$ H-FAU. Lonyi et al.,¹⁸⁵ measured the following acidity scale: H-MFI \sim HMOR \sim H-BEA $>$ H-USY $>$ HY using N₂ as the probe, in good agreement with n-hexane conversion. Theoretical calculations by Brändle and Sauer,¹⁸⁶ in contrast, indicate that deprotonation energy is higher for highly siliceous H-FAU than for H-MOR and H-MFI, thus supporting a higher acidity of H-FAU and a lowest one for H-MFI. More recently, Simperler et al.¹⁷³ calculated the following intrinsic acidity scale: H-MFI $>$ H-MOR $>$ H-MTW $>$ H-FER $>$ H-FAU. However, the same authors calculated a different scale for the strength of hydrogen bond with acetonitrile: H-MFI $>$ H-FAU $>$ H-MOR $>$ H-MTW $>$ H-FER, which indicates that the interaction is negatively affected (weakened) by steric hindrance in the case of smaller pore zeolites. In the very recent work on neopentane hydrogen/deuterium exchange Walspurger et al.¹⁸⁷ found the reactivity scale H-MOR $>$ H-MFI $>$ H-BEA $>$ H-FAU and concluded that it is strongly influenced (favored) by the smaller size of the pores. In both cases a relevant role of confinement effects has been suggested. A similar conclusion was obtained by Xu et al.,¹⁸⁸ who, on the basis of kinetic measurements, concluded that the active sites of MFI, BEA, MOR, and FAU protonic zeolites have very similar strengths, with a relevant role of local geometric factors.

6.2.3.1.2. External versus Internal Sites in the Zeolite Catalysis: "Selectivation" of Zeolites. Catalytic active sites also exist on the external surface and at the pore mouth of zeolite crystals. These sites are considered to be responsible for unwanted nonselective catalysis^{164,165,189} as in the case of alkyl aromatic conversions over H-MFI. On the other hand, H-zeolites also catalyze reactions of molecules that do not enter the cavities due to their bigger size. Therefore, the external surface of zeolites is certainly active in acid catalysis. Additionally, the bulk versus surface Si/Al composition of a zeolite could be different, and different preparation procedures can allow modification of this ratio.^{164,165}

The external surfaces of H-FER,^{190,191} H-MFI,^{191,192} and H-MOR¹⁹³ have been studied by IR spectroscopy of adsorbed hindered nitriles. The results on H-FER are confirmed using pyridine,^{92,191} lutidine, and aromatic hydrocarbons.¹⁹⁴ Terminal silanols and Lewis acid sites exist at the external surface of H-FER, H-MFI, and H-MOR. Interestingly, the acidity of the external silanol OH groups of zeolites can be enhanced with respect to those of silica. The very strong bridging Brønsted acid sites, instead, do not apparently exist at the external surface, being totally confined at the internal surface. Otero Arean et al.¹⁹⁵ obtained similar results on H-MFI using adamantane-carbonitrile as the probe. ¹H NMR spectra of different protonic zeolites show peaks in the 1.3–2.2 ppm range attributed to external nonacidic silanols (see Figure 18).^{170,174}

Interesting data have been obtained by the investigation of the acidity of ITQ-2, a layered material produced by exfoliation of MCM-22 (H-MWW) zeolite.^{196–198} They showed that upon exfoliation the band due to bridging OH groups decreases strongly in intensity, whereas the band due to terminal silanols strongly increases. This indicates that bridging sites cannot resist when the cavity disappears and they become exposed at the surface. The bridges probably open to give terminal silanols. Some authors, however, report

the existence on the surface of sites with intermediate acidity between silanols and bridging OH groups they consider to be not directly detectable in IR spectra. Possibly they are indistinguishable spectroscopically from terminal silanols, as suggested by Trombetta et al.^{92,190–192}

As cited above, the adsorption of hindered nitriles reveals the presence of Lewis sites at the external surface of H-FER, H-MFI, and H-MOR,^{190–193} after previous outgassing at 673–773 K. Recently, van Bokhoven et al. showed that, in these conditions, tricoordinated Al species can be detected by in situ XANES at the Al–K-edge on H-MOR and H-BEA.¹⁹⁹ These authors propose these species is at framework position, but they could not determine if these sites are internal or external. According to Trombetta et al.^{92,190–192} the external surface of protonic zeolites is similar to that of silica alumina. This is reasonable because at the external surface of zeolites the “rigidity” of the crystalline structure is relaxed and the cavity effects, obviously, do not exist.

A largely used strategy to avoid unwanted unselective reactivity at the external surface is to limit it by producing large well-crystallized zeolite crystals.¹⁶³ The “selectivation”^{162,200} of the zeolite behavior may also be obtained by inertization of the external surface through silanization with alkoxy silanes, which can destroy the external Lewis sites,^{201,202} precoking of the external surface and/or most of the active sites, poisoning of the external acid sites by hindered bases (such as 2,6-di-*tert*-butylpyridine),²⁰³ dealumination causing changes in the pore structure, etc.

6.2.3.1.3. Extra-framework Material in Protonic Zeolites. Zeolite catalysts are actually applied frequently after treatments tending to increase their stability and also, in some cases, to further enhance surface acidity and shape selectivity effects. These treatments, such as steam dealumination, can cause the decrease of the framework Al content and the release from the framework of aluminum-containing species that contribute to stabilizing the framework, but can also contain additional catalytically active acid sites. These particles can also narrow the size of the zeolite channels or their mouths, so improving the shape selectivity effects. Extra-framework material (EF) is composed by very small particles mostly containing Al cations complexed by OH groups but sometimes also involving silicate species, likely interacting with the framework walls, located in the cavities or on the external surface. It can arise from the preparation or the activation procedure or by addition of components by impregnation or ion exchange. The presence of EF gives rise to the presence of strong additional bands in the IR OH stretching spectrum. In general, IR bands above 3750 cm⁻¹, and in the region of 3730–3650 cm⁻¹ in protonic zeolites, are attributed to OH groups on EF materials. In Figure 15 the experiments of low-temperature CO adsorption on two H-MFI zeolites are compared. Sample A contains traces of EF material, whereas sample B contains much more. The bands at 3780 and 3670 cm⁻¹, much more evident in the case of sample B, are in fact due to EF. The band at 3670 cm⁻¹ shifts down to 3470 cm⁻¹ upon CO adsorption. The shift $\Delta\nu \sim 200$ cm⁻¹ is lower than that of bridging OH groups ($\Delta\nu > 300$ cm⁻¹) but still indicates quite strong Brønsted acidity for the OH groups of EF.

Similarly, the detection of octahedral Al ions in ²⁷Al NMR techniques is evidence of EF. Several authors also attribute Lewis acidity of zeolites to extra-framework species, neglecting the evidence of their presence also at the external surface of the framework.

Hydrothermal treatment producing EF species has been reported to affect positively the isobutylene selectivity upon *n*-butylene conversion over H-FER²⁰⁴ and the activity of H-MOR for light alkane conversion.²⁰⁵ Some authors believe that EF is released at the external surface of zeolites.²⁰⁶ The use of hindered nitriles, however, showed that the EF material produced by thermal treatment in H-MOR is in the interior of the side pockets.²⁰⁷ Similarly, in a sample of H-MFI EF material was found to be located in the interior of the channels.²⁰⁸ Tricoordinated Al ions, as detected by XANES on heat-treated H-MOR and H-BEA,¹⁹⁹ could be precursors for EF formation.

6.2.3.1.4. Adsorption and Protonation of Molecules in the Zeolite Cavities and the Confinement Effect. Strongly basic probe molecules can be easily protonated in the cavities of the zeolites (Figure 13 for pyridine on H-MOR). Ammonia is strongly adsorbed in the form of ammonium ions at low coverages, whereas it gives rise to the “dimeric” N₂H₇⁺ cation, formed by hydrogen bonding between an ammonia molecule and the ammonium cation, at higher coverages, on H-ZSM-5.^{79,209,210} The ammonium ions may be stabilized by H-bonding interactions with oxygen atoms in the cavity.

In the case of the adsorption of water, instead, the first H₂O molecule is likely only H-bonded on the Brønsted sites of protonic zeolites.²¹¹ It is still not fully clear whether neutral or ionic dimeric and polymeric water species are formed at higher coverages²¹² or whether both species coexist.

According to theoretical studies,²¹³ highly reactive hydrocarbons, such as olefins, are protonated by the Brønsted sites of the zeolites, with the formation of carbenium ions as transition states and alkoxide species as stable intermediates. Experimental studies confirm this: it has been shown, in fact, that olefins produce, at low temperature (150–250 K), H-bonded species²¹⁴ on bridging OH groups. Protonation of isobutylene is observed at slightly higher temperatures, giving rise to detectable *tert*-butoxy groups,²¹⁴ which are also formed by adsorption followed by skeletal isomerization of *n*-butylenes at 0 °C. These species later initiate cationic polymerization to give polyisobutylene. In the copresence of aromatics, a concerted mechanism is foreseen by theory, with rapid alkylation of the aromatic.²¹⁵ Experimental^{80,216} as well as theoretical data⁷⁹ show that besides the interactions of the functional groups of the reactive molecules with the zeolite Brønsted sites, the van der Waals interactions of other unreactive groups of atoms with the zeolite cavity walls may be very relevant and stabilize the intermediates. These interactions may vary significantly as a function of the type of the zeolite and the dimension and shape of the cavities as well as the Al and proton content and the presence of EF. Also, they depend on the size and shape of the molecule. These “confinement effects” give the cavities of the single-zeolite structures unique solvation and reactivity environments and play a relevant role in the catalysis by zeolites. They also explain the discrepancies among the acid strengths measured using different probes and different techniques.

6.2.3.1.5. Some Particular Protonic Zeolites Applied in Industry. Ferrierite (H-FER). The framework of the FER zeolite (Figure 19) gives rise to two kinds of intersecting channels, one of which is formed by 10-membered silicate rings along the [001] direction, with diameters 4.2 × 5.4 Å, the other being formed by 8-membered rings along the [010] with diameters 3.5 × 4.8 Å. It is consequently denoted a medium pore zeolite. It frequently has quite high Al content (Si/Al ratio = 8) but may be also prepared in a very highly

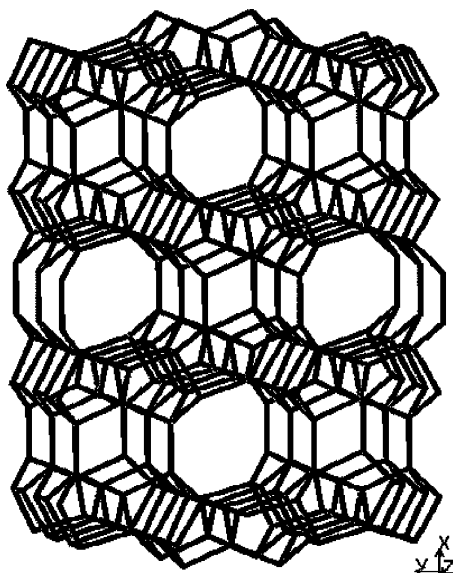


Figure 19. FER (ferrierite) zeolite structure. (Reprinted with permission from ref 160.)

siliceous form. It presents an unsplit OH stretching band near 3595 cm^{-1} , with slight shifts depending on the Al content and recording temperature (Figures 14 and 16).

The adsorption of hindered nitriles allowed independent investigation of the OH groups located in the two channels of H-FER. In fact, the monobranched probe isobutyronitrile enters only the larger channels of H-FER, where the OH groups vibrate at 3591 cm^{-1} , leaving free the OH groups of the smaller channels, which absorb at 3598 cm^{-1} ,¹⁹³ in good agreement with the neutron scattering data of Martucci et al.²¹⁷ The ^1H NMR peak for bridging OH groups of H-FER has been observed unsplit at 4.4 nm .²¹⁸

H-FER zeolite was the focus of much interest in the 1990s for its high catalytic activity and selectivity for the *n*-butylene skeletal isomerization to isobutylene,²¹⁹ a potentially very relevant process in view of gasoline reformulation.²²⁰ A commercial process, IsomPlus (Lyondell–CDTech) is available and worked industrially at least for some years.²²¹ The reaction occurs near $350\text{ }^\circ\text{C}$ near ambient pressure. The selectivity to isobutylene grows with time on stream when coking also proceeds and *n*-butylene conversion decreases progressively. Quite frequent catalyst regeneration is consequently needed, using swing reactors.²²⁰

Still, controversy exists on the reaction mechanism (monomolecular versus bimolecular, with cracking of an octene cation) and on a possible role of carbonaceous materials as “active site” in the reaction.^{204,222,223} One of the features of the catalyst allowing high selectivity to isobutylene is the impossible (or very highly hindered) diffusion of aromatics in the small pores of ferrierite. Aromatics are among the main products over other larger pore zeolites such as H-ZSM5.⁹² It is evident that a product shape selectivity effect occurs. Theoretical data²²⁴ also suggested that a transition state shape selectivity effect may occur, just limiting the possibility of formation of C8 adducts that can crack unselectively, giving rise to $\text{C}_3 + \text{C}_5$ hydrocarbons. This may be even more effective in the case of partially coked materials, so allowing improved shape selectivity.

On the other hand, it has been shown that monobranched compounds may diffuse much better in the larger channels of FER structure than in the smaller ones, where access of branched compounds is strongly hindered. Compounds with

the *tert*-butyl group appear to be unallowed to enter both channels, at least at room temperature. This suggests that the isomerization reaction should not involve as stable intermediates compounds with the *tert*-butyl group. On the other hand, due to the small size of the pores of H-FER, it seems still difficult to understand how coke and reactants can coexist in the same cavity. It is possible that coking mostly occurs at the external surface and in the larger channels, along the [001] direction, whereas the more selective reaction should occur on the smaller channels along [010].

ZSM5 (H-MFI). The structure of MFI zeolite (Figure 20) contains two types of intersecting channels, both formed by

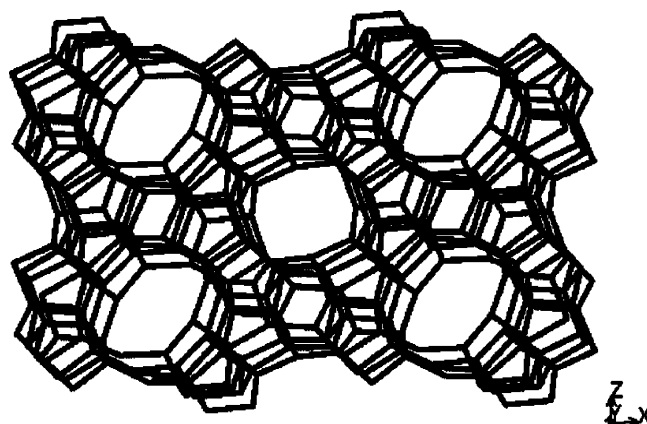


Figure 20. MFI zeolite structure. (Reprinted with permission from ref 160.)

10-membered silicate rings, characterizing this material as a medium-pore zeolite. One channel type is straight and has a nearly circular opening ($5.3 \times 5.6\text{ \AA}$) along [010], whereas the other one is sinusoidal and has an elliptical opening ($5.1 \times 5.5\text{ \AA}$), along [100]. The Si/Al ratio may vary from infinity (silicalite-1) to near 10. The bridging hydroxy groups show a single band that shifts from 3595 to 3620 cm^{-1} by varying the Si/Al ratio and measurement temperature (see Figures 1, 14, 15, and 17). Although the channels of H-MFI and framework oxygen positions are very similar each other, and never is the νOH band found to be split, the benzene-driven access of pivalonitrile²²⁵ suggests that the OH groups in the channel intersection absorb at a slightly higher frequency ($3610\text{--}3620\text{ cm}^{-1}$) than those located in the channels $3610\text{--}3590\text{ cm}^{-1}$. ^1H NMR studies (Figure 18) allowed peaks, usually in the range from 4.1 to 4.3 ppm, to be assigned to the acidic protons of H-MFI.^{172,226,227} Interestingly, some studies found the peak split into two^{228,229} or even four components with the more intense peak at 3.8 ppm.²³⁰ The inelastic neutron scattering study of Jobic et al.²¹¹ showed that the deformation mode $\gamma\text{-OH}$ is split for H-MFI, suggesting that at least two very different OH groups actually exist.

The channels of the MFI structure allow the diffusion of benzene and monosubstituted benzenes as well as of *p*-xylene. The diffusion of ortho and meta disubstituted benzenes is far more difficult.¹⁹⁴ This allows shape selectivity in favor of mono- or para-disubstituted benzenes. An example of this behavior is the application of “selectivated H-ZSM5” in the selective toluene disproportionation (STDP) process,^{162,200} allowing the highly selective production of benzene and *p*-xylene from toluene. With a zeolite treated with silicon-containing compounds at the external surface (to limit reaction out of the channels), the pore mouths of

which may also be narrowed by silication or precoking, working in the vapor phase at 420–480 °C, 20–40 bar, WHSV 3–5 h⁻¹ small toluene conversion per pass, the selectivity *p*-xylenes/total xylenes may be >80%, with cycle lengths of more than 1 year.²³¹ H-MFI catalysts find a number of other applications in the field of gas-phase aromatics chemistry. They are the catalysts of the Mobil-Badger process of benzene alkylation by ethylene for the ethylbenzene synthesis, performed in the vapor phase at 390–450 °C.^{232,233} Interestingly, H-MFI is not a good catalyst of the benzene alkylation by propene for the cumene synthesis, producing an excess of *n*-propylbenzene. This has been attributed to the too high temperature needed to overcome the aromatics diffusion constraints in the 10-membered channels.²³⁴ These constraints limit activity of H-MFI in liquid phase aromatics alkylations.

The channel size of MFI also does not allow the easy diffusion, if at all, of molecules containing the *tert*-butyl group.²²⁵ This is probably the reason for the almost total inactivity of H-MFI in isobutane/butylene alkylation,³³ the products and intermediate species of which contain the *tert*-butyl group. For the same reason H-ZSM5-based catalysts with SiO₂/Al₂O₃ ratios of at least 20, containing ca. 40 wt % of a binder (Al₂O₃ or SiO₂), have been developed to obtain olefin oligomers with relatively high linearity and low branching that can be applied for use as diesel blending fuels [conversion of olefins to diesel (COD) from Lurgi-Süd Chemie²³⁵].

A product shape selectivity effect is also at the basis of the development of H-MFI catalysts for the Mobil methanol to gasoline (MTG) and the Mobil olefin to gasoline/distillate (MOGD) processes,^{236,237} developed in the 1980s. The main products of both processes are hydrocarbon mixtures useful as gasoline components. In the case of the MOGD process, well-defined iso-olefinic products are obtained. Selectivation of a H-MFI-based catalyst by poisoning the external surface with 2,6-di-*tert*-butylpyridine allows the production, even from propene oligomerization, of nearly linear C₂₀₊ products, with a small amount of methyl branching.²⁰²

A reactant shape selectivity effect allows the use of H-MFI (usually containing also a hydrogenating metal) for the selective cracking of linear paraffins in the catalytic dewaxing of lube oils [such as the Mobil selective dewaxing process (MSDW)]. Linear paraffins enter and diffuse easily in the MFI cavities, whereas the entrance of branched isomers is hindered. Thus, conversion of linear compounds is favored with respect to those of branched isomers.²³⁸

An important recent application of H-ZSM-5 is as a component of fluid catalytic cracking catalysts based on REUSY zeolites. H-ZSM-5 cracks selectively the C₅₊ olefins, resulting in a reduced gasoline olefinicity and increased gaseous olefins production.²³⁹

H-MFI zeolite can also be applied as a heterogeneous acid catalyst in the water phase.²⁴⁰ A process for cyclohexene hydration to cyclohexyl alcohol in water using highly siliceous H-ZSM-5 zeolite from Asahi Kasei operates successfully at ~120 °C.²⁴¹

Beta Zeolite (H-BEA). The framework of BEA zeolite (Figure 21) gives rise to two different channel types, both formed by 12-membered rings but with definitely different diameters, one (0.55 × 0.55 nm) in the medium pore range, the other (0.76 × 0.64 nm) in the large pore range. The Si/Al ratio is typically in the 10–30 range, although particular

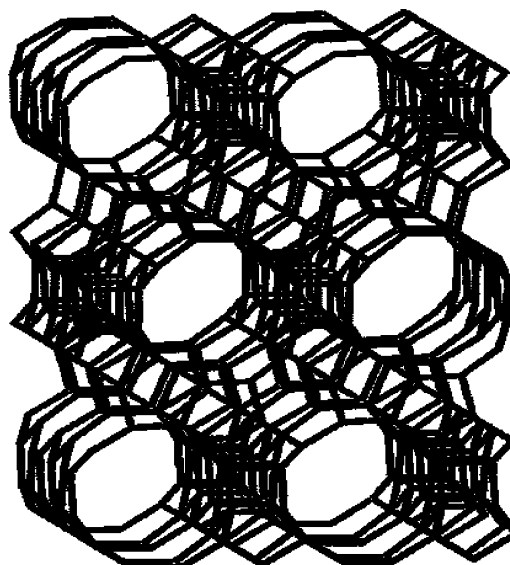


Figure 21. BEA (beta) zeolite structure. (Reprinted with permission from ref 160.)

preparations allow this ratio range to be expanded down to 5²⁴² or up to infinity.^{102,243}

The H-BEA structure is relatively fragile, and calcination or steaming above 400 °C causes progressive dealumination with deposition of extra-framework aluminum (EF-Al) inside the channels.^{244,245} Crystallographic faults are frequently observed in BEA zeolite, and a structural model was proposed by Jansen et al.²⁴⁶ to explain local defects creation by distorted layers connection. IR spectroscopy experimental data supporting the presence of these local defects have been reported in the literature.²⁴⁷ Actually, the structure of BEA is reported to be an intergrowth of two or three polymorph types.

In the case of H-BEA the band of bridging OH groups is a little split in at least two components (ν OH ~ 3608 cm⁻¹ and ~ 3620–3612 cm⁻¹).^{176,178} Kotrel et al.¹⁷⁶ observed that only the intensity of the low-frequency component correlates with the catalytic activity in *n*-hexane cracking for Na-poisoned H-BEAs. A more detailed analysis¹⁹³ arising from experiments of adsorption of the hindered *tert*-butyl-containing probe pivalonitrile (PN) suggests that the OHs located at the smaller channels (unaccessible to PN) are quite homogeneous (sharp band at 3609 cm⁻¹), whereas those in the larger channels (accessible to PN) are likely much more abundant and are definitely heterogeneous (three components at 3628, 3608, and 3590 cm⁻¹). Also, ¹H NMR studies reveal a significant heterogeneity of the bridging OH groups of H-BEA with four δ _H components at 3.28, 3.84, 4.42, and 5.21 ppm.²³⁰

The size of the larger channels of H-BEA allows quite easily the diffusion of aromatics as well as of molecules containing the *tert*-butyl group. The size of the cavity may perhaps be reduced by dealumination, producing EF material. This is considered to be beneficial, for example, for the selective acylation of 2-methoxynaphthalene over H-BEA.²⁴⁸ An IR study on H-BEA¹⁷⁸ suggests that at least two different types of extra-framework structures exist in unleached H-BEA zeolite. One of them is characterized by the presence of H-bonded OH groups responsible for a broad absorption in the 3700–3200 cm⁻¹ region and for strong Lewis acid sites. These features decrease by calcination, disappear by acid leaching, and are related to structures that are internal

to the zeolite pores. They are identified as Al hydroxo-ions interacting with the internal wall of the zeolite cavities. These species, presumably highly dispersed into the channels, probably do not hinder so much the channels. With heating they likely dehydrate, coalescing into bigger particles (those associated with the OH stretching band at 3785 cm^{-1}) that give rise to the improved shape selectivity effect observed in the acylation of 2-methoxynaphthalene.²⁴⁸ IR data provide also evidence for the presence of defects in the relatively perfect BEA sample obtained by double acid leaching. In fact, this sample shows a small fraction of terminal silanols that are inaccessible both to pyridine and to pivalonitrile. However, the frequency of these residual sites is 3744 cm^{-1} , that is, nearly intermediate between that of the sites considered to be external (3747 cm^{-1}) and those considered to be internal (3736 cm^{-1}). This suggests that some big holes exist, which are, however, in contact with the external atmosphere by very small channels.

H-BEA zeolite finds industrial application in the Polimeri Europa-ENI²⁴⁹ and in the UOP Q-Max²⁵⁰ processes for the liquid-phase synthesis of cumene by alkylation of benzene with propene (see Table 4). In both cases H-BEA-based catalysts catalyze selectively both the alkylation reaction, in multi-fixed-bed catalytic reactors, with a large excess of benzene, and also the transalkylation reaction, by which benzene reacts with polyisobutylbenzene to produce additional cumene in a separate fixed bed reactor. The ENI catalyst, denoted PBE-1, is composed of a mixture of very small and uniform beta-zeolite particles with a binder, showing both zeolite microporosity and extrazeolite mesoporosity. Experimental results reported by the ENI group²⁵¹ show that H-BEA, working with 3.8 MPa total pressure, at $150\text{ }^{\circ}\text{C}$ and WHSV $1\text{--}5\text{ h}^{-1}$, gives rise to better selectivity to cumene than other medium- or large-pore zeolites such as MOR, ERB-1 (H-MWW), USY, and MTW, with lower coproduction of propylene oligomers and n-propylbenzene. A computational study²⁵¹ shows that cumene diffusion is much better on large- than on medium-pore zeolites (where the isopropyl group causes some hindering), whereas the diffusion of diisopropylbenzenes is more hindered in beta zeolite than in other large-pore zeolites, showing that in this case product shape selectivity occurs. The catalyst can be fully regenerated by coke burning, needed every 2–3 years, and should last for at least three cycles with proper care.²⁴⁹ According to the patent literature it seems that also the Lummus/UOP EBOne liquid-phase ethylbenzene synthesis process works with a H-BEA-based catalyst.²⁵²

MCM-22 (H-MWW). MCM-22, isotypic with the so-called ERB-1 zeolite, possesses a unique crystal structure (Figure 22), denoted MWW, containing two independent non-intersecting pore systems.²⁵³ One of the channel systems contains two-dimensional sinusoidal 10-membered silicate ring channels (diameters = $4.1 \times 5.1\text{ \AA}$), whereas the other system consists of large supercages (12-membered) with dimensions of $7.1 \times 7.1 \times 18.1\text{ \AA}$. The supercages stack one above another through double-prismatic six-membered rings and are accessed by slightly distorted elliptical 10-membered connecting channels ($4.0 \times 5.5\text{ \AA}$). In general, the synthesized MCM-22 zeolites crystallized as very thin plates with large external surface area,²⁵⁴ on which 12-membered hemisupercage pockets ($7.0 \times 7.1 \times 7.1\text{ \AA}$) are exposed.

In a recent DFT study²⁵⁵ the most favorable sites for framework Al substitutions have been calculated, which

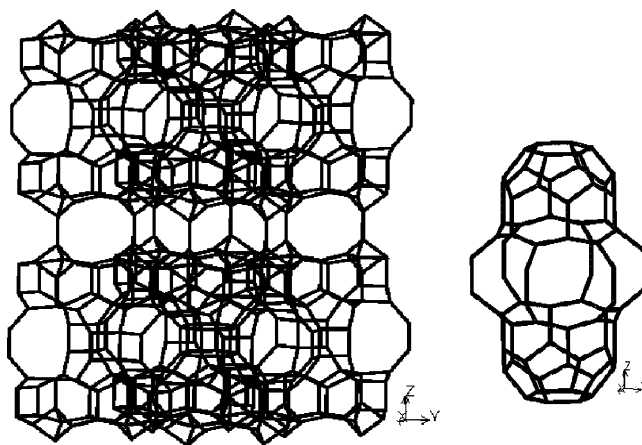


Figure 22. MWW (MCM-22) zeolite structure. (Reprinted with permission from ref 160.)

indicated that two acid sites should be located on the 12-membered ring in the supercages and a third one should be in the 10-membered ring sinusoidal channels.

Four hydroxyl bands were detected in the IR spectrum of pure MCM-22 samples. The large band centered at 3626 cm^{-1} was resolved into two single components at 3628 and 3618 cm^{-1} , which were assigned to Si(OH)Al groups located in supercages and in sinusoidal channels. The shoulder at 3585 cm^{-1} was attributed to Si(OH)Al groups positioned in a hexagonal prism between two supercages.^{256–258} The fourth component (3670 cm^{-1}) was ascribed to the AlOH groups linked to extra-framework Al species. The exfoliation of MCM-22 zeolite to produce the so-called ITQ-2 zeolite results in the strong decrease or the disappearance of the band of bridging OH groups, suggesting that at the external surface and in the hemisupercage pockets only terminal silanols exist, although relevant acidity is retained.^{195–197}

Mobil's proprietary MCM-22 zeolite is the catalyst of the EBMax liquid-phase ethylbenzene process, performed at $160\text{--}220\text{ }^{\circ}\text{C}$. In the EBMax process, benzene is fed to the bottom of the liquid-filled multibed reactor. Ethylene is cofed with benzene and also between the catalyst beds to quench the reaction heat. Typical benzene to ethylene feed ratios are in the range of 3–5. MCM-22 is also the component of the catalyst of the liquid-phase Mobil-Raytheon process for cumene synthesis.^{231–233} This catalyst competes with those based on H-BEA (ENI and UOP) and H-MOR (Dow) (see Table 4). According to Corma et al.²⁵⁹ MCM-22 may perform slightly better than H-BEA at higher temperatures ($220\text{ }^{\circ}\text{C}$), whereas H-BEA may perform better at lower temperatures ($180\text{ }^{\circ}\text{C}$). In both cases, however, the Si/Al ratio as well as the morphological properties of the zeolite and of the binder must be finely tuned to optimize the performances.²⁵⁰

The MCM-22 zeolite catalyst is more monoalkylate-selective than most large-pore zeolites and is very stable. Cycle lengths in excess of 3 years have been achieved.²³² The excellent selectivity to monoalkylated products is attributed to the confinement effect within the 12-membered ring pore system where the reaction occurs and the easy desorption of alkylbenzenes from the pockets.²³³ Mechanistic studies suggest that the reaction should occur in the hemisupercages exposed at the surface. If this theory is true, MCM-22 should be a zeolite working mostly at the external surface, where, however, the zeolite structure is in some way retained. It is unlikely that the active sites are, in this case,

the bridging OH groups, seemingly not existing as such at the open surface.^{195–197} However, spectroscopic data suggest that benzene could enter the supercages and react there with olefins.²⁵⁷ This point should be the subject of further investigation. The particularly high stability of MCM-22 is attributed to the unique feature of the existence of a buried T (Si or Al) atom not accessible to a channel wall.

Mordenite (H-MOR). The orthorhombic mordenite structure (Figure 23) is characterized by nearly straight channels

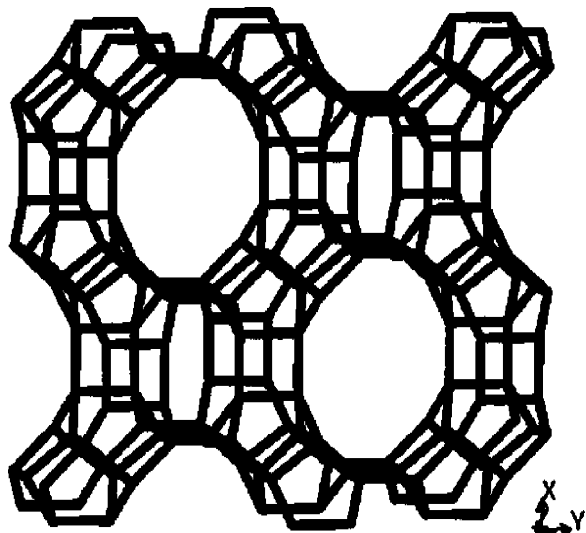


Figure 23. MOR (mordenite) zeolite structure. (Reprinted with permission from ref 160.)

running along the [001] crystallographic direction, which are accessible through 12-membered silicon–oxygen rings $6.5 \times 7.0 \text{ \AA}$ wide. Additionally, 8-ring “side pockets” exist in the [010] direction, the opening of which is $3.4 \times 4.8 \text{ \AA}$. The side pockets connect the main channels to a distorted 8-ring “compressed” channel also running parallel to the [001] direction, but having an elliptical small opening, $5.7 \times 2.6 \text{ \AA}$ wide.

IR spectra show, for typical H-MOR with a Si/Al ratio of 10, a strong slightly asymmetric band centered at 3605 cm^{-1} (Figures 14 and 17). Several recent studies have been devoted to the characterization and to localization of the “framework” protonic sites in H-MOR by IR spectroscopy.^{207,260–264} Several authors reported that the OH groups in the so-called side pockets and smaller channels are associated with a band located at distinctly lower frequencies (near 3580 cm^{-1}) with respect to those located in the main channels. Distinct Brønsted sites in H-MOR have also been identified through NMR techniques.^{265,266}

Studies on the adsorption of hindered nitriles^{193,207,264,267} allowed three families of bridging OH groups to be distinguished in H-MOR. As shown in Figure 24, propionitrile (Figure 24b) (as acetonitrile) shifts the entire OH band found at 3605 cm^{-1} in the activated sample (Figure 24a). Isobutyronitrile (i.e., 2-methylpropionitrile) leaves unperturbed a weak band at 3588 cm^{-1} . Pivalonitrile (i.e., 2,2-dimethylpropionitrile) interacts with a few OH groups and leaves a strong band at 3609 cm^{-1} . 2,2-Diphenylpropionitrile (not shown here) does not perturb¹⁹³ at all the bridging OH groups. In parallel, the ABC type broad absorptions associated with strong H-bonding of the nitriles with the bridging OH groups grow. Thus, the hydroxy groups responsible for the band at 3588 cm^{-1} are available to interact with linear nitriles, but not to branched and aromatic ones: they are

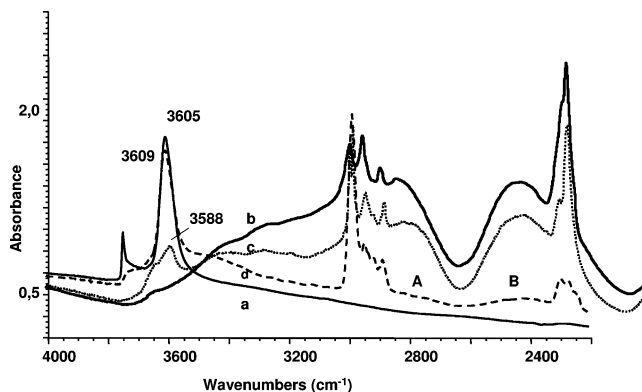


Figure 24. IR spectra of a H-MOR zeolite (Si/Al a.r. 10) after outgassing at $450 \text{ }^\circ\text{C}$ (a) and after contact at room temperature with propionitrile vapor (b), isobutyronitrile vapor (c), and pivalonitrile vapor (d).

likely located inside the side pockets. Others interact with linear and monobranched nitrile (isobutyronitrile), but not with doubly branched pivalonitrile, and with aromatic nitriles, too: they, absorbing at 3609 cm^{-1} , are likely at the intersection between side pockets and main channels. The small dimension of the main channel of mordenite and the rigidity of the pivalonitrile²⁰⁷ and benzonitrile²⁶⁷ molecules do not allow the rotation and the bending of the probes, which, consequently, cannot probe such an intersection.²⁰⁷ A third family interacts with all nitriles investigated except 2,2-diphenylpropionitrile.¹⁹³ They absorb at 3605 cm^{-1} and are thought to stand near the center of the main channels. 2,2-Diphenylpropionitrile is so large a molecule that it cannot enter even the main channels of mordenite. Consequently, this molecule probes the external surface only of H-MOR, where no bridging OH groups are found; however, terminal silanols are mostly located there, together with Lewis sites. Three families of bridging OH groups have also been found, later, by Marie et al.²⁶⁸

According to the structural data of Alberti,²⁶⁹ the access to some of the oxygen sites (in particular O4 and O8, i.e., pointing toward the chain of four-membered rings) should be fully hindered to probe molecules. This observation of Alberti means that, if these positions are occupied by free OH groups, the corresponding IR band should not be perturbed by probes. Nevertheless, IR studies show that acetonitrile, propionitrile, and CO interact with all free OH groups of H-MOR. This allowed Bevilacqua et al.^{207,264} to conclude that such positions could not carry hydroxy groups. An alternative possibility we now propose is that OH groups located in these positions are H-bonded, being responsible for the broad OH stretching modes with the maximum near 3300 cm^{-1} in Figure 17.

A study with dealuminated H-MOR (Si/Al ar 45) showed that the band of residual OH groups observed at 3604 cm^{-1} is fully perturbed by pivalonitrile and that thermal dealumination produces EF species with OH groups inaccessible also to isobutyronitrile.²⁶⁴ This suggests that dealumination mostly occurs in the side pockets and in the compressed channels, leaving the most exposed OH groups of the main channels free for catalysis. However, extensive dealumination may make the side pockets accessible to large probes such as alkylpyridines.²⁷⁰

The adsorption of different probes shows that monosubstituted aromatic compounds and compounds having the *tert*-butyl group diffuse in the main channels, but are not allowed to enter the side pockets. Even the access of *n*-hexane in the

side pockets is hindered.²⁶⁴ The entrance of ortho disubstituted benzenes may be hindered also in the main channels.²⁶⁷ Pyridine is protonated in the main channels²⁶⁴ (Figure 13). Small amounts of quite strong Lewis sites are mostly if not entirely located at the external surface.¹⁹³ These data definitely suggest that acid catalysis occurs predominantly in the main channels, although the location of Na ions and EF material in the side pockets may stabilize the structure and influence in some way the catalytic phenomenon.

Dealuminated mordenite is the basic structure of commercial catalysts for C4–C6 paraffin skeletal isomerization,^{271–273} based on alumina-bound Pt-H-MOR with SiO₂/Al₂O₃ ~ 15–17. Dealumination to a framework/extra-framework Al ratio of ~3 improves the catalytic activity.²⁷⁴ The catalyst works near 250 °C, so at a definitely higher temperature than those based on chlorided alumina, when the thermodynamics is less favorable, but is more stable and more environmentally friendly. This catalyst may be applied, for example, with the IPSORB process of IFP.²⁷⁵ This agrees with the quite easy diffusion of branched molecules in the main channels.

As said, also monosubstituted benzene diffuses easily in the main channels of H-MOR, whereas ortho disubstituted benzenes are hindered from diffusion.²⁶⁷ In agreement with this, H-MOR also catalyzes selective conversions of aromatics. Dealuminated H-MOR is the catalyst of the Dow-Kellogg cumene synthesis process (Table 4²⁵⁰). Noble metal containing H-MOR is also applied for the disproportionation of toluene to benzene + an equilibrium mixture of xylenes, generally at 20–40 bar and 380–500 °C, with excess hydrogen (H₂/hydrocarbon 1–6) and WHSV 1–6 h⁻¹.²³¹

Zeolite Omega (H-MAZ). Zeolite omega, a large-pore zeolite with a silica–alumina ratio in the range of 4–10, is the synthetic isotype of the mineral mazzite²⁷⁶ (topological code MAZ). In its unit cell (Figure 25), 36 tetrahedral atoms

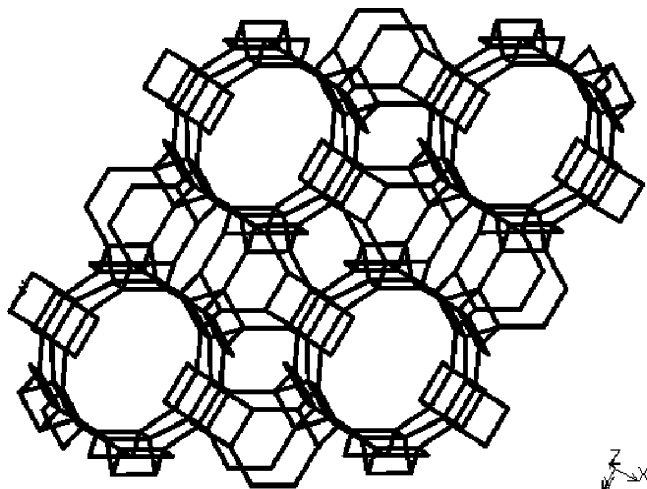


Figure 25. MAZ (mazzite, omega) zeolite structure. (Reprinted with permission from ref 160.)

bridged by oxygen atoms form gmelinite-type cages and 12-membered cylindrical channels along the [001] direction with 7.4 Å diameters. In addition to its large-pore system, secondary mesoporous structure could be created by mild dealumination,²⁷⁷ which may facilitate the transport of reactant and reduce the deposition of coke. The IR spectra show a complex band due to bridging OH stretching modes: according to McQueen et al.²⁷⁸ two components are observed at 3615 and 3600 cm⁻¹ in the case of a partially

dealuminated mazzite sample, whereas according to Guisnet et al.²⁷⁹ up to five components can be distinguished in differently dealuminated samples. Shigeishi et al.²⁸⁰ found two peaks at 3626 and 3606 cm⁻¹ assigned to structural hydroxy groups. According to these authors the peak at 3626 cm⁻¹ would shift down to 3247 cm⁻¹, upon low-temperature CO adsorption, with a shift of 379 cm⁻¹, which would indicate an exceptionally strong acidity of these OH groups.

Zeolite omega is apparently the basic structure of modern zeolitic C4–C6 paraffin skeletal isomerization catalysts cited under development by Süd Chemie as HYSOPAR catalysts, reported to be characterized by their outstanding tolerance of feedstock poisons such as sulfur (even more than 100 ppm) and water with very high catalyst lives.^{272,273} The catalyst is alumina-bound Pt-H-MAZ with Si/Al ~ 16, working at 250 °C with WHSV 1.5 h⁻¹ and a H₂/hydrocarbon ratio of 4. Pt and hydrogen have the effect of reducing coking and hydrodesulfurizing S-containing compounds. It may be applied in the so-called CKS ISOM process licensed by Kellogg, Brown and Root. This catalyst is reported to be more effective than Pt-H-MOR commercial catalysts and more stable than the catalysts based on chlorided aluminas and sulfated zirconia.^{272,273}

Faujasite (H-FAU: H-Y, H-USY, RE-Y). The faujasite structure (Figure 26) is formed by wide supercages (13 Å

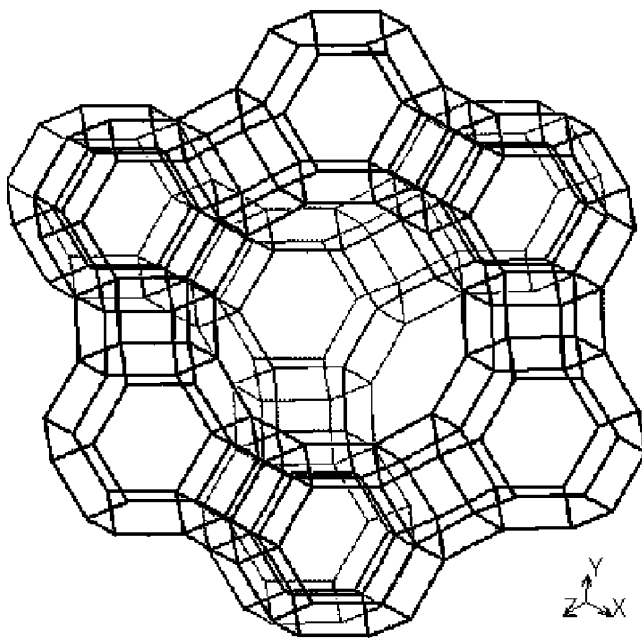


Figure 26. FAU (faujasite) zeolite structure. (Reprinted with permission from ref 160.)

diameter) accessed through 12-membered silicate rings with 7.4 Å diameter, much smaller sodalite cages accessed through 6-membered silicate rings, and hexagonal prisms connecting the sodalite cages. All of the catalytic chemistry of faujasites is supposed to occur in the supercages. The aluminum content in faujasite is generally very high, the theoretical Si/Al ratio being as low as 1. Faujasites with Si/Al ratio near 1 are usually denoted X-zeolites. Faujasites with Si/Al ratio higher than 2 are usually denoted Y-zeolites and are more stable in the protonic form, denoted H-FAU or H-Y. The multiplicity of the hydroxy groups can be very clearly observed, two well-defined although weak bands appearing for bridging OH groups (Figure 14). The high-frequency HF band (3626 cm⁻¹) has been assigned to bridging OH groups located in

the supercage and accessible to most molecules, whereas the low-frequency LF band (3562 cm^{-1}) has been assigned to OH groups located near the middle of the six bond rings connecting the sodalite cages,^{281,282} being possibly weakly H-bonded through the cavity.¹⁶⁷ The LF OH groups can H-bond with molecules located in the supercages, but are possibly unable, for steric reasons, to protonate them. In a recent study, Romero Sarria et al. observed, by the use of trimethylamine as a probe, a third component that is not perturbed at all by the probe, at 3501 cm^{-1} , assigned to OH groups in the hexagonal prisms.^{283,284} The ^1H MAS NMR spectrum (Figure 18) shows a peak at 3.9 ppm that is perturbed by deuteroacetonitrile and is assigned to the hydroxy groups in the supercages. Another peak at 4.8 ppm is not accessible to the probe and is consequently assigned to hydroxy groups in the sodalite cages.

H-Y (H-FAU) zeolites for their practical application at high temperature in reaction or regeneration must be stabilized by steam dealumination, generally performed at $T > 773$ on the $\text{NH}_4\text{-Y}$ precursor. The resulting materials are hydrothermally more stable (the so-called ultrastable Y zeolite, USY). Their structure and acidic properties are greatly influenced by the dealumination process, which generates extra-framework alumina possessing Lewis acidity and inducing enhanced Brønsted acidity within the material. Cairon et al.²⁸⁵ have demonstrated that this extra-framework material possesses a non-negligible Brønsted acidity of its own. Although still not fully understood and a point of much debate in the literature, the generation of this extra-framework material has been shown to greatly modify the catalytic properties of the zeolite. The spectra of USY samples may contain, besides the OH stretchings of H-Y, three less intense bands at 3673, 3603, and 3525 cm^{-1} . These last three bands were attributed to hydroxyl groups present on extra-framework material (EF), high-frequency OH groups interacting with this extra-framework material (HF'), and LF groups involved in similar interaction (LF').²⁸⁶ Niwa et al.²⁸⁷ attributed to a new OH absorbing at 3595 cm^{-1} the enhanced acidity of USY treated with ethylenediaminetetracetic acid. According to Navarro et al.,²⁸⁸ steam-treated Y zeolites with EF aluminum removed by any known method have access to the CO probe molecule and also to LF OH groups. After these treatments HF OH groups with exceptionally strong acidity ($\Delta\nu\text{OH}$ with CO 443 cm^{-1}) should be formed.²⁸⁸

According to ^{27}Al 3Q NMR and ^{29}Si MAS NMR studies, van Bokhoven et al.²⁸⁹ concluded that the extra-framework octahedral EF Al species causes a perturbation on framework tetrahedral Al ions. In agreement with this, DFT studies suggest that EF Al species would tend to coordinate to oxygen atoms near the framework Al atoms.²⁹⁰ In this way, an enhancement of the Brønsted acidity of the regular framework sites discussed above can be obtained. However, it seems that EF species possess their own Brønsted acidity, having been identified as silica-alumina debris where part of Al is in a flexible octahedral environment.^{291,292} According to Menezes et al.²⁹³ MQMAS NMR and IR experiments show that tetrahedral Al species are also formed by steaming in USY and give rise to Lewis acidity, which however, is not completely removed by leaching. Very recently, Xu et al. showed that the structure of zeolite Y may collapse and be restructured, but this may give rise to quite different materials.²⁹⁴

The main component of fluid catalytic cracking (FCC) catalysts today is rare-earth (RE) containing FAU zeolites

(RE-Y or RE-USY), such as La-H-Y zeolites. The IR spectra of REY samples^{193,295–297} (Figure 14) show two main bands centered at 3629 and 3532 cm^{-1} , with shoulders at 3610 and 3550 cm^{-1} . Additional bands are found weakly split at 3690, 3676 cm^{-1} and at 3744 cm^{-1} , the last very weak. In particular, the weak band at 3744 cm^{-1} is assigned to silanol groups likely located at the external surface of the zeolite, whereas the split band at 3690 and 3676 cm^{-1} is usually assigned to extra-framework material. The couple of bands at 3629 and 3532 cm^{-1} (with shoulders at 3610 and 3550 cm^{-1}) are typical of bridging Si–OH–Al Brønsted acidic sites of FAU zeolites, although the lower frequency component, being very sensitive to the nature of the rare earth cation, certainly involves an interaction with such cations. The HF band split at 3629 and 3610 cm^{-1} does not undergo substantial hindering, being strongly perturbed by basic probes,¹⁹³ and is consequently due to bridging OH groups exposed in the supercage of the faujasite structure. On the contrary, the LF band split at 3532 and 3550 cm^{-1} is likely due to OH groups located in the sodalite cage, in agreement with previous assignments, so being able to interact only weakly with the probe molecules located in the supercage.

FCC is an autothermic process whereby the strongly endothermic catalytic cracking step is coupled with the strongly exothermic coke-burning catalyst regeneration step. The catalyst continuously moves from the riser where the cracking reaction occurs at $\sim 540\text{ }^\circ\text{C}$, 2 bar, residence time $\sim 3\text{--}10\text{ s}$, to the regenerator, where the burning of coke gives rise to a gas rich in CO (so still useful for further heat generation by burning) and the temperature is enhanced again to $730\text{ }^\circ\text{C}$, 2 bar, residence time $\sim 15\text{ min}$.²⁹⁸ The catalyst must be very stable to high-temperature hydrothermal treatment to resist such a cyclic process.

Besides RE-Y and RE-USY, the most used FCC catalyst today, several other components are present,^{299–302} such as an alumina or silica-alumina matrix or binder, kaolin, and H-ZSM5-containing additives to improve performances and quality of the products. To obtain a deeper cracking of sulfur compounds upon the FCC process, further additives (e.g., ZnAl_2O_4) may be used.

USY is also a typical component or support of hydrocracking catalysts, to provide acidity. The catalyst contains a sulfur-resistant hydrogenation phase, such as Ni–W sulfide. The reaction is performed at $300\text{--}450\text{ }^\circ\text{C}$ under 50–200 atm of hydrogen. A heavy low-value feed is transformed into lighter fractions. Hydrodesulfurization, hydrodenitrogenation, hydrodearomatization, and hydrodealkylations occur. The wide dimension of the channels of faujasite allow quite heavy molecules to be cracked. Deactivation by coking occurs, but USY-based catalysts are less easily coked than those based on silica-alumina.³⁰³

USY containing Pt is probably the catalyst of the AlkyClean process proposed by Akzo Nobel/ABB Lummus^{33,304} for solid-catalyzed isobutane/butylene alkylation. The catalyst works at $40\text{--}90\text{ }^\circ\text{C}$ ³⁰⁵ and is rejuvenated in the liquid phase by hydrogen–isobutane mixture and regenerated at $250\text{ }^\circ\text{C}$ by hydrogen in the gas phase. Multiple reactors are used to allow for continuous alkylate production/catalyst rejuvenation cycles. Regeneration is performed intermittently. Also, the catalyst proposed by Lurgi and Süd Chemie (Lurgi Eurofuel), where reaction occurs at $50\text{--}100\text{ }^\circ\text{C}$, is likely based on acid faujasite.³³ Alternative regeneration procedures of USY-based

catalysts are under study, such as supercritical isobutane regeneration at 60 °C and 111 bar.³⁰⁶

6.2.3.1.6. New Developments in the Synthesis of Zeolite-like Materials. The synthesis of new zeolites and of zeolite-like materials is still the object of intensive investigation. Among the most interesting recent results, we can cite the synthesis of several zeolites with framework element substitution such as silicogermanate and silico-alumino-germanate zeolites, some of which have very large pores such as IM-12, with 14- and 12-membered rings,³⁰⁷ and ITQ-33, with 18- and 10-membered rings.³⁰⁸ Particularly interesting appears also to be the development of zeolite-derived delamination materials, such as ITQ-2³⁰⁹ and ITQ-6,³¹⁰ derived from MWW and FER zeolites, respectively. In particular, ITQ-2 has been reported to have an extremely large surface area (840 m²/g) with respect to typical zeolites (400–500 m²/g) and to carry very high density of surface acid sites, although mainly associated to terminal silanol groups.^{195–197} It has very promising properties as a support for hydrocracking and hydrogenation catalysts.³¹¹

6.2.3.2. Microporous and Mesoporous Silica-aluminas (SAs). The structural details of the oxides resulting from coprecipitation or co-gelling of Si and Al compounds are still largely unclear. Commercial materials are available with any composition starting from pure aluminas to pure silicas. The silica-rich materials are generally fully amorphous and are called “silica-aluminas”. They behave as strongly acidic materials and have been used for some decades (1930–1960) as catalysts for catalytic cracking processes and still find relevant industrial application.³¹²

After the work of Kresge et al.³¹³ at Mobil, and the possibly even previous work of researchers of Toyota,³¹⁴ mesoporous silicas and SAs containing large pores with sizes from a few to many nanometers, have been developed. Different materials, denoted with the abbreviations MCM-41, FSM-16, HMS, SBA, MSU, KIT-1, MSA, and ERS-8, with different mostly mesoporous pore structure, may be obtained by different preparation procedures. Although sometimes considered like very large pore zeolites, these materials are essentially amorphous SAs with nonstructural although sometimes ordered mesopores. The surface chemistry of these materials appears to be closely similar to that of amorphous microporous SAs. ²⁷Al MAS NMR studies provided evidence for tetrahedral coordination of Al in SAs, although variable amounts of octahedral Al species as well as pentacoordinated or distorted tetrahedral Al are also present.^{315,316} According to Omegna et al.^{291,292} two kinds of octahedrally coordinated Al species actually exist in SAs. Part of it in fact changes its coordination when the adsorption of bases such as ammonia occurs, converting into tetrahedral. This is possibly associated with surface aluminum species that, upon the effect of a base, generate a Brønsted acidic site by bridging of a silanol over Al cation.

The IR spectra of SAs always present a very sharp band near 3747 cm⁻¹ (Figures 12 and 27) certainly due to terminal silanols, spectroscopically very similar to those of pure silicas and of any silica-containing material. A tail toward lower frequencies is likely due (as on pure silica too) to H-bonded and geminal silanols. Several papers reported the complete absence of bands assignable to bridging OH groups^{190,285,317} despite the remarkable Brønsted acidity of SAs detected, for example, by protonation of ammonia, pyridine (Figure 13), and amines and also by the strong H-bonding with nitriles^{92,318,319} and CO⁹⁴ and by calorimetric measurements,³²⁰

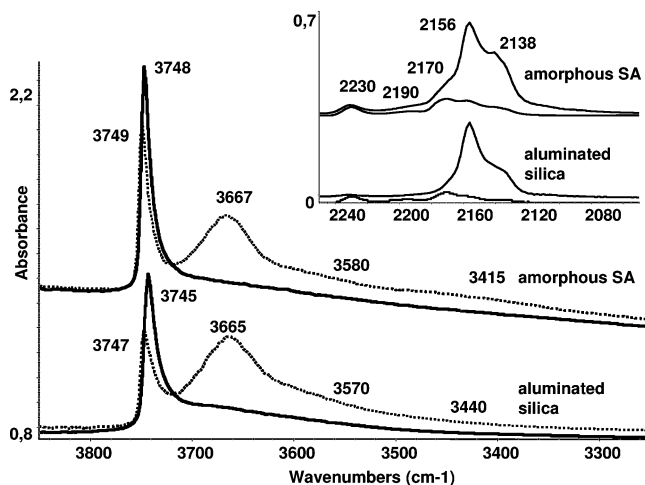


Figure 27. IR spectra of commercial silica-alumina from STREM (13% Al₂O₃) and of aluminated silica (6.5% Al₂O₃ impregnated via Al nitrate on silica gel)⁹⁴ activated by outgassing at 500 °C and cooled to 130 K (solid lines) and in contact with CO gas (10 Torr) at 130 K (point lines). (Inset) IR adsorbed CO in contact with CO gas (10 Torr) at 130 K and after outgassing at 110 K.

as well as deduced by its catalytic activity. In Figure 27, upper spectra, the IR spectra of a commercial SA sample (13% Al₂O₃) after activation and upon low-temperature adsorption of CO are reported. The adsorption of CO causes the shift of the maximum of the OH stretching band of silanol groups down to 3667 cm⁻¹ ($\Delta\nu \sim 80$ cm⁻¹) but with an additional component near 3580 cm⁻¹ ($\Delta\nu \sim 170$ cm⁻¹). To these features a ν CO band at 2156 cm⁻¹ corresponds. These features are also observed on silica and show that part of the surface is composed by pure SiO₂ and is very weakly acidic. However, an additional ν OH component is found near 3415 cm⁻¹, that, if it is due to the perturbation of part of free silanol groups absorbing at ~ 3747 cm⁻¹, corresponds to $\Delta\nu \sim 330$ cm⁻¹. This is evidence of a Brønsted acidity similar to or even stronger than that of the bridging OH groups of most zeolites. To this corresponds a ν CO band at 2170 cm⁻¹, actually similar to that found for zeolites (see Figure 15). Further ν CO bands at 2230 and 2190 cm⁻¹ are associated with CO interacting with very strong Lewis acidic Al³⁺ ions.⁹⁴

Some papers emphasized the additional presence of very small bands near 3600 cm⁻¹ in the spectra of mesoporous SAs,^{321–323} supposed to be due to bridging zeolite-type sites (see in the inset in Figure 12 a strongly expanded spectrum). Also, theoretical works at least up to the end of 1990s, modeled the active site for zeolites and SA in the same way, as Al–(OH)–Si bridging hydroxy groups. Accordingly, some authors stated that the active site for SA and protonic zeolites is the same (i.e., it is constituted by the bridging hydroxy groups bonded to a silicon and an aluminum atom).³²⁴

New results have been reported in very recent papers. Gora-Marek et al. re-proposed the existence of bridging OH groups on mesoporous SA.^{325,326} In contrast, Crépeau et al.³²⁷ did not find any other species except terminal silanols on their strongly Brønsted acidic SA samples. The same result has been reported by Luan and Fornier for SBA-15.³²⁸ Garrone et al.³²⁹ showed that small amounts of water adsorbed on mesoporous silica-alumina produce a weak band at 3611 cm⁻¹ together with another at 3697 cm⁻¹ (symmetric and asymmetric OH stretchings) and that adsorbed water adsorbs CO, showing significant protonic acidity. This,

however, reflects the acidity of water as such, which is enhanced by coordination on the Lewis sites of any acidic oxide, including pure alumina and titania.^{70,71} On the other hand, water vapor is reported to act as a poison for silica-alumina acid catalysts. Bevilacqua et al.⁹⁴ reinvestigated the surface hydroxy groups and the surface acidity of silica, silicalite, mesoporous and microporous SAs, silicated aluminas, aluminated silicas, and some zeolites by IR spectroscopy. CO, pyridine, and lutidine have been used as molecular basic probes. The data suggest that the bridging hydroxy group of Si–OH–Al is a fully stable structure only in the cavities of zeolites, where they produce the strong bands at 3630–3500 cm⁻¹ well correlated with the framework Al content. Extremely small bands near 3610 cm⁻¹ may be found on some SA samples only (mostly prepared in organic media) and on aluminated silicas after activation by outgassing, thus being not due to adsorbed water. These bands certainly correspond to very few OH groups, and impurities (such as bicarbonates) might contribute to their formation. It has been suggested that, in disordered mesoporous or microporous amorphous materials, zeolite-like pores may accidentally form and host zeolite-like bridging hydroxy groups.

Our conclusion,⁹⁴ in agreement with Crépeau et al.,³²⁷ is that acidity-enhanced terminal silanols represent the predominant Brønsted acid sites in nonzeolitic materials based on combinations of silica and alumina. Bridging sites, if they actually exist, and adsorbed water are not the components mainly responsible for the Brønsted acidity of SA. Brønsted acidity is, in fact, evident also for samples in whose spectrum the band near 3610 cm⁻¹ is not present at all, in full absence of water.

¹H MAS NMR studies^{327,330–333} and ²⁷Al MAS NMR techniques^{291,292,334} agree with the IR data showing that structurally different sites are active on SAs, with respect to zeolites. Proton NMR spectra of activated SAs in fact usually show a single peak at 1.7–1.8 ppm assigned to terminal silanols, with a broader component located at variable positions between 2.5 and 3.8 ppm, attributed to Al–OH or to more acididic OH groups. In contrast, the typical bridging OH of zeolites resonates sharply above 3.8 ppm (see above and Figure 18).

The lack of substantial formation of the bridging OH sites by reacting silica surfaces with Al ions or alumina surfaces with silicate ions, and also on mixed oxides such as SA, provides evidence for a substantial instability of the Si–OH–Al bridge, which is likely stabilized by the rigidity of the zeolite framework and/or by some interaction of the proton with the opposite wall of the cavity. On the other hand, it must also be mentioned that, on the surface of SA, very strong Lewis acid sites can be detected⁹⁴ (Figure 27). They are certainly due to highly uncoordinated Al ions and correspond to the strongest Lewis sites of transitional alumina or perhaps are even stronger, due to the induction effect of the covalent silica matrix. This makes SA also a very strong catalyst for Lewis acid-catalyzed reactions. Al ions near terminal silanols can cause a relevant strengthening of the acidity of terminal silanols. Different mechanisms for this behavior have been reported in the literature and are discussed in ref 66.

Amorphous microporous SA, used in the past for fixed and moving bed catalytic cracking starting from the 1940s,³³⁵ still finds a number of applications as acid catalysts, for example, the dehydrochlorination of halided hydrocar-

bons.^{42,336} Also, SAs are used as supports of sulfide catalysts for hydrotreatings^{303,337} and of catalysts for ring opening of polycyclic compounds, useful for the improvement of the technical and environmental quality of diesel fuels.³³⁸

Several recent studies have appeared concerning the possible industrial application of mesoporous SAs and the comparison with microporous SA and zeolite as catalysts for several reactions of industrial interest such as alkylation of aromatics³³⁹ and propene oligomerization.³⁴⁰ The catalytic activity of mesoporous SAs appears to be frequently higher than that of microporous SAs, but lower than that of zeolites. A recent contribution underscored the inverse relationship of the pore sizes of mesoporous SAs and catalytic activity in n-hexane conversion showing the role of confinement effects in the acid catalysis.³⁴¹ SAs may also act as binders in catalysts such as those for the modern FCC process.

Recently, the buildup of strong Brønsted acid centers in the walls of mesoporous SAs has been attempted to enhance their catalytic activity and hydrothermal stability while taking advantage of their unusual porosity. This can be made with the incorporation of “zeolite seeds” in the framework.³⁴² Alternatively, mesostructured SAs have been prepared by surfactant-mediated hydrolysis of zeolites, with retention of five-ring subunits and, consequently, Brønsted acid centers.³⁴³

6.2.3.3. Alumina-Rich Silica-aluminas and Silicated Aluminas. Several commercial aluminas actually contain small amounts of silica mainly for stabilization against the phase transformation to corundum. Alumina-rich silica-aluminas produced by coprecipitation methods have been the object of some interest and of a few investigations. According to Trombetta et al.³⁴⁴ and Daniell et al.³⁴⁵ they have the structure of γ -alumina, silica being mostly located at the surface. Similar materials have been investigated more recently by the Topsøe group and found to be very active for the dimethyl ether (DME) synthesis from methanol at 300 °C and atmospheric pressure.³⁴⁶ The presence of silica would increase acidity and resistance to coking. Similar materials, denoted “activated alumina”, are possibly those used in the condensation step of the Topsøe technology for large-scale production of DME, for the coproduction of methanol, and DME from syngas.³⁹

The so-called “silicated aluminas”, obtained by a “reactive” deposition of silica precursors [such as tetraethoxysilane (TEOS)] onto the surface of γ -alumina, are a relevant class of materials reported as excellent catalysts for the skeletal isomerization of butylenes to isobutylene at 400–450 °C.^{92,347–349} Pt-containing silicated aluminas have also been patented for this reaction.³⁴⁸ A similar catalyst composed of silica and alumina is reported to be used in the ARCO *tert*-butyl alcohol dehydration process to produce pure isobutylene: the reaction occurs in the vapor phase at 260–370 °C at about 14 bar, with a conversion of 98%.³⁵⁰

The addition of silicate species to alumina (at the surface or in the bulk) gives rise to terminal silanols but does not produce bands in the region of bridging OH groups, nor is relevant Brønsted acidity observed. This is explained by supposing that the silicate species tend to maximize the interaction with the bulk of alumina by orienting three oxygen atoms toward the bulk, whereas the fourth necessarily stands up, with respect the surface. To limit the free energy, the fourth oxygen standing up bonds with a proton. It seems obvious that it cannot bend to bridge surface aluminum cations. The resulting Brønsted acidity is consequently that

of isolated silanols, weak, although enhanced by the vicinity of Al ions.⁹²

6.2.3.4. Aluminated Silicas. The addition of small amounts of aluminum oxide species at the surface of preformed silica gives rise to those species we called aluminated silicas.⁹⁴ In Figure 27 the spectra of an aluminated silica sample, as such and upon low-temperature CO adsorption, are compared with the corresponding spectra recorded for a commercial amorphous silica-alumina. These materials appear to be very similar to each other, with strong Lewis acidity, due to surface uncoordinated Al³⁺ ions, and Brønsted acidity associated with acidity-enhanced silanol groups.⁹⁴ To these materials belong, likely, the catalysts for the MTBE cracking Snamprogetti process (described as “based on silica”³⁵¹) performed in the gas phase at 140–150 °C, for the production of high-purity isobutylene.

6.2.4. SAPO-34

Silicoaluminophosphate (SAPO) molecular sieves are topologically similar to small- or medium-pore zeolites, in which phosphorus, aluminum, and silicon atoms occupy the tetrahedral positions. These materials appear to be characterized by a high thermal stability. SAPO-34 is isomorphous to chabazite (CHA), the structure of which is shown in Figure 28. The chabazite topology might be described as layers of

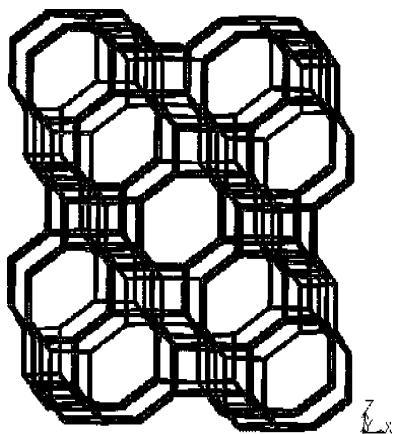


Figure 28. CHA (chabazite) zeolite structure. (Reprinted with permission from ref 160.)

double 6-membered rings that are interconnected by units of 4-membered rings. The double 6-membered-ring layers stack in an ABC sequence. This leads to a framework with a regular array of barrel-shaped cages with 9.4 Å diameter, interconnected by 8-membered-ring windows (3.8 × 3.8 Å). The chabazite structure contains only one unique tetrahedral site but four different oxygen atoms in the asymmetric unit, giving four possible acid site configurations, depending on to which of the oxygen atoms the proton is attached^{169,352}

After activation, SAPO-34 gives five IR peaks in the range of 3000–4000 cm⁻¹ representing five types of hydroxyl groups. Two peaks at 3625–3628 and 3598–3605 cm⁻¹ can be attributed to two types of Si(OH)Al groups. The bridging group absorbing at ~3600 cm⁻¹ is assumed to be localized in the hexagonal prism, forming an H-bond with adjacent oxygen atoms of the framework, whereas the isolated bridging OH groups pointing toward the center of the elliptical cage would give rise to a vibration frequency at ~3625 cm⁻¹. The lower frequency OH groups are considered to be a little less acidic than the high-frequency ones. Both have acid strength comparable to those of zeolites, including

chabazite, and are the active sites for acid-catalyzed reactions. The other peaks at 3675, 3743, and 3748 cm⁻¹, with very low intensity, are assigned to P–OH, Si–OH, and Al–OH groups, respectively, which are generated by the defect sites of SAPO-34 surface.^{352,353}

SAPO-34 is an excellent catalyst for the conversion of methanol to ethylene and propylene in the so-called methanol to olefin (MTO) process. The structure of SAPO-34 along with the small sizes of certain organic molecules is key to the MTO process, developed by UOP and Norsk Hydro.^{354,355} The small pore size of SAPO-34 restricts the diffusion of heavy and/or branched hydrocarbons, and this leads to high selectivity to the desired small linear olefins.

Under reaction conditions, at 400–550 °C, the deactivation by coke of SAPO-34 (containing 10% Si) is very fast, although activity is completely recovered after subsequent combustion of coke with air. The catalyst has demonstrated the degree of attrition resistance and stability required to handle multiple regenerations and fluidized bed conditions over the long term. The better performances of SAPO-34 with respect to H-chabazite as the catalyst have been related to the tunable density of acidity that allows the coking rate to be limited.³⁵⁶ The catalytic performance of SAPO-34 is improved if the surfaces of the crystals are doped with silica by heating with polydimethylsiloxane or an alkyl silicate.³⁵⁷

6.2.5. Acid Catalysts from Clays

Clays may be applied in the field of adsorption and catalysis, as cheap and readily available materials. Their catalytic activity, however, is generally weak, and activation procedures (e.g., acid treating and delamination) are needed to increase surface area and acidity. Kaolin is a usual component of FCC catalysts (20–50%) and reacts with Ni and V compounds,³⁵⁸ so preserving the active component, zeolite REUSY, from contamination. Although it is generally supposed to act as a mesoporous matrix in which reactant and product molecules diffuse to reach the active zeolite particles, it has been shown that kaolin, despite its poor acidity, participates in the reaction, catalyzing the cracking of the largest molecules that do not enter the zeolite cavities.³⁵⁹

6.2.5.1. Acid-Treated Clays. Among the earliest cracking catalysts applied in the Houdry fixed bed catalytic cracking process were acid-activated bentonite clays, these being replaced in the 1940s by synthetic silica-aluminas³⁵⁵ and in the 1960s by large-pore Y-zeolites.

Smectite clays (Figure 29) are sheet silicates⁸⁹ in which a layer of octahedrally coordinated cations is sandwiched between two tetrahedral phyllosilicate layers (2:1 layer type). To complete the coordination of the cations, hydroxy groups are also present in the layers, the theoretical formula for each layer being Al₂Si₄O₁₀(OH)₂. Among these clays, montmorillonites and saponites are the most widely present in nature. In the case of montmorillonites (bentonites) Mg substitutes for Al in the octahedral layers, and hydrated alkali or alkali-earth cations in the interlayer space compensate for the charge defect. In saponites, additional Al for Si substitution occurs in the tetrahedral sheets.

The acidity of such clays is relatively low and their surface area is also relatively low. In Figure 30 (upper spectra), the IR spectra of Ca-montmorillonite (Detercal P1) are reported. The strong OH stretching band centered at 3645 cm⁻¹ is due to bulk hydroxy groups, whereas the weak one at 3742 cm⁻¹ is due to terminal silanols. The adsorption of pivalonitrile

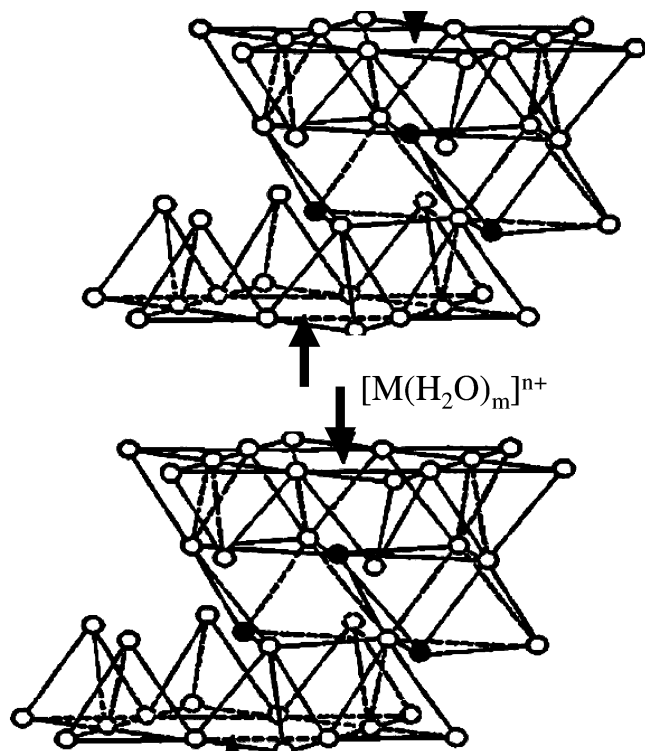


Figure 29. Schematics of the structure of smectites. White balls represent oxygen atoms, black balls are hydroxy groups, and arrows show cavities in the layers structure.

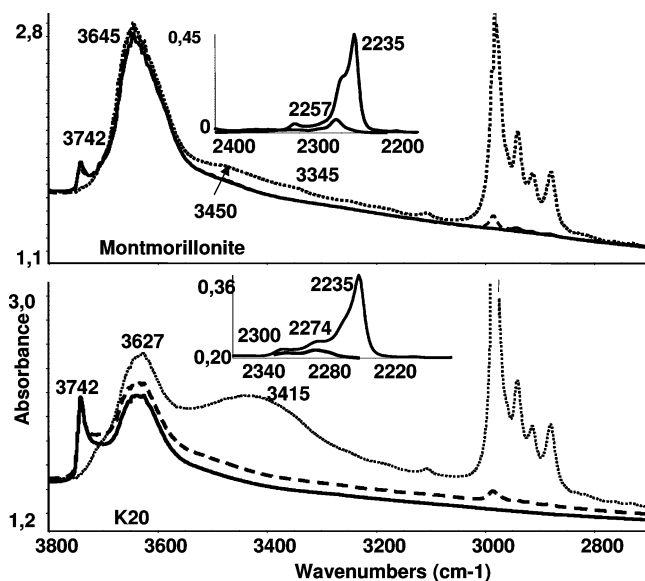


Figure 30. IR spectra of Detercal P1, a natural calcium-rich bentonite (montmorillonite 97%) of North African origin (Nador, Morocco), used as received from Industria Chimica Carlo Laviosa S.p.A. (Livorno, Italy) and of K20 acid-treated montmorillonite from Süd Chemie after outgassing at 400 °C (solid lines), after adsorption of pivalonitrile (dotted lines), and subsequent outgassing at room temperature (broken lines). (Inset) CN stretching bands of adsorbed pivalonitrile.

shows that terminal silanols are exposed at the surface and that their acidity is mostly similar to that found on pure silica ($\Delta\nu \sim 300 \text{ cm}^{-1}$ upon pivalonitrile adsorption) but with some more acidic site ($\Delta\nu \sim 400 \text{ cm}^{-1}$). The experiment do not detect any Lewis site.

Both acidity and surface area can be significantly enhanced by acid treatment, as done since very early times. Acid-treated montmorillonites are today commercial products and

can be purchased from a variety of commercial sources. Different grades of acid-activated montmorillonites are tailored to different applications. The process by which natural calcium bentonites are acid-activated involves treatment of the uncalcined clay with mineral acids of variable concentration and for different duration at $\sim 100 \text{ }^\circ\text{C}$. Such a treatment leads to leaching of aluminum, magnesium, and iron cations from the octahedral layer, to partial removal of aluminum ions from the tetrahedral layer that relocate in the interlayer space, and to the reduction of cation exchange capacity. During acid activation, swelling also occurs at the edges of clay platelets, which open up and separate while still remaining tightly stacked at the center. The surface area increases notably, and pore diameters increase and assume a three-dimensional form.

The acidity of H^+ -montmorillonite (0.65 mequiv/g) is evaluated to correspond to highly negative Hammett functions, $-8.2 < H_0 < -5.6$, that become even more negative by further acid treatment.⁸³

IR spectroscopy³⁶⁰ allows characterization of the surface Brønsted acidity as due to terminal silanols, located at the external surface of the “tetrahedral” layers. In Figure 30 (lower spectra) the spectra of the K20 acid-treated montmorillonite from Süd Chemie³⁶¹ are reported after vacuum activation and after adsorption of pivalonitrile. Acid treatment results in a strong growth of the band of the surface silanol groups at 3742 cm^{-1} , which are still weakly Brønsted acidic but much more abundant, and in the appearance of strong and medium Lewis acid sites (pivalonitrile CN stretching bands at 2300 and 2275 cm^{-1}) at least in part due to Al^{3+} ions in low coordination. On the other hand, acid-activated clays may be not stable in their acid form, undergoing autotransformation that results in a very sensitive dependence of the acidity on the water content of the clay. The interconversion that may occur among Brønsted and Lewis sites makes difficult the interpretation of the experimental data.³⁶²

Clays and acid-treated clays are today largely used in the petrochemical industry mostly as adsorbants for purification and decoloration of oils.³⁶¹ However, they are still also proposed as catalysts for several acid-catalyzed reactions^{363,364} such as cracking of heavy fractions,³¹² etherifications, esterifications, alkylation. They have also been considered for industrial applications in the fields of hydroprocessing and hydroisomerization³⁶⁵ and mild hydrocracking³⁶⁶ and as a support for other acid catalysts.³⁶⁷

Recently, a new clay-derived material, called LRS-1, a de-laminated phyllosilicate, has been developed; its Brønsted acidity appears to be definitely higher, with zeolitic-type bridging hydroxy group.³⁶⁸

6.2.5.2. Pillared Clays (PILC) and Acidic Porous Clay Heterostructures (PCH). Exchanging the charge-compensating cations of a smectite clay with an oligomeric polyoxometal cation (such as the $[\text{Al}_{13}\text{O}_4(\text{OH})_{24}(\text{H}_2\text{O})_{12}]^{7+}$ Keggin-type ion) results in a two-dimensional porous material known as pillared clay.^{369,370} Upon heating, the cationic pillars form oxide clusters that permanently open the clay layers, creating an interlayer space of molecular dimensions and a well-defined pore system (schematized in Figure 31).

The pillaring process may generate Brønsted and Lewis acid centers in the interlayer region of the clay, depending upon the starting clay and the pillaring agent. If the pillaring process is repeated on a pillared clay, the cation exchange capacity (CEC) of which was previously restored, both

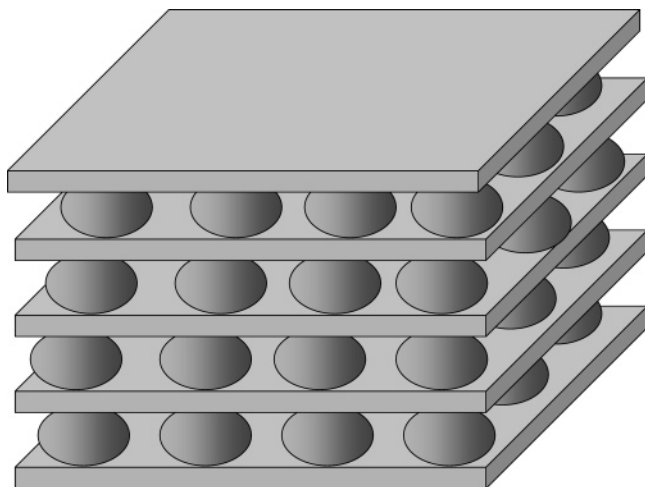


Figure 31. Schematics of the morphology of pillared clays.

thermal stability and the number of acid sites were found to increase. The intercalation of the aluminum Keggin ion between the layers, and the following pillaring process, is quite different in the tetrahedrally substituted saponite and in the octahedrally substituted montmorillonite.³⁷¹ In montmorillonites the proton released during calcination can migrate into the octahedral sheets' vacant sites, but this does not occur in saponites, where they remain located in the interlayer spacing. Moreover, pillars in pillared saponite are presumably strongly anchored to the layer by covalent Al–O–Al, whereas in pillared montmorillonites there is no evidence of this pillar/layer anchoring. By analyzing the pillaring process³⁷² by molecular modeling, it was proposed that a more homogeneous distribution of the pillars must be achieved in pillared tetrahedrally Al/Si-substituted smectites.

The IR spectra of saponite and of alumina pillared saponite are compared in Figure 32. Pillaring increases the intensity

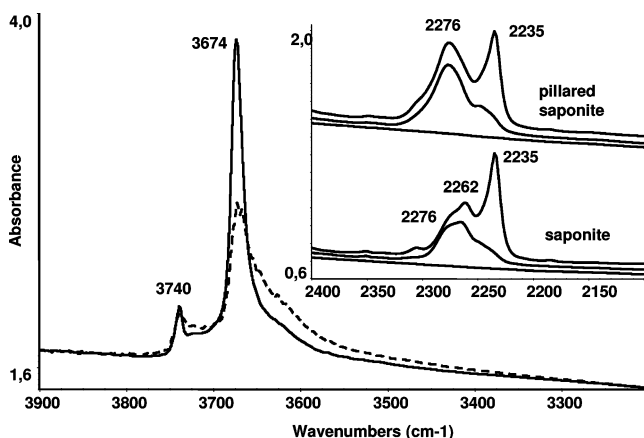


Figure 32. IR spectra of natural saponite C27 from Tolsa (Spain) (solid line) and of alumina-pillared saponite³⁷² (broken line) after outgassing at 400 °C. (Inset) CN stretching bands of pivalonitrile adsorbed on the sample in contact with the vapor (upper) and outgassed at room temperature (lower).

ratio between the bands of free surface silanols (3740 cm^{-1}) and internal OH groups (3674 cm^{-1}). Additionally, new OH bands are observed in the region of 3730–3600 cm^{-1} , likely due to AlOH groups of the pillars. Pivalonitrile adsorption reveals the increase of octahedrally coordinated Al^{3+} acting as medium-strong Lewis acid sites. In fact, IR spectroscopy studies³⁷⁰ show that pillars in pillared montmorillonite are structurally similar to spinel-type alumina, with strongly

acidic tetrahedral Al^{3+} cations, whereas pillars in pillared saponite are more similar to corundum-type alumina, with less acidic octahedral Al^{3+} cations.

Efforts have been made to obtain by clay pillaring large-pore materials stable to regeneration treatments to perform cracking of very large molecules ($>8 \text{ \AA}$).³⁷³ In any case, materials based on pillared clays are applied in some catalytic cracking processes^{312,374} and as molecular sieves. They may also be useful as medium-acidity supports of noble metal catalysts for diesel³⁷⁵ and gas oil³⁶⁵ hydrotreating. Also, the catalytic activity of pillared clays in acid catalysis,³⁶¹ in particular of ethylene glycol synthesis from ethylene oxide hydration and formation of ethylene glycol ethers³⁷⁶ and propene oxide from n-propanol,³⁷⁷ appears to be of industrial interest. Further development of PILCs as industrial catalysts has been limited up to now due to inhomogeneous porosity and difficulties in the control of the preparation and of the final porosity.³⁷⁸ An interesting recent development in this field consists in the preparation of acid porous clay heterostructures (PCH) by the surfactant-directed assembly of mesostructured silicas³⁷⁹ and silica-aluminas³⁸⁰ in the two-dimensional galleries of 2:1 layered silicates. These materials are reported to have strong acidity, stability to 750 °C, and a particularly porous structure.

6.2.6. Pure and Mixed or Supported Transition Metal Oxides: Titania, Zirconia, Tungsta, and Their Combinations

The oxides of tetravalent transition metals, such as zirconias and titanias, are definitely ionic network solids. The ionicity of their metal–oxygen bond, associated with the medium size of the cations,⁷⁰ corresponds to the formation of Lewis acid–base surface character, whereas the Brønsted acidity of their surface hydroxy groups is definitely weak. The Lewis acidity of these catalysts is medium-strong, lower than that of alumina.

Zirconia is a polymorphic material. It presents three structures that are thermodynamically stable in three different temperature ranges. Monoclinic zirconia (baddeleyite) is the room temperature form, tetragonal zirconia is stable above 1200 K, and cubic zirconia is stable above 2400 K. Tetragonal and cubic zirconia, however, may exist as metastable forms at room temperature, mostly if stabilized by dopants such as yttrium. Frequently, zirconia powders as prepared are mixed tetragonal and monoclinic.³⁸¹ Several characterization studies have been performed on pure zirconias and showed they are typical ionic materials, characterized by medium Lewis acidity, significant surface basicity, and very low Brønsted acidity, if possessing any at all. CO adsorption experiments^{127,382} provide evidence for two slightly different types of Lewis acidic Zr^{4+} ions on both monoclinic and tetragonal zirconia. On the other hand, the qualities of the sites are very similar in the two phases, but a little stronger sites exist on the tetragonal phase. Slightly different concentrations of Lewis sites can be found on the two solids, depending on outgassing temperature. CO_2 adsorption studies³⁸² reveal significant basicity.

Pure zirconia or zirconia doped with alkali or alkali-earth cations is applied industrially for some alcohol dehydration and dehydrogenation reactions in the fine chemicals field.³¹² Zirconia finds many actual or potential applications as a catalyst support.

Titania is also a polymorphic material: the most usual phases are anatase and rutile, the latter being always

thermodynamically stable. Also, titanias are highly ionic oxides with medium-high Lewis acidity, significant basicity, and weak Brønsted acidity, if possessing any at all. Characterization data show that on anatase stronger Lewis acid sites are usually detectable than on rutile.^{383,384} Anatase is usually prepared by precipitation and is largely used in the catalysis field, for example, as the support for vanadia-based selective oxidation catalysts³⁸⁵ as well as for vanadia–tungsta and vanadia–molybdena catalysts for the selective catalytic reduction of NO_x .³⁸⁶ Titania may also be used as a support of sulfided hydrodesulfurization catalysts. As a catalyst, titania finds relevant application in the Claus process as an alternative to alumina, in particular for the first higher temperature bed where hydrolysis of COS and CS_2 also occurs.³⁸⁷ Titania–anatase is also the basic component of most photocatalysts.

Titania and zirconia may be combined with silica³⁸⁸ and alumina,^{389,390} as well as each other,³⁹¹ to give interesting and useful high-surface area and high-stability materials. These materials retain high Lewis acidity associated with the Al^{3+} , Ti^{4+} , and Zr^{4+} cations, as well as medium-weak Brønsted acidity, associated with silanols and other hydroxy groups. Titania–aluminas are important materials as catalyst supports, for example, for hydrodesulfurization catalysts.^{392,393}

Tungsten oxide (WO_3) has many crystal structures, most of which, however, are distorted forms of the ReO_3 type cubic structure. These structures, in which hexavalent tungsten is in more or less distorted octahedral sixfold coordination, have a highly covalent character, associated with the very high charge and very low size of the W^{6+} cation.⁷⁰ This material has very strong acidity of both the Lewis and Brønsted types.³⁹⁴ Pure WO_3 and silica-supported WO_3 have had industrial application as acid catalysts, for example, for commercial direct hydration of ethylene to ethanol in the gas phase.³⁹⁵

Much interest has been devoted recently to tungstated oxides^{396,397} as catalysts. Tungstated titanias are investigated mainly in relation to their use as active components of vanadia catalysts for the selective catalytic reduction of NO_x by ammonia,³⁸⁵ a reaction in which catalyst acidity plays a relevant role. Tungstated zirconia is mostly investigated in relation to its activity in the paraffin skeletal isomerization reaction.^{398–400} Anatase and tetragonal zirconia give rise to better catalysts than rutile and monoclinic zirconia. The presence of wolframate species on both titania and zirconia causes an increase of the Lewis acid strength, an almost full disappearance of the surface anions acting as basic sites, and the appearance of a very strong Brønsted acidity.^{401–404} The tungstate ions^{405,406} on ionic oxides in dry conditions are tetracoordinated with one short $\text{W}=\text{O}$ bond (mono-oxo structure), responsible for a strong IR and Raman band near 1010 cm^{-1} (Figure 33) at near or less than the monolayer coverage. This is the case of $\text{WO}_3\text{-TiO}_2$ supports for vanadia SCR catalysts, which usually contain $\sim 10\%$ WO_3 w/w and have $\sim 70\text{ m}^2/\text{g}$. In the presence of water the situation changes greatly. According to the Lewis acidity of wolframyl species, it is believed that they can react with water and be converted in a hydrated form⁴⁰⁶ or be polymerized.³⁹⁷ Polymeric forms of tungstate species are supposed to form at higher coverages,^{397,407} as an intermediate step before the formation of separate WO_3 particles. The evidence of the real existence of polymeric tungstated species, to which high catalytic activity is attributed,⁴⁰⁸ is the shift upward of the $\text{W}=\text{O}$ stretching mode and of the UV absorption edge.³⁹⁷ Both of

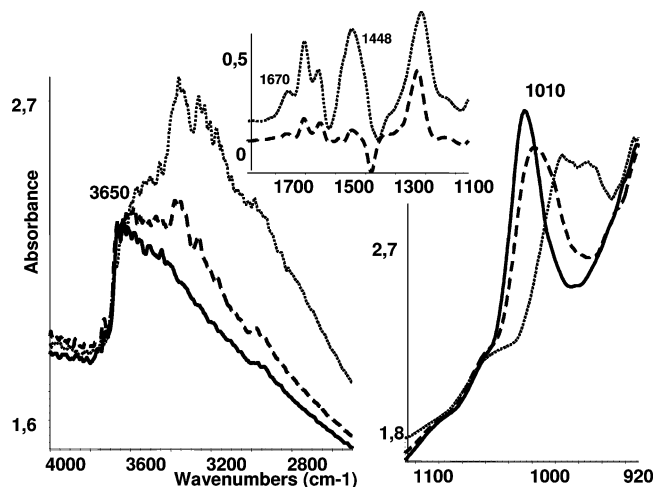


Figure 33. IR spectra of 10% $\text{WO}_3\text{-ZrO}_2$ ($85\text{ m}^2/\text{g}$) after activation by outgassing at $450\text{ }^\circ\text{C}$ (a) in contact with ammonia vapor and outgassing at room temperature (b) and at $150\text{ }^\circ\text{C}$ (c). (Inset) Subtraction spectra showing the bands of adsorbed ammonia and ammonium ions.

these phenomena, however, could alternatively be due to the heterogeneity of monomeric wolframates. Splittings of the $\text{W}=\text{O}$ modes as well as new characteristic $\text{W}-\text{O}-\text{W}$ modes, expected for oligomeric species, are in fact not observed either in IR or in Raman spectra.⁴⁰⁶ At high coverages (more than the monolayer) as for $\text{WO}_3\text{-ZrO}_2$ paraffin isomerization catalysts, WO_3 particles are well evident in Raman spectroscopy analysis.³⁹⁷ Residual surface OH groups of such materials do not present well-defined sharp bands but quite broad features (Figure 33), suggesting that the OH groups are in fact involved in H-bondings.

A particular feature of tungsta-based catalysts concerns the possible reduction of tungsten oxide to lower oxidation states, which make them active catalysts also for selective oxidation.⁴⁰⁹ The presence of tungstate species influences very much the redox properties of vanadia–titania SCR catalysts.⁴¹⁰ UV–vis studies by Gutierrez-Alejandre et al.^{403,411} contributed to underscore the possible role of the semiconducting nature of zirconia and titania in these catalytic materials. In fact, in the same conditions, insulating support materials such as aluminas seem to give rise to less active tungstated catalysts in acid catalysis, despite their even stronger, or equivalent,⁴¹² acidity. Monoclinic zirconia, in whose bulk Zr ions have coordination seven and half-oxygen ions have coordination three (in contrast to both cubic and tetragonal ZrO_2 in which coordination is eight at Zr and four at oxygen), has an optical gap significantly lower than that of tetragonal zirconia,³⁸¹ which gives better catalysts. In parallel, also rutile has an optical gap significantly lower than that of anatase (which gives more active catalysts).⁴¹³ The hypothesis of the generation, upon reduction in hydrogen, of stronger Brønsted acid sites has been proposed.^{414,415} The semiconductivity of the support may influence this phenomenon.

The strong Brønsted acidity of tungstated oxides (see Figure 33, where ammonia is shown to be protonated to give bands at 1670 and 1448 cm^{-1} , typical of NH_4^+ ions) is essentially related to the high acidity of tungstic acid species, whereas the redox properties of tungstic acid species, which may be influenced by the semiconducting/insulating and dispersing/nondispersing behavior of the support, may favor the generation of protonic centers by reduction and/or may

be related to nonacid catalytic steps, such as partial paraffin oxidative dehydrogenation to olefins, which is likely a step in paraffin skeletal isomerization. Pt and Mn promoted $\text{WO}_3\text{-ZrO}_2$ catalysts are very active, for example, in the isomerization of *n*-hexane at 220–250 °C.⁴¹⁶ The so-called EMICT (ExxonMobil Isomerization Catalyst Technology) catalyst, based on promoted $\text{WO}_3\text{-ZrO}_2$, is reported to be very effective in C5–C6 paraffin skeletal isomerization at 175–200 °C even in the presence of 20 ppm of water and to be fully regenerable.⁴¹⁷ In this case the redox properties of the catalyst might also be involved in the oxydehydrogenation of alkane to alkenes that later are protonated and promote a chain skeletal isomerization reaction, as for sulfated zirconia (see below). Reduced tungsten oxides are also mentioned as good catalysts for olefin methathesis.⁴¹⁸

6.2.7. Sulfated Zirconia

Sulfation of metal oxides introduces quite strong Brønsted acidity and, in general, enhances the catalytic activity in acid-catalyzed reactions. For example, sulfation of alumina enhances its catalytic activity in *n*-butylene skeletal isomerization.⁴¹⁹

Zirconia (tetragonal more than monoclinic), when sulfated, becomes very active for some hydrocarbon conversion reactions such as *n*-butane skeletal isomerization.⁴²⁰ A similar behavior has also been found for sulfated zirconia–titania¹⁸⁵ and, although less pronounced, for sulfated titania–anatase.⁴¹⁹

Spectroscopic studies showed that the sulfate ions⁴²¹ on ionic oxides in dry conditions at low coverage are tetracoordinated with one short S=O bond (mono-oxo structure). At higher coverage, disulfate species are assumed to exist,^{422,423} although a real proof of this probably does not exist. However, sulfate species are strongly sensitive to hydration. Lewis acidity and basicity of zirconia disappear in part by sulfation, but the residual Lewis sites are a little stronger. However, Brønsted acidity is also formed. IR spectra show a band in the range of 3645–3630 cm^{-1} ,^{422,423} which is shifted by 139 cm^{-1} upon low-temperature CO adsorption,⁴²² so measuring a medium-weak Brønsted acid strength. In contrast, the Brønsted acid strength of sulfated oxides measured by IR through the surface “olefin oligomerization” method is superior to that of silica-alumina and comparable to that of protonic zeolites.⁴²⁴ The measurement of the Hammett constant⁸³ gives values more negative than those of pure sulfuric acid, thus allowing the definition of these materials as “superacidic”. Characteristic ¹H MAS and broad line NMR signals⁴²⁵ with chemical shifts larger than those of zeolite protons have been found. Microcalorimetric ammonia chemisorption studies⁴²⁶ and ammonia TPD experiments⁴²⁷ suggested that dry sulfated zirconia surfaces have Brønsted acidity not stronger than that of protonic zeolites. Water is reported to be needed for high catalytic activity⁴²⁸ and, according to Katada et al.,⁴²⁹ should generate “superacidic” Brønsted centers. In contrast, water is cited as a poison during commercial application in paraffin isomerization.^{272,273}

The very high catalytic activity of sulfated zirconia, in particular for C4–C6 paraffin isomerization, appears when a certain number of requirements are satisfied: in particular, it must be prepared by an amorphous sulfated precursor calcined at $T \geq 550$ °C in order to have a tetragonal sulfated phase and be properly activated.⁴³⁰ The catalytic activity of these materials may be enhanced by promoters such as Mn and Fe ions, which, however, do not increase the catalyst acidity.

Recent studies showed convincing evidence of the existence of an *n*-butane oxidative dehydrogenation step, probably induced by the reduction of sulfate species, during the induction period with the formation of water molecules and butylene.^{431,433} Protonation of butylene gives rise to the sec-butyl cation that leads to a chain mechanism. This chain may involve direct isomerization of the butyl cation and hydride transfer from *n*-butane (monomolecular mechanism) or dimerization, isomerization, cracking, and hydrogen transfer (bimolecular mechanism). According to the experimental evidence that the presence of any olefins increases the butane isomerization reaction rate, it has been proposed that the skeletal isomerization reaction could more likely occur on an “olefin modified site” (i.e., a carbenium ion) than on the protonic site, giving rise to a bimolecular pathway having the characteristics of a monomolecular one.⁴³²

Thus, the protonic acidity of these materials, arising from the presence of sulfuric acid species, is certainly strong. The presence of small amounts of water is likely required to retain surface hydroxylation. However, in parallel with what has been discussed for tungstated oxides, the semiconducting nature of zirconia (and titania to a lower extent) coupled with the reducibility of sulfate species may play an important role in the behavior of the catalyst, in nonacidic steps. The other sulfated oxide that has been reported recently to be superacidic, as deduced by Ar TPD,^{433,434} and even more active than sulfated zirconia in paraffin isomerization, is sulfated tin oxide, that is, another semiconducting material.

Sulfated zirconia-based catalysts have already been used in industrial application for C4–C6 paraffin isomerization processes and are commercialized, for example, by Süd Chemie (HYSOPAR-SA catalysts) constituted by Pt-promoted sulfated zirconia.^{272,273} They work at temperatures (180–210 °C) intermediate between those of the competing chlorided alumina and zeolite catalysts, similar to those of $\text{WO}_3\text{-ZrO}_2$ -based catalysts, with final comparable performances, moderate limits in the allowed feed purity, and possible regeneration.

6.3. Solid Acids

6.3.1. Sulfonic Acid Resins

Ion exchange resins were introduced in the 1960s and find today wide application as catalysts in the hydrocarbon industry.^{435–437} The most used materials are macroreticular sulfonated polystyrene-based ion-exchange resins with 20% divinylbenzene, such as the materials of the Amberlyst family produced by Rohm and Haas.⁴³⁸ The acidity of these materials, having surface area near 50 m^2/g , is associated with the strong acidity of the aryl-sulfonic acid groups Ar-SO₃H. These are actually the active sites in nonpolar conditions, but at high water or alcohol contents in the medium, the less active solvated protons act as the acids.⁴³⁹ These materials are prepared as “gel” resins in the form of uniform beads, and as “macroporous” materials. Due to restricted diffusion, the acid sites in the gels are accessible only when the beads are swollen. Macroporous resins are prepared with permanent porosity; thus, more acid sites are accessible also in nonswelling solvents, although diffusion of the reactant in the polymer matrix is also determinant.⁴⁴⁰ The number of acid sites in sulfonated polystyrene is relatively high, 4.7 equiv/kg for Amberlyst-15 and 5.4 equiv/kg for the hypersulfonated resin Amberlyst-36. However, the acid strength is considered to be relatively low, the Hammett

acidity function being evaluated as $H_0 = -2.2$. Another limit of these materials consists in the limited stability temperature range, $<150\text{--}180\text{ }^\circ\text{C}$. Materials with comparable activities (e.g., Dowex from Dow Chemicals, Indion from Ion Exchange Ltd., India) can be found in the market.

The application of these materials is limited to relatively nondemanding acid-catalyzed reactions in the liquid phase. They are in fact the catalysts for branched olefin etherification processes such as MTBE,⁴⁴¹ ETBE, and TAME syntheses. In the SNAMPROGETTI process, MTBE synthesis is performed in the liquid phase at $40\text{--}80\text{ }^\circ\text{C}$ and $7\text{--}15$ atm C_4 cut pressure, with a water-cooled multitubular reactor and an adiabatic finishing reactor in series.⁴⁴² CDTEch proposes catalytic distillation reactors using cylindrical bales containing the ion-exchange resin in the packing of the tower.⁴⁴³ The MTBE process may be modified to obtain MTBE/isobutylene dimer coproduction.⁴⁴⁴ The same catalysts and modified MTBE processes are applied today for isobutylene di- and trimerization.⁴⁴⁵ The reaction conditions are similar, but the inactive alcohol *tert*-butanol (TBA) is added instead of methanol. TBA does not react with isobutylene, but its presence strongly increases dimer selectivity, although decreasing isobutylene conversion. Working with a real C_4 cut also linear butylenes react with isobutylene to a small extent.⁴⁴⁶ Similar resins are also amply used in phenol alkylation processes.⁴² In this case the reaction temperature is in the range of $100\text{--}130\text{ }^\circ\text{C}$. Oligomerization of propene and isoamylene can also be performed.

Sulfonated polystyrene polydivinylbenzene resins are deactivated by basic impurities in the feed such as nitriles (typically present in the C_4 cut after FCC),⁴⁴⁷ as well as by cations such as Na^+ and Fe^{3+} .⁴⁴⁸ Washing procedures can be applied to the catalysts to rejuvenate them. By using water-cooled multitubular reactors, the hot spot due to the exothermic reaction is, when the bed is fresh, at the entrance of the tubes, but it tends to move toward the exit by increasing time on stream due to partial deactivation of the bed. This allows the progressive catalyst deactivation to be followed. When the hot spot is at the exit of the bed, the catalyst must be substituted.⁴⁴¹ In the use of sulfonated resins for olefin oligomerization catalyst, fouling by higher oligomers may occur.

Nafion is a strongly acidic resin produced by DuPont,⁴⁴⁹ a copolymer of tetrafluoroethylene and perfluoro-3,6-dioxo-4-methyl-7-octenesulfonyl fluoride, converted to the proton (H^+) form. Nafion is definitely more acidic than polystyrene-based sulfonic resins. This material, largely used in electrochemical processes as membrane for chlor-alkali cells and as electrolyte for proton exchange membrane fuel cells (PEMFC), may also act as a very strong Brønsted acid solid catalyst. It carries the strongly acidic terminal $-\text{CF}_2\text{CF}_2\text{SO}_3\text{H}$ group, which is, however, converted into solvated protons in the presence of water.⁴⁵⁰ This material is both chemically stable (as expected due to the fluorocarbon nature of the backbone) and thermally stable up to $280\text{ }^\circ\text{C}$, at which temperature the sulfonic acid groups begin to decompose. It is commercialized in the form of membranes, beads, and dispersions in water and aliphatic alcohol solutions.

It is generally accepted that perfluorinated resin sulfonic acids are very strong acids with values of the Hammett acidity function ($H_0 = -11$ to -13) which allow the application of the term "superacid". However, the surface area of this material is very low, the density of the protonic sites in the pure polymer is very small (0.9 equiv/kg), and

their availability also is very small. Consequently, the activity of this material either in nonswelling solvents or in the gas phase is very low. This limited very much actual application in catalysis.

A new perspective was born with the development of Nafion resin/silica nanocomposites, which may function in nonswelling solvents. This material has been successfully tested in several reactions such as isobutane/butylene alkylation.⁴⁵¹ Attempts to develop industrial processes have been reported, for example, for the liquid-phase oligomerization of tetrahydrofuran and for the oligomerization of olefins.⁴⁵²

The used Nafion-based catalysts can be regenerated by washing with nitric acid. However, a relevant limit of Nafion-based materials is related to unsafe disposal and to the toxicity of their thermal degradation products in the case of heating above $280\text{ }^\circ\text{C}$.⁴⁴⁹

6.3.2. "Solid Phosphoric Acid"

The so-called "solid phosphoric acid" catalyst (SPA) was developed by UOP in the 1930s.^{453,454} It is produced by mixing phosphoric acid 85% with Kieselguhr (a natural form of highly pure silica) followed by extrusion and calcination. The heat treatment causes the partial polymerization of orthophosphoric acid H_3PO_4 to pyrophosphoric acid $\text{H}_4\text{P}_2\text{O}_7$, and higher polymers such as triphosphoric acid $\text{H}_5\text{P}_3\text{O}_{10}$, as well as the formation of silicon phosphates such as $\text{Si}_5\text{O}(\text{PO}_4)_6$, hexagonal SiP_2O_7 , $\text{Si}(\text{HPO}_4)_2\cdot\text{H}_2\text{O}$, and $\text{SiHP}_3\text{O}_{10}$.⁴⁵⁵ However, the real constitution of the acid phase strictly depends on water content in the catalyst, which is also greatly influenced by the amount of water vapor in the feed during the reaction.⁴⁵⁶

According to a recent NMR study, the acidity of this catalyst is associated with a liquid or glassy solution of phosphoric acid oligomers supported on the silicon phosphate phases.⁴⁵⁵ The IR spectrum of the SPA catalyst (Figure 34)

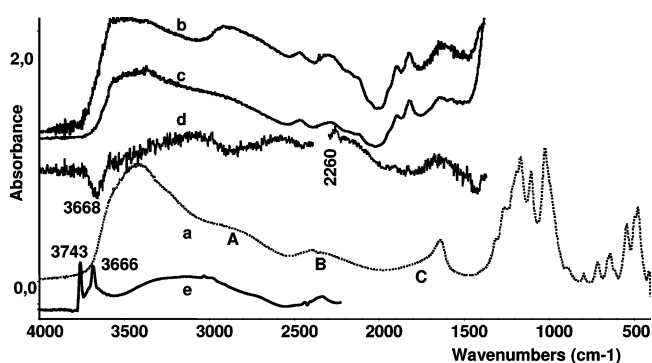


Figure 34. IR spectra of solid phosphoric acid in a KBr pressed disk in the air (a) and in a self-supporting pressed disk after outgassing at $300\text{ }^\circ\text{C}$ (b) and $400\text{ }^\circ\text{C}$ (c); (d) subtraction spectrum after pivalonitrile adsorption over PSA outgassed at $400\text{ }^\circ\text{C}$; (e) IR spectrum of an 8% silica-supported H_3PO_4 catalyst after outgassing at $400\text{ }^\circ\text{C}$.

shows the typical features of strong hydrogen bonds (A, B broad features) between POH groups and water molecules. Pressed disks of the pure powder do not transmit the IR radiation at all. After outgassing, partial water desorption occurs, and the sample transmits the IR radiation, still showing features due to water molecules. No clear evidence is found for protonated water species. The adsorption of a nitrile as a probe reveals also the existence, on the outgassed sample, of free POH groups absorbing at 3658 cm^{-1} , which

are perturbed upon adsorption and form a negative band in the subtraction spectrum (Figure 34d). These free POH groups appear to be the most available to adsorbates. The position of the band is similar to that observed on low coverage supported H_3PO_4 on silica (Figure 34e), as well as on phosphoric acid supported on other oxides⁴⁵⁷ and on metal phosphates and pyrophosphates,^{458,459} and their Brønsted acidity, as measured by the hydrogen bonding and by the olefin oligomerization method via IR, is significant, but definitely lower than that of silica-alumina and zeolites (Table 8). Interestingly, no bands of free silanol groups are observed in the case of SPA, whereas they are evident for silica-supported phosphoric acid. Also, the skeletal spectrum of SPA shows that silica, as such, does not exist in the SPA bulk. No Lewis acidity is found. The Hammett acidity function of SPA has been evaluated to be in the range from -5 to -7 .⁴⁵⁵

SPA is the catalyst for gas-phase propene and isobutylene oligomerization industrial processes^{460,461} producing polymerate gasoline, and it is still used for cumene synthesis from propene and benzene (see Table 4). According to Cavani et al.⁴⁵⁶ the hydration state of the catalyst affects in opposite ways the activities in olefin oligomerization and cumene synthesis and also affects strongly the catalyst lifetime. However, excessive water in the feed leads to loss of mechanical properties of the catalyst and its destruction, mostly due to the hydrolysis of silicon phosphates. Acid leaching and coking are additional causes of deactivation.

Reaction temperature for industrial propene and isobutylene oligomerization to trimers and tetramers (UOP, IFP processes⁴⁶⁰) is 150 – 250 °C at 18 – 80 atm, with relatively high space velocities to limit coking. A total of 250 – 300 ppm of water in the feed is recommended, and catalyst life may be more than 1 year.⁴⁵⁵ Multiple fixed bed or multitubular reactors are used.

SPA can also be used to produce diesel-range olefin oligomers.⁴⁶² The selectivity to such products has been shown to have a peak when the concentration of pyrophosphoric acid $\text{H}_4\text{P}_2\text{O}_7$ in the catalyst becomes relatively high and space velocities are low.⁴⁶³ Recently, the preparation of the catalyst has been modified to improve the crushing strength, which is controlled by the relative amounts of the silicon ortho- and pyrophosphate phases present. A new commercial catalyst was formulated that requires no binders and showed a 30% increase in catalyst lifetime.⁴⁶⁴

For gas-phase UOP cumene synthesis typical reaction temperatures are 200 – 260 °C, at pressures of 30 – 45 bar, with a large excess of benzene (5:1 to 10:1 benzene to propene) to limit multiple alkylation (Table 4).^{42,231,232,250} Typical reactors are multiple fixed bed with quenching to control the exothermic reaction temperature. A total of 100 – 150 ppm of water is recommended, and the catalyst life may be more than 1 year.⁴⁵⁵ The catalyst cannot be regenerated.²³²

Solid phosphoric acid is also used for the direct hydration of ethylene to ethanol in the liquid phase at 230 – 300 °C and 60 – 80 atm⁴⁶⁵ and to produce other alcohols by acid-catalyzed hydration of olefins. The phosphoric acid is continually lost from the carrier, and water must be supplied with the feed. The use of different carriers results in diminution of the catalytic activity.

6.3.3. Niobic Acid and Niobium Phosphate

Hydrated niobium oxides (niobic acids) calcined at moderate temperatures of 100 – 300 °C are reported to show a

strong acidic character ($H_0 = -5.6$)^{466,467} with many potential applications in catalysis,^{468,469} displaying both Lewis and Brønsted acidity.^{70,470} Proton NMR data indicate that Brønsted acidity of niobic acid is very high, possibly comparable with that of protonic zeolites.⁴⁷¹ The IR spectrum⁴⁷² of niobic acid, after outgassing at 100 °C, shows a strong band at 1612 cm^{-1} , asymmetric with a tail toward higher frequencies and a component at 1440 cm^{-1} (Figure 35). At higher frequen-

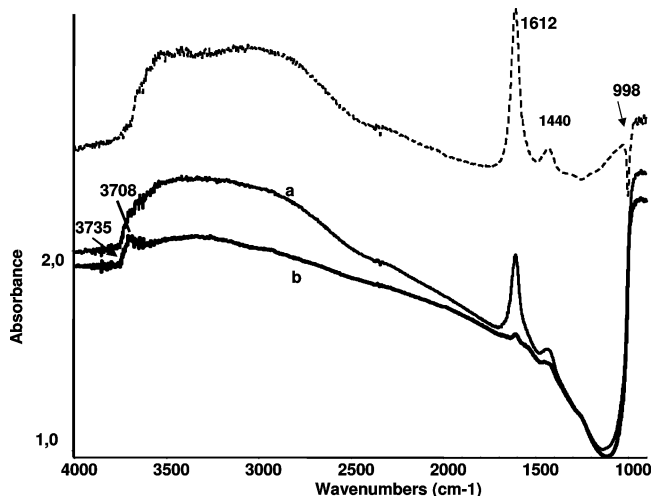


Figure 35. IR spectrum of niobic acid supplied by CBMM (Companhia Brasileira de Metalurgia e Mineracao) after outgassing at 100 °C (a) and 200 °C (b); broken line, subtraction $a - b$.

cies, a broad absorption is found in the region of 3600 – 2500 cm^{-1} , due to OH stretchings of H-bonded water and hydroxy groups. These absorptions decrease significantly by outgassing at 200 °C. After this treatment, a quite sharp peak at 3708 cm^{-1} , with a shoulder near 3735 cm^{-1} , is observed, assigned to free Nb–OH surface groups. A broad absorption centered near 3300 cm^{-1} resists this treatment, whereas the bands at 1612 and 1440 cm^{-1} are now very weak. The difference spectrum also shows that the desorption of water causes the appearance of a sharp feature at 998 cm^{-1} , associated with Nb=O double-bond stretchings. The spectrum we observe of adsorbed water (desorbed mostly in the 100 – 200 °C range) contains features (in particular, the component at 1440 cm^{-1}) that, according to Zecchina et al.,¹⁸¹ should be fingerprints of protonated water species $[\text{H}(\text{H}_2\text{O})_n]^+$. In contrast, the more recent work of Stoyanov et al.⁴⁷³ allows the doublet at 1612 and 1440 cm^{-1} to be attributed to a splitting of the deformation mode of $[\text{H}_3\text{O}]^+$, due to its lowered symmetry. In any case, the Brønsted acidity of niobic acid is confirmed. Nb–OH and Nb=O groups become present at the surface after water desorption. Adsorption of nitriles indicates that Nb–OH groups are less acidic than the bridging hydroxy groups of zeolites.⁷⁰ Nb cations, observed after heating at 400 °C, also show strong Lewis acidity. Niobic acid is reported to crystallize as niobium oxide at 853 K, so losing all of its water and hydroxide species.

The products of the combination of niobium oxide and phosphoric acid are niobium phosphates^{472,474} and phosphoric acid-treated niobic acid,⁴⁷⁵ both reported to be materials potentially useful in acid catalysis. FT-IR spectra of the niobium phosphate samples also show the sharp band of the P–OH groups near 3668 cm^{-1} , as well as a weak band at 3700 cm^{-1} assigned to Nb–OH groups. The spectra of adsorbed water are similar, indicating the formation of $[\text{H}(\text{H}_2\text{O})_n]^+$ species. The hydrogen bonding of acetonitrile

with the surface hydroxy groups of the niobium phosphate samples is significantly stronger than that niobic acid,⁴⁶⁶ suggesting that POH groups are stronger Brønsted acids than NbOH groups.

Both niobic acid and niobium phosphate find application as insoluble solid catalysts in water phase²⁴⁰ and are applied in the industry for some fine chemical acid-catalyzed processes,⁴⁶⁸ such as the fructose dehydration reaction.^{476,477} Acid–base titrations realized in different polar liquids showed a better performance of niobium phosphate than niobic acid could be related to the higher effective acidity of its surface.⁴⁷¹ As reported by Tanabe⁴⁶⁸ niobic acid and niobium phosphate are patented as alternatives to solid phosphoric acid for ethylene hydration to ethyl alcohol in the gas phase at 200 °C.

6.3.4. Heteropolyacids

The most common and thermally stable primary structure of heteropolyacids (HPAs)^{478,479} is that of the Keggin unit that consists of a central atom (usually P, Si, or Ge) in a tetrahedral arrangement of oxygen atoms, surrounded by 12 oxygen octahedra containing mostly tungsten or molybdenum. There are four types of oxygen atoms found in the Keggin unit: the central oxygen atoms, two types of bridging oxygen atoms, and terminal oxygen atoms. The secondary structure takes the form of the Bravais lattices, with the Keggin units located at the lattice positions. Heteropolyacids possess waters of crystallization that bind the Keggin units together in the secondary structure by forming water bridges. Tertiary structures can be observed when heavy alkali salts are formed.

The acidity of the heteropolyacids is purely Brønsted in nature. Because the Keggin unit possesses a net negative charge, charge-compensating protons or cations must be present for electroneutrality. The acid form of heteropolyacids is generally soluble in water and acts as a liquid acid and as a homogeneous acid catalyst in water solutions, as well as in liquid biphasic systems.^{480,481} Evaluation of acid strength in solution has shown that HPAs composed of tungsten are more acidic than those composed of molybdenum, and the effect of the central atom is not as great as that of the addenda atoms. Nevertheless, phosphorus-based HPAs are slightly more acidic than silicon-based HPAs. This gives the general order of acidity as $\text{H}_3\text{PW}_{12}\text{O}_{40} > \text{H}_4\text{-SiW}_{12}\text{O}_{40}$ and $\text{H}_3\text{PW}_{12}\text{O}_{40} > \text{H}_4\text{PMo}_{12}\text{O}_{40}$.⁴⁸² A similar trend is found in gas-phase catalytic experiments.⁴⁸³

The surface area of solid HPA is generally very low (few m^2/g), and this makes protons accessible to the reactants very few. The salts of HPAs with large cations such as Cs^+ , K^+ , Rb^+ , and NH_4^+ , when obtained by precipitation from aqueous solution of the parent acid $\text{H}_3\text{PW}_{12}\text{O}_{40}$, are micro/mesoporous materials with much larger surface areas, up to $200 \text{ m}^2/\text{g}$. Thus, in the case of partial cation exchange, such as for $\text{Cs}_x\text{H}_{3-x}\text{PW}_{12}\text{O}_{40}$, the number of protons accessible to non-polar reactant molecules is very much enhanced, and in parallel also the catalytic activity is enhanced.

According to several studies, $\text{H}_3\text{PW}_{12}\text{O}_{40}$, one of the most stable and strongest acids in the Keggin series, has acid sites stronger than those of H-ZSM5 zeolite and even has superacidic centers as shown by adsorption calorimetry experiments.⁴⁸⁴ It has also been shown that its acid strength depends strongly on the presence of crystallization water: H_0 varies from -5.6 for $\text{H}_3\text{PW}_{12}\text{O}_{40} \cdot 10 \text{ H}_2\text{O}$ to -8.2 for $\text{H}_3\text{-PW}_{12}\text{O}_{40} \cdot 6 \text{ H}_2\text{O}$ to -12.8 for $\text{H}_3\text{PW}_{12}\text{O}_{40} \cdot (1-2) \text{ H}_2\text{O}$. In

agreement with this, it has been found that $\text{H}_3\text{PW}_{12}\text{O}_{40}$ and $\text{Cs}_{1.9}\text{H}_{1.1}\text{PW}_{12}\text{O}_{40}$ are very active for the isomerization of n-butane to isobutane at 473 K, but their catalytic activity decreased when small amounts of water were added.⁴⁸⁵ The Cs^+ forms of heteropolyacids are generally not soluble in water but can work as heterogeneous catalysts in liquid water or in liquid water/organic biphasic systems.^{240,452}

Dehydrated $\text{H}_3\text{PW}_{12}\text{O}_{40}$ shows a well-evident ^1H MAS NMR peak at 9 ppm, assigned to protons bonded to surface bridging oxygens of the anion.⁴⁸⁶ The IR spectrum shows a broad band centered at 3100 cm^{-1} , assigned to two families of H-bonded OH groups,^{487,488} although, based on the more recent work of Stoyanov et al.,⁴⁷³ both the NMR peak and the IR band could correspond to H_3O^+ . All protons are reported to be able to protonate pyridine up to forming py_2H^+ cations.⁴⁸⁸ In the hydrated form, the formation of a “pseudo-liquid phase” occurs, with the formation of H_5O_2^+ , corresponding to the disappearance of the NMR peak. Water molecules as well as acidic protons are nearly uniformly distributed in the solid.⁴⁸⁶ The location of protons, according to Uchida et al.,⁴⁸⁶ is schematized in Figure 36.

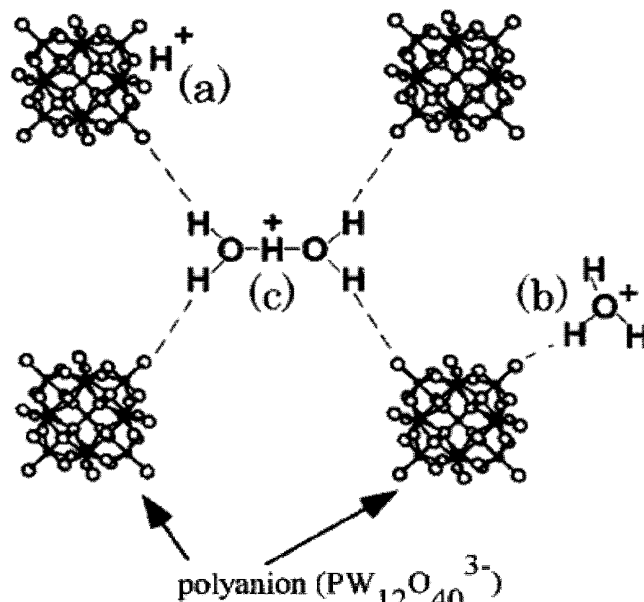


Figure 36. Protons in the acid $\text{H}_3\text{PW}_{12}\text{O}_{40}$ depending on hydration (taken from ref 486).

Solid HPAs are active as heterogeneous catalysts for several gas-phase and liquid-phase hydrocarbon conversion reactions^{489,479} and have been the subject of several theoretical investigations.⁴⁹⁰ However, their use in the industry for gas-phase reactions seems to be still very limited, if at all, possibly due to their rapid deactivation.⁴⁹¹ The commercial application of Cs-modified phosphotungstic and silicotungstic acids for the gas-phase esterification of ethylene to ethyl acetate has been reported.⁴⁵²

They have been used also industrially for the hydration of olefins to alcohols, such as the syntheses of isopropyl alcohol from propene and of *tert*-butyl alcohol from isobutylene²⁴⁰ and for the synthesis of poly(tetramethylene ether)-glycol from tetrahydrofuran.⁴⁵²

Other heteropolyacid structures exist besides Keggin-type phases. In particular, the so-called Wells–Dawson structures, with the $\text{H}_6\text{P}_2\text{W}_{18}\text{O}_{62} \cdot n \text{ H}_2\text{O}$ stoichiometry, also give rise to strong acid catalysts.^{492,493} The structure, known as the α isomer, possesses two identical “half-units” of the central

atom surrounded by nine octahedral units XM_9O_{31} linked through oxygen atoms. The isomeric β structure originates when a half-unit rotates $\pi/3$ around the $X-X$ -axis. Similarly to many heteropoly anions, the Wells–Dawson structure can be chemically manipulated to generate “holes” by removing up to six WO_6 units (from X_2M_{18} to X_2M_{12}). Wells–Dawson phosphotungstic acid $\text{H}_6\text{P}_2\text{W}_{18}\text{O}_{62}$ shows high acidity and performs as an effective catalyst in different reactions⁴⁹² such as MTBE synthesis and isobutane/butylene alkylation and may catalyze reactions in the liquid phase and in the gas phase.

6.3.5. Friedel–Crafts Type Solids

As already cited, the classical Friedel–Crafts chemistry implies liquid-phase catalysis mostly performed with metal chloride catalysts activated by proton donor species. Due to the severe drawbacks of these catalytic systems, the substitution of these systems with solid catalysts is under development.⁵⁷ In the field of refinery, catalysts based on solid halided aluminas have been used for decades.

6.3.5.1. Chlorided Alumina. Chloride ion at the surface of alumina, produced by adsorption of HCl or by surface decomposition of alkyl chlorides, or residual chloride ion from incomplete decomposition of AlCl_3 from the preparation method, or finally chloride ion from the deposition of AlCl_3 further enhances the acidity of alumina. As shown in Figure 37, the IR spectrum of the surface hydroxy groups is

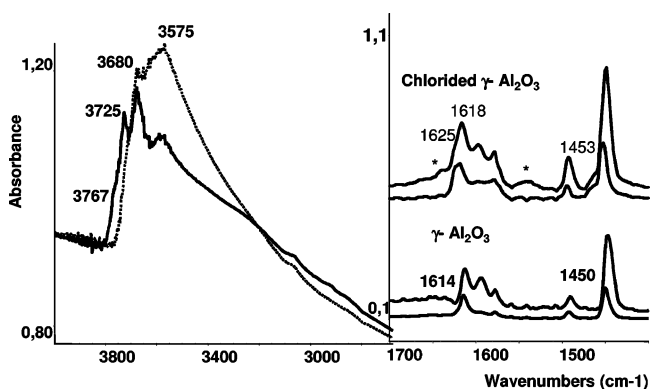


Figure 37. IR spectra of a commercial $\gamma\text{-Al}_2\text{O}_3$ sample from Condea (surface area = $174\text{ m}^2/\text{g}$) as such (solid line) and chlorided by treatment with ethyl chloride at $300\text{ }^\circ\text{C}$ (dotted line), both outgassed at $350\text{ }^\circ\text{C}$. (Inset) Adsorbed pyridine after outgassing at room temperature (upper) and $100\text{ }^\circ\text{C}$ (lower).

modified, with the disappearance of the higher frequency aluminas OH groups.^{106,135,494,495} Chlorided aluminas are very acidic materials, with a H_0 value evaluated to be around -14 ⁴⁹⁶ and high catalytic activity in demanding reactions, such as isobutane/butylene alkylation.⁴⁹⁷ The adsorption of pyridine (Figure 37) shows that, in the same conditions, more acidic Al^{3+} cations are formed on chlorided alumina (band at 1625 cm^{-1}) than on the parent $\gamma\text{-Al}_2\text{O}_3$ and that few Brønsted sites (absorption denoted by asterisks) able to protonate pyridine are also formed by chlorination.

Chlorided aluminas have been used for decades as the catalytically active support for Pt-based catalysts for naphtha re-forming^{498,499} as well as the catalyst for C4 and C5 paraffin skeletal isomerization.^{272,273} The chlorided alumina based catalysts require the continuous addition of small amounts of acidic chlorides to maintain high catalyst activities. In effect, chlorided hydrocarbons, such as alkyl chlorides,^{135,434}

trichloroethylene,⁵⁰⁰ and CCl_4 ,⁵⁰¹ decompose on alumina at $150\text{--}400\text{ }^\circ\text{C}$, producing HCl that is adsorbed on alumina.

For paraffin isomerization,^{272,273} the feed to these units must be free of water and other oxygen sources to avoid catalyst deactivation and potential corrosion problems. Catalysts are non-regenerable, their lifetimes being usually in the range of 2–3 years. However, they work at very low temperature ($150\text{--}200\text{ }^\circ\text{C}$), and this allows more favorable equilibrium conditions, so their performances are better than with MOR and MAZ zeolite-based catalysts or sulfated and tungstated zirconia.

In the catalytic re-forming process,^{498,499} which works at much higher temperature ($\sim 500\text{ }^\circ\text{C}$) with depentanized naphtha, the chlorided alumina support acts as the catalyst of skeletal isomerization of linear paraffins as well as of alkylcyclopentanes. Also in this case chlorine compounds are fed to allow a constant chlorine content in the catalyst.

Chlorided alumina is probably the basic component of the catalyst of the solid-catalyzed UOP alkylene process for isobutane/butylene alkylation to isooctane.⁵⁰² The catalyst should contain metals for the hydrogenation function and possibly alkali metal ions to moderate catalyst acidity, preventing excessive cracking and coking. After reaction occurring in a riser, the catalyst is disengaged and moves to the reactivation zone, where hydrogen is fed with isobutane, for hydrogenation and washing. Part of the catalyst is transported to a separate reactivation vessel where also regeneration occurs.⁵⁰² The reaction temperature is $10\text{--}40\text{ }^\circ\text{C}$, and the isobutane to olefin ratio in the reactor is 8–15.

Drawbacks common to these processes concern the difficult regenerability of the catalyst, the deliquescent behavior of aluminum chloride with the consequent leaching, corrosion, and disposal problems.

6.3.5.2. Aluminum Fluoride, Fluorided Alumina, and Solids Containing Boron Trifluoride. Fluorination of alumina with HF causes the progressive formation of AlF_3 polymorphs $\alpha\text{-AlF}_3$ more than $\beta\text{-AlF}_3$.⁵⁰³ Fluorided aluminas can also be prepared by impregnation of NH_4F followed by thermal decomposition. Aluminum fluoride and fluorided aluminas are perhaps the strongest Lewis acidic solids, as deduced by the adsorption of basic probes (ν_8a of pyridine at 1627 cm^{-1} , ν_{CN} of pivalonitrile at 2309 cm^{-1} ; Table 7). In parallel, both present also strong Brønsted acidity.^{504,505} AlF_3 catalysts show surface OH groups that are able to protonate pyridine and strong Lewis acid sites.⁵⁰⁶ Fluorination of alumina causes the progressive disappearance of the OH groups absorbing at 3790 and 3770 cm^{-1} , with the progressive growth of bands at 3730 and 3655 cm^{-1} .⁵⁰⁷ According to Corma et al.⁵⁰⁸ the total number of Lewis acid sites decreases when the fluorine content increases, whereas the number of sites with strong acidity exhibits a maximum for samples with 2–4% of fluorine content. Also, the number of Brønsted acid sites presents a maximum for the same fluorine content, despite the fact that only a small fraction of the sites created by fluorination exhibits strong acidity.

Aluminum fluoride and fluorided aluminas can be used at higher temperatures than chlorided aluminas and AlCl_3 . They are largely used industrially in the field of the chemistry of fluorocarbons and fluorochlorocarbons⁵⁰⁹ and have been proposed for several acid-catalyzed hydrocarbon conversions (such as benzene alkylation, where a very high selectivity to monoalkylated products has been claimed⁵⁰⁷) and as support for hydrodesulfurization catalysts.⁵¹⁰

BF₃ is also a very strong Lewis acidic compound, giving rise to Brønsted superacidic behavior with proton-donor species. Attempts to produce stable very acidic solids based on BF₃ have been reported in the literature. Impregnation of BF₃ onto alumina gives rise to solid acids, for which interesting activity in the isobutane/butylene alkylation has been found.³³ Similar materials have been apparently used in industrial ethylbenzene synthesis catalysis (Alkar UOP process).^{42,54} However, leaching of BF₃ and its reactivity with water to produce volatile compounds are relevant drawbacks.

6.3.5.3. Supported Liquid-Phase Catalysts. Attempts to produce acid solids based on liquid superacids are also in progress. The activity of triflic acid in isobutane/butylene alkylation has been studied by Olah and co-workers.⁵¹¹ Triflic acid supported on silica is used in the Haldor Topsøe FBA process of isobutane/butylenes alkylation.^{512,513} The reaction occurs at 273–293 K in a fixed bed reactor. The catalyst, however, may be withdrawn without stopping the production and transported in a regeneration unit. Traces of acid are leached into the product, which must be purified. A ¹H NMR study showed that the peak position of the triflic acid proton at 12 ppm is substantially unchanged in the case of the silica-supported catalyst until a water-to-acid molar ratio of 1, whereas it shifts to 10 ppm at higher water content, possibly according to the formation of the TFA·2H₂O complex. The IR OH stretching band is reported to be at 3397 cm⁻¹.⁵¹³

7. Conclusions

The data summarized in this review provide sufficient evidence of three main trends in the research and development on acid catalysis in the chemical industry. The first trend consists, as usual in industrial practice, in producing better performing catalytic materials, in order to obtain more efficient industrial chemical processes. With this in mind, the exploitation of liquid superacidity performing acid-catalyzed processes at low temperature and, if possible, improving selectivity, is an evident target. This could also allow a more extensive use of poorly reactive paraffins for chemical processes, in substitution of the more reactive, but more expensive, olefins. From this perspective, the development of acidic ionic liquids seems to be quite promising. However, not all newly investigated and apparently promising materials also show promise in terms of safety and environmental friendliness.

A second trend is certainly related to the efforts in improving the safety and environmental friendliness of industrial processes. This is quite evident considering the progressive evolution of the industrial catalysts from the very first pollutant and corrosive liquid catalysts (such as sulfuric acid and aluminum chloride-based liquids) to more easily recoverable (but dangerous) liquids (HF), then to deliquescent solids still presenting some pollution and corrosion problems (such as chlorided aluminas and solid phosphoric acid), and finally to more environmentally friendly solids such as zeolites and, when possible, clays. These solid materials are in fact fully recoverable⁵¹⁴ and easily separable from the reactant mixture. They can also be regenerated with several lifecycles and can be disposed of with less concern. All of these efforts have been successfully included in several relevant industrial processes. For example, considering the field of aromatics alkylation processes, such as ethylbenzene and cumene syntheses, the introduction of zeolite catalysts established new processes that are not only safer and more environmentally friendly but also more efficient.

There are, however, less successful examples. Attempts to develop new solid-catalyzed processes for the production of alkylate gasoline have not been very successful, so far. In fact, new solid catalytic materials such as those based on chlorided alumina and supported triflic acid are probably not that valid in terms of environmental friendliness. In any case, the practical application of solid catalysts for isobutane/butylene alkylation, even in the case of the zeolite-based ones, is still at the initial stage now, and a conclusive evaluation of the performances is still premature. In the case of paraffin isomerization, the development of metal oxides (such as WO₃–ZrO₂) and of zeolite-based catalysts allowed a clear improvement of the environmental friendliness of the process. However, these new catalysts are less active than the previous ones based on chlorided alumina.

The third trend consists in developing new acid-catalyzed processes able to produce new useful organic chemicals or better products or to transform different raw materials. This is the case, for example, of the several efforts aimed toward the production of reformulated and less polluting fuels. The recent development of new processes such as olefin oligomerization to diesel fuels, hydrodearomatization and ring opening of gasoils to improve the quality of diesel fuels, and hydrodesulfurization and octane gain of FCC gasolines, has been obtained with the development of new catalysts and fine-tuning of their activity and properties, including acidity. This is certainly a field that may change in the near future its goals, with the more extensive use of biomasses, and perhaps also with the return to coal, as the raw materials for fuels and chemicals.

As always, the efforts of developing new catalysts goes together with the development of new processes and new reactor solutions. This is the case, for example, of the development of different cyclic reaction/catalyst regeneration systems, that is, those used for catalytic cracking and catalytic re-forming, and more recently catalytic dehydrogenation of paraffins and isobutane/butylenes alkylation. This is also the case of the development of processes based on the shift of the alkylation and transalkylation steps in the case of benzene alkylations and, similarly, the more extensive use of catalytic distillation reactors, as well as of complex reactors in which different catalytic beds perform different reactions (such as isomerization and hydrogenation).

Acid catalysis has been a crucial discipline in the industrial organic chemistry of oil refining and petrochemistry, giving a unique contribution to the development of greener chemical processes. Its role will be also relevant in the consolidation of a new industrial organic chemistry based on renewables.

8. References

- (1) Smil, V. *Energy in the World History*; Westview Press: Boulder, CO, 1994.
- (2) Olah, G. A.; Molnár, A. *Hydrocarbon Chemistry*, 2nd ed.; Wiley: New York, 2003.
- (3) Arrhenius, S. A. Recherches sur la conductibilité galvanique des électrolytes. Ph.D. thesis, University of Uppsala, Sweden, 1984. Arrhenius, S. A. *Z. Phys. Chem.* **1887**, *1*, 631.
- (4) Brønsted, J. N. *Recl. Trav. Chim. Pays Bas* **1923**, *42*, 718.
- (5) Lowry, T. M. *Chim. Ind. (London)* **1923**, *42*, 43. Lowry, T. M. *Trans. Faraday Soc.* **1924**, *20*, 13.
- (6) Lewis, G. N. *Valency and Structure of Atoms and Molecules*; Wiley: New York, 1923.
- (7) Atkins, P. N. *Physical Chemistry*; Oxford University Press: Oxford, U.K., 1997; p 294.
- (8) Kazansky, V. B. *Topics Catal.* **2000**, *11/12*, 55.
- (9) Hammett, L. P. *Physical Organic Chemistry*; McGraw-Hill: New York, 1940.
- (10) Fărcașiu, D.; Ghenciu, A. *J. Am. Chem. Soc.* **1993**, *115*, 10901.

- (11) Stoyanov, E. S.; Kim, K. C.; Reed, C. A. *J. Am. Chem. Soc.* **2006**, *128*, 8500.
- (12) Hall, N. F.; Conant, J. B. *J. Am. Chem. Soc.* **1927**, *49*, 3047.
- (13) Gillespie, R. J. *Acc. Chem. Res.* **1968**, *1*, 202.
- (14) Olah, G. A.; Prakash, G. K.; Sommer, J. *Superacids*; Wiley: New York, 1985.
- (15) Olah, G. A. *J. Org. Chem.* **2005**, *70*, 2413.
- (16) Olah, G. A. *J. Org. Chem.* **2001**, *66*, 5943.
- (17) Reed, C. A.; Kim, K. C.; Bolskar, R. D.; Mueller, L. *Science* **2000**, *289*, 101.
- (18) Reed, C. A. *Chem. Commun.* **2005**, 1669.
- (19) Pearson, R. G. *J. Am. Chem. Soc.* **1963**, *85*, 3533.
- (20) Pearson, R. G. *Acc. Chem. Res.* **1993**, *26*, 250.
- (21) Bartmess, J. E.; McIver, R. T. In *Gas Phase Ion Chemistry*; Aue, D. H., Bowers, M. T., Eds.; Academic Press: New York, 1979; Vol. 2, p 87.
- (22) www.nist.org.
- (23) Dewar, M. J. *J. Chem. Soc.* **1946**, 406.
- (24) Vogel, P. *Carbocation Chemistry*; Elsevier: New York, 1985.
- (25) Kilpatrick, M.; Luborsky, F. E. *J. Am. Chem. Soc.* **1953**, *75*, 577.
- (26) Olah, G. A.; Schlosberg, R. H. *J. Am. Chem. Soc.* **1968**, *90*, 2726.
- (27) Hogeveen, H.; Bickel, A. *Recl. Trav. Chim. Pays-Bas* **1967**, *86*, 1313.
- (28) Olah, G. A.; Prakash, G. K.; Sommer, J. *Science* **1979**, *206*, 13.
- (29) Esteves, P. M.; Ramirez-Solis, A.; Mota, C. J. A. *J. Phys. Chem. B* **2001**, *105*, 4331.
- (30) Sommer, J.; Jost, R. *Pure Appl. Chem.* **2000**, *72*, 2309.
- (31) Francis, A. W. *Ind. Eng. Chem.* **1928**, *20*, 277.
- (32) Farcasiu, D.; Ghenciu, A. *J. Am. Chem. Soc.* **1993**, *115*, 10901.
- (33) Feller, A.; Lercher, J. A. *Adv. Catal.* **2004**, *48*, 229.
- (34) http://www.stratco.dupont.com/alk/alkylation_02.html.
- (35) <http://www.exxonmobil.com/refiningtechnologies/index.html>.
- (36) Shorey, S. W. Motor fuel alkylation with CDAlkySM Process technology, <http://www.cdtech.com>.
- (37) Malone, M. F.; Huss, R. S.; Doherty, M. F. *Environ. Sci. Technol.* **2003**, *37*, 5325.
- (38) Albright, L. F. *Ind. Eng. Chem. Res.* **2002**, *41*, 5627.
- (39) <http://www.topsoe.com>.
- (40) Sillanpää, A. J.; Simon, C.; Klein, M. L.; Laasonen, K. *J. Phys. Chem. B* **2002**, *106*, 11315.
- (41) Esteves, P. M.; Ramirez-Solis, A.; Mota, C. J. A. *J. Am. Chem. Soc.* **2002**, *124*, 2672.
- (42) Frank, H. G.; Stadelhofer, J. W. *Industrial Aromatic Chemistry*; Springer-Verlag: Berlin, Germany, 1988.
- (43) Olson, A. C. *Ind. Eng. Chem.* **1960**, *52*, 833.
- (44) http://www.fuelstechnology.com/soft_processoverview.htm.
- (45) Olah, G. A.; Nojima, M.; Kerekes, I. *Synthesis* **1973**, 779, 780.
- (46) Olah, G. A.; Mathew, T.; Goeppert, A.; Török, B.; Bucsi, I.; Li, X.-Y.; Wang, Q.; Marinez, E. R.; Batamack, P.; Aniszfeld, R.; Surya Prakash, G. K. *J. Am. Chem. Soc.* **2005**, *127*, 5964.
- (47) Nowak, F. M.; Himes, J. F.; Mehlberg, R. L. Advances in hydrofluoric acid (HF) catalyzed alkylation, <http://www.uop.com/objects/NPRASpr2003HFAlky.pdf>.
- (48) Kirschner, B.; Seitsonen, A. P.; Hutter, J. *J. Phys. Chem. B* **2006**, *110*, 11475.
- (49) Evering, B. L. *Adv. Catal. Relat. Subj.* **1954**, *6*, 197.
- (50) Conrad Zhang, Z. *Adv. Catal.* **2006**, *40*, 153.
- (51) Smith, G. P.; Dworkin, A. S.; Pagni, R. M.; Zingg, S. P. *J. Am. Chem. Soc.* **1989**, *111*, 525.
- (52) Zhao, Z. K.; Quiao, W. H.; Li, Z. S.; Wang G. R.; Cheng, L. B. *J. Mol. Catal. A: Chem.* **2004**, *222*, 207.
- (53) Tarakeshvar, P.; Lee, J. Y.; Kim, K. S. *J. Phys. Chem. A* **1998**, *102*, 2253.
- (54) Stefanidakis, G.; Gwin, J. E. In *Chemical Processing Handbook*; McKetta, J. J., Ed.; Dekker: New York, 1993; p 80.
- (55) Chianese, A.; Annesini, M. C.; De Santis, R.; Marrelli, L. *Chem. Eng. J.* **1981**, *22*, 151.
- (56) U.S. Patent 4554383.
- (57) Sartori, G.; Maggi, R. *Chem. Rev.* **2006**, *106*, 1077.
- (58) Albright, L. F.; Eckert, R. E. *Ind. Eng. Chem. Res.* **2001**, *40*, 4032.
- (59) Brilman, D. W. F.; van Swaaij, W. P. M.; Versteeg, G. F. *Ind. Eng. Chem. Res.* **1997**, *36*, 4638.
- (60) Taft, R. W., Jr. *J. Am. Chem. Soc.* **1952**, *74*, 5372.
- (61) Carrizales-Martínez, G.; Fermat, R.; González-Alvarez, V. *Chem. Eng. J.* **2006**, *125*, 89.
- (62) Lee, B.-C.; Outcalt, S. L. *J. Chem. Eng. Data* **2006**, *51*, 892.
- (63) Camper, D.; Becker, C.; Koval, C.; Noble, R. *Ind. Eng. Chem. Res.* **2006**, *45*, 445.
- (64) Imelik B., Vedrine, J. C., Eds. *Catalyst Characterisation, Physical Techniques for Solid Materials*; Plenum Press: New York, 1994.
- (65) Knözinger, H. In *Handbook of Heterogeneous Catalysis*; Ertl, G., Knözinger, H., Weitkamp, J., Eds.; Wiley-VCH: Weinheim, 1997; Vol. 2, pp 707–732.
- (66) Busca, G. In *Metal Oxides: Chemistry and Applications*; Fierro, J. L. G., Ed.; CRC Press: Boca Raton, FL, 2005; p 247.
- (67) Sun, C.; Berg, J. C. *Adv. Colloids Interface Sci.* **2003**, *105*, 151.
- (68) Auroux, A. *Topics Catal.* **2002**, *19*, 205.
- (69) Niwa, M.; Katada, N. *Catal. Surv. Jpn.* **1997**, *1*, 215.
- (70) Busca, G. *Phys. Chem. Chem. Phys.* **1999**, *1*, 723.
- (71) Busca, G. *Catal. Today* **1998**, *41*, 191.
- (72) Haw, J. F.; Teng, X. *Adv. Catal.* **1998**, *42*, 115.
- (73) Hunger, M.; Weitkamp, J. In *In Situ Spectroscopy of Catalysts*; Weckhuysen, B. M., Ed.; American Scientific Publishers: Stevenson Ranch, CA, 2004; p 166.
- (74) Ganapathy, S.; Kumar, R.; Delevoye, L.; Amoureux, J. P. *Chem. Commun.* **2003**, 2076.
- (75) Gorte, R. J. *Catal. Lett.* **1999**, *62*, 1.
- (76) Bellamy, L. J.; Hallam, H. E.; Williams, R. E. *Trans. Faraday Soc.* **1958**, *54*, 1120.
- (77) Paukshtis, E. A.; Yurchenko, E. N. *Russ. Chem. Rev. Engl. Transl.* **1983**, *52*, 242.
- (78) Pazé, C.; Bordiga, S.; Lamberti, C.; Salvalaggio, M.; Zecchina, A.; Bellussi, G. *J. Phys. Chem. B* **1997**, *101*, 4740.
- (79) Teunissen, E. H.; van Santen, R. A.; Janssen, A. P. J.; van Duijneveldt, F. B. *J. Phys. Chem.* **1993**, *97*, 203.
- (80) Onida, B.; Monelli, B.; Borello, L.; Fiorilli, S.; Geobaldo, F.; Garrone, E. *J. Phys. Chem. B* **2002**, *106*, 10518.
- (81) Bolis, V.; Broyer, M.; Barbaglia, A.; Busco, C.; Foddanu, G. M.; Ugliengo, P. *J. Mol. Catal. A: Chem.* **2003**, *204–205*, 561.
- (82) Benesi, H. A.; Winquist, B. H. C. *Adv. Catal.* **1978**, *27*, 97.
- (83) Tanabe, K.; Misono, M.; Ono, Y.; Hattori, H. *New Solid Acids and Bases, Their Catalytic Properties*; Elsevier: Amsterdam, The Netherlands, 1989.
- (84) Corma, A. *Chem. Rev.* **1995**, *95*, 559.
- (85) Roberie, T. G.; Hildebrandt, D.; Creighton, J.; Gilson, J. P. In *Zeolites for Cleaner Technologies*; Guisnet, M., Gilson, J. P., Eds.; Imperial College Press: London, U.K., 2002; p 57.
- (86) Sie, S. T. *Appl. Catal. A: Gen.* **2001**, *212*, 129.
- (87) Avidan, A. A.; Shinnar, R. *Ind. Eng. Chem. Res.* **1990**, *29*, 931.
- (88) Sanfilippo, D.; Miracca, I. *Catal. Today* **2006**, *111*, 133.
- (89) Griffen, D. T. *Silicate Crystal Chemistry*; Oxford University Press: Oxford, U.K., 1992.
- (90) Vogel, W. *Chemistry of Glass*; American Ceramic Society: Columbus, OH, 1985.
- (91) Dorémieux-Morin, C.; Heeribout, L.; Dumousseaux, C.; Fraissard, J.; Hommel, H.; Legraud, A. P. *J. Am. Chem. Soc.* **1996**, *118*, 13040.
- (92) Trombetta, M.; Busca, G.; Rossini, S.; Piccoli, V.; Cornaro, U.; Guercio, A.; Catani, R.; Willey, R. J. *J. Catal.* **1998**, *179*, 581.
- (93) Dijkstra, T. W.; Duchateau, R.; van Santen, R. A.; Meetsma, A.; Yap, G. P. A. *J. Am. Chem. Soc.* **2002**, *124*, 9856.
- (94) Bevilacqua, M.; Montanari, T.; Finocchio, E.; Busca, G. *Catal. Today* **2006**, *116*, 132.
- (95) Marrone, M.; Montanari, T.; Busca, G.; Conzatti, L.; Costa, G.; Castellano, M.; Turturro, A. *J. Phys. Chem. B* **2004**, *108*, 3563.
- (96) Astorino, E.; Peri, J.; Willey, R. J.; Busca, G. *J. Catal.* **1995**, *157*, 482.
- (97) Zecchina, A.; Bordiga, S.; Spoto, G.; Marchese, L.; Petrini, G.; Leofanti, G.; Padovan, M. *J. Phys. Chem.* **1992**, *96*, 4991.
- (98) Flego, C.; Dalloro, L. *Micropor. Mesopor. Mater.* **2003**, *60*, 263.
- (99) Heitmann, G. P.; Dahlhoff, G.; Hölderich, W. F. *J. Catal.* **1999**, *186*, 12.
- (100) Cambor, M. A.; Corma, A.; Diaz-Caban, M.-J.; Baerlocher, C. *J. Phys. Chem. B* **1998**, *102*, 44.
- (101) Corma, A.; Rey, F.; Rius, J.; Sabater, M. J.; Valencia, S. *Nature* **2004**, *431*, 287.
- (102) Fernández, A.-B.; Marinas, A.; Blasco, T.; Fornés, V.; Corma, A. *J. Catal.* **2006**, *243*, 270.
- (103) Wefers, K.; Misra, C. *Oxides and Hydroxides of Aluminum*; Alcoa: Pittsburgh, PA, 1987.
- (104) Oberlander, R. K. In *Applied Industrial Catalysis*; Leach, B. E., Ed.; Academic Press: New York, 1984; Vol. 3, p 64.
- (105) Berty, J. M. In *Applied Industrial Catalysis*; Leach, B. E., Ed.; Academic Press: New York, 1984; Vol. 1, p 207.
- (106) Lavalley, J. C.; Benaissa, M.; Busca, G.; Lorenzelli, V. *Appl. Catal.* **1986**, *24*, 249.
- (107) Zhang, Z.; Hicks, R. W.; Pauly, T. R.; Pinnavaia, T. J. *J. Am. Chem. Soc.* **2002**, *124*, 1592.
- (108) Lippens, B. C.; de Boer, J. H. *Acta Crystallogr.* **1964**, *17*, 1312.
- (109) Chen, F. R.; Davis, J. G.; Fripiat, J. J. *J. Catal.* **1992**, *133*, 263.
- (110) Soled, S. *J. Catal.* **1983**, *81*, 252.
- (111) Zhou, R. S.; Snyder, R. L. *Acta Crystallogr. B* **1991**, *47*, 617.
- (112) Tsyganenko, A. A.; Smirnov, K. S.; Rzhavskij, A. M.; Mardilovich, P. P. *Mater. Chem. Phys.* **1990**, *26*, 35.
- (113) Wolverton, C.; Hass, K. C. *Phys. Rev. B* **2001**, *63*, 24102.
- (114) Sohlberg, K.; Pantelides, T. S.; Pennycook, S. J. *J. Am. Chem. Soc.* **2001**, *123*, 26.

- (115) Sohlberg, K.; Pennycook, S. J.; Pantelides, T. S. *Chem. Eng. Commun.* **2000**, *181*, 107.
- (116) Digne, M. Ph.D. thesis, Ecole Normale Supérieure de Lyon.
- (117) Krokididis, X.; Raybaud, P.; Gobichon, A.-E.; Rebours, B.; Euzen, P.; Toulhoat, H. *J. Phys. Chem. B* **2001**, *105*, 5121.
- (118) Wilson, S. J.; Mc Connel, J. D. C. *J. Solid State Chem.* **1980**, *34*, 35.
- (119) Hyde, B. G.; Andersson, S. *Inorganic Crystal Structures*; Wiley: New York, 1989; p 156.
- (120) John, C. S.; Alma, N. C. M.; Hays, G. R. *Appl. Catal.* **1983**, *6*, 341.
- (121) Pechartroman, C.; Sobrados, I.; Iglesias, J. E.; Gonzales, Carreno, T.; Sanz, J. *J. Phys. Chem. B* **1999**, *103*, 6160.
- (122) Abbattista, F.; Delmastro, S.; Gozzelino, G.; Mazza, D.; Vallino, M.; Busca, G.; Lorenzelli, V.; Ramis, G. *J. Catal.* **1989**, *117*, 42.
- (123) Cocke, D. L.; Johnson, E. D.; Merrill, R. P. *Catal. Rev. Sci. Eng.* **1984**, *26*, 163.
- (124) Dumesic, J. A.; Fripiat, J. J., Eds. Acidity in aluminas, amorphous and crystalline silico-aluminates. *Topics Catal.* **1997**, *4*.
- (125) Morterra, C.; Magnacca, G. *Catal. Today* **1996**, *27*, 497.
- (126) Auroux, A.; Gervasini, A. *J. Phys. Chem.* **1990**, *94*, 6371.
- (127) Bolis, V.; Cerrato, G.; Magnacca, G.; Morterra, C. *Thermochim. Acta* **1998**, *312*, 63.
- (128) Guillaume, D.; Gautier, S.; Despujol, J.; Alario, F.; Beccat, P. *Catal. Lett.* **1997**, *4*, 213.
- (129) Liu, X.; Truitt, R. E. *J. Am. Chem. Soc.* **1997**, *119*, 9856.
- (130) Lundie, D. T.; McInroy, A. R.; Marshall, R.; Winfield, J. M.; Jones, P.; Dudman, C. C.; Parker, S. F.; Mitchell, C.; Lennon, D. *J. Phys. Chem. B* **2005**, *109*, 11592.
- (131) Busca, G.; Rossi, P. F.; Lorenzelli, V.; Benaissa, M.; Travet, J.; Lavalley, J. C. *J. Phys. Chem.* **1985**, *89*, 5433.
- (132) Knözinger, H.; Krietenbrink, H.; Müller, H. D.; Schulz, W. *Proceedings of the 6th International Congress on Catalysis*, London, 1976; p 183.
- (133) Busca, G. *Catal. Today* **1996**, *27*, 457.
- (134) Pistarino, C.; Finocchio, E.; Romezzano, G.; Bricchese, F.; DiFelice, R.; Busca, G.; Baldi, M. *Ind. Eng. Chem. Res.* **2000**, *39*, 2752.
- (135) Carmello, D.; Finocchio, E.; Marsella, A.; Cremaschi, B.; Leofanti, G.; Padovan, M.; Busca, G. *J. Catal.* **2000**, *191*, 354.
- (136) Busca, G.; Finocchio, E.; Lorenzelli, V.; Trombetta, M.; Rossini, S. A. *J. Chem. Soc., Faraday Trans.* **1996**, *92*, 4687.
- (137) Hong, Y.; Chen, F. R.; Fripiat, J. J. *Catal. Lett.* **1993**, *17*, 187.
- (138) Peri, J. B. *J. Phys. Chem.* **1965**, *69*, 211.
- (139) Tsyganenko, A.; Filimonov, V. N. *Spectrosc. Lett.* **1972**, *5*, 477.
- (140) Knözinger, H.; Ratnasamy, P. *Catal. Rev. Sci. Eng.* **1978**, *17*, 31.
- (141) Busca, G.; Lorenzelli, V.; Ramis, G.; Willey, R. J. *Langmuir* **1993**, *9*, 1492.
- (142) Busca, G.; Lorenzelli, V.; Sanchez Escribano, V.; Guidetti, R. *J. Catal.* **1991**, *131*, 167.
- (143) Tsyganenko, A. A.; Mardilovich, P. P. *J. Chem. Soc., Faraday Trans.* **1996**, *92*, 4843.
- (144) Fripiat, J.; Alvarez, L.; Sanchez Sanchez, S.; Martinez Morades, E.; Saniger, J.; Sanchez, N. *Appl. Catal. A: Gen.* **2001**, *215*, 91.
- (145) Digne, M.; Sautet, P.; Raybaud, P.; Euzen, P.; Toulhoat, H. *J. Catal.* **2002**, *211*, 1.
- (146) Lambert, J. F.; Che, M. *J. Mol. Catal. A: Chem.* **2000**, *162*, 5.
- (147) Malpartida, I.; Larrubia Vargas, M. A.; Alemany, L. J.; Finocchio, E.; Busca, G. *Appl. Catal., B*, in press, and unpublished results from this laboratory.
- (148) Tretyakov, N. E.; Filimonov, V. N. *Kinet. Katal.* **1972**, *13*, 815.
- (149) Trombetta, M.; Busca, G.; Rossini, S.; Piccoli, V.; Cornaro, U. *J. Catal.* **1997**, *168*, 334.
- (150) Mohammed Saad, A. B.; Ivanov, V. A.; Lavalley, J. C.; Nortier, P.; Luck, F. *Appl. Catal. A: Gen.* **1993**, *94*, 71.
- (151) Pines, H.; Manassen, J. *Adv. Catal. Relat. Subj.* **1966**, *16*, 49.
- (152) Hu, Y. C. In *Chemical Processing Handbook*; McKetta, J. J., Ed.; Dekker: New York, 1993; p 768.
- (153) Liu, Z.; Sun, C.; Wang, G.; Wang, Q.; Cai, G. *Fuel Process. Technol.* **2000**, *62*, 161.
- (154) HF alkylation process, <http://www.engelhard.com>.
- (155) Okada, K.; Otsuka, N. *J. Am. Ceram. Soc.* **1986**, *69*, 652.
- (156) Barrer, R. M. *Zeolites and Clay Minerals as Sorbents and Molecular Sieves*; Academic Press: New York, 1978.
- (157) Chen, N. Y.; Garwood, W. E.; Dwyer, F. G. *Shape Selective Catalysis in Industrial Applications*, 2nd ed.; Dekker: New York, 1996.
- (158) Guisnet, M.; Gilson, J. P., Eds. *Zeolites for Cleaner Technologies*; Imperial College Press: London, U.K., 2002.
- (159) Beck, L. W.; Davis, M. E. *Micropor. Mesopor. Mater.* **1998**, *22*, 107.
- (160) Baerlocher, Ch.; McCusker, L. B. *Database of Zeolite Structures*, <http://www.iza-structure.org/databases>.
- (161) Baerlocher, Ch.; Meier, W. M.; Olson, D. H. *Atlas of Zeolite Framework Types*, 5th ed.; Elsevier: Amsterdam, The Netherlands, 2001.
- (162) Sherman, J. D. *Proc. Natl. Acad. Sci. U.S.A.* **1999**, *96*, 3471.
- (163) Armaroli, T.; Simon, L. J.; Digne, M.; Montanari, T.; Bevilacqua, M.; Valtchev, V.; Patarin, J.; Busca, G. *Appl. Catal. A: Gen.* **2006**, *306*, 78.
- (164) Kim, J.-H.; Kunieda, T.; Niwa, M. *J. Catal.* **1998**, *173*, 433.
- (165) Kunieda, T.; Kim, J.-H.; Niwa, M. *J. Catal.* **1999**, *188*, 431.
- (166) Eichler, U.; Brändle, M.; Sauer, J. *J. Phys. Chem. B* **1997**, *101*, 10035.
- (167) Schroder, K. P.; Sauer, J.; Leslie, M.; Catlow, C. R. A.; Thomas, J. M. *Chem. Phys. Lett.* **1992**, *188*, 320.
- (168) Domokos, L.; Lefferts, L.; Seshan, K.; Lercher, J. A. *J. Mol. Catal. A: Chem.* **2000**, *162*, 147.
- (169) Regli, L.; Zecchina, A.; Vitillo, J. G.; Cocina, D.; Spoto, G.; Lamberti, C.; Lillerud, K. P.; Olsbye, U.; Bordiga, S. *Phys. Chem. Chem. Phys.* **2005**, *7*, 3197.
- (170) Hunger, M. *Catal. Rev. Sci. Eng.* **1997**, *39*, 345.
- (171) Haw, J. F. *Phys. Chem. Chem. Phys.* **2002**, *4*, 5431.
- (172) Huang, J.; Jiang, Y.; Marthala, V. R. R.; Wang, W.; Sulikowski B.; Hunger, M. *Micropor. Mesopor. Mater.* **2007**, *99*, 86.
- (173) Simperler, A.; Bell, R. G.; Anderson, M. W. *J. Phys. Chem. B* **2004**, *108*, 7142.
- (174) Kazansky, V. B.; Seryk, A. I.; Semmer-Herledan, V.; Fraissard, J. *Phys. Chem. Chem. Phys.* **2003**, *5*, 966.
- (175) Miyamoto, Y.; Takada, N.; Niwa, M. *Micropor. Mesopor. Mater.* **2000**, *40*, 271.
- (176) Kotrel, S.; Rosynek, M. P.; Lunsford, J. H. *J. Catal.* **1999**, *182*, 278.
- (177) Corma, A.; Fornés, V.; Forni, L.; Marquez, F.; Martinez-Triguero, J.; Moschetti, D. *J. Catal.* **1998**, *179*, 451.
- (178) Trombetta, M.; Busca, G.; Storaro, L.; Lenarda, M.; Casagrande, M.; Zambon, A. *Phys. Chem. Chem. Phys.* **2000**, *2*, 3529.
- (179) Farcasiu, D.; Leu, R.; Corma, A. *J. Phys. Chem. B* **2002**, *106*, 928.
- (180) Zecchina, A.; Bordiga, S.; Spoto, G.; Scarano, D.; Spanò, G.; Geobaldo, F. *J. Chem. Soc., Faraday Trans.* **1996**, *92*, 4863.
- (181) Zecchina, A.; Geobaldo, F.; Spoto, G.; Bordiga, S.; Ricchiardi, G.; Buzzoni, R.; Petrini, G. *J. Phys. Chem.* **1996**, *100*, 16584.
- (182) Auroux, A. *Topics Catal.* **2002**, *19*, 205.
- (183) Miyamoto, Y.; Takada, N.; Niwa, M. *Micropor. Mesopor. Mater.* **2000**, *40*, 271.
- (184) Thibault-Starzyk, F.; Travet, A.; Saussey, J.; Lavalley, J. C. *Topics Catal.* **1998**, *6*, 111.
- (185) Lonyi, F.; Kovacs, A.; Valyon, J. *J. Phys. Chem. B* **2006**, *110*, 1711.
- (186) Brandle, M.; Sauer, J. *J. Am. Chem. Soc.* **1998**, *120*, 1556.
- (187) Walspurger, S.; Sun, Y.; Sido, A. S. S.; Sommer, J. *J. Phys. Chem. B* **2006**, *110*, 18368.
- (188) Xu, B.; Sievers, C.; Hong, S. B.; Prins, R.; van Bokhoven, J. A. *J. Catal.* **2006**, *244*, 163.
- (189) Paparatto, G.; Moretti, E.; Leofanti, G.; Gatti, F. *J. Catal.* **1987**, *105*, 227.
- (190) Trombetta, M.; Busca, G.; Lenarda, M.; Storaro, L.; Pavan, M. *Appl. Catal. A: Gen.* **1999**, *182*, 225.
- (191) Trombetta, M.; Busca, G. *J. Catal.* **1999**, *187*, 521
- (192) Trombetta, M.; Armaroli, T.; Gutiérrez-Alejandre, A.; Ramirez, J.; Busca, G. *Appl. Catal. A: Gen.* **2000**, *192*, 125.
- (193) Montanari, T.; Bevilacqua, M.; Busca, G. *Appl. Catal. A: Gen.* **2006**, *307*, 21.
- (194) Armaroli, A.; Bevilacqua, M.; Trombetta, M.; Gutiérrez-Alejandre, A.; Ramirez, J.; Busca, G. *Appl. Catal. A: Gen.* **2001**, *220*, 181.
- (195) Otero Arean, C.; Escalona Platero, E.; Penarroya Mentruit, M.; Rodriguez Delgado, M.; Llabbres Xamena, F. X.; Garcia Raso, A.; Morterra, C. *Micropor. Mesopor. Mater.* **2000**, *34*, 55.
- (196) Corma, A.; Diaz, U.; Fornés, V.; Guil, J. M.; Martínez-Triguero, J.; Creighton, E. J. *J. Catal.* **2000**, *191*, 218.
- (197) Onida, B.; Borello, L.; Monelli, B.; Geobaldo, F.; Garrone, E. *J. Catal.* **2003**, *214*, 191.
- (198) Gora-Marek, K.; Datka, J. *Stud. Surf. Sci. Catal.* **2005**, *158*, A, 837.
- (199) Van Bokhoven, J. A.; van der Eerden, A. M. J.; Koningsberger, D. C. *J. Am. Chem. Soc.* **2003**, *125*, 7435.
- (200) Halgeri, A. B.; Das, J. *Catal. Today* **2002**, *73*, 65.
- (201) Borzatta, V.; Busca, G.; Poluzzi, E.; Rossetti, V.; Trombetta, M.; Vaccari, A. *Appl. Catal. A: Gen.* **2004**, *257*, 85.
- (202) Montanari, T.; Herrera Delgado, M. C.; Bevilacqua, M.; Busca, G.; Larrubia Vargas, M. A.; Alemany, L. J. *J. Phys. Chem. B* **2005**, *109*, 879.
- (203) Hsia Chen, C. S.; Bridger, R. F. *J. Catal.* **1996**, *161*, 687.
- (204) Mériaudeau, P.; Naccache, C. *Adv. Catal.* **1999**, *44*, 505.
- (205) Van Bokhoven, J. A.; Tromp, M.; Koningsberger, D. C.; Miller, J. T.; Pieterse, J. A. Z.; Lercher, J. A.; Williams, B. A.; Kung, H. H. *J. Catal.* **2001**, *202*, 129.
- (206) Remy, M. J.; Stanica, D.; Poncelet, G.; Feijen, E. J. P.; Grobet, P. *J. Phys. Chem.* **1996**, *100*, 12440.
- (207) Bevilacqua, M.; Busca, G. *Catal. Commun.* **2002**, *3*, 497.
- (208) Trombetta, M.; Armaroli, T.; Gutiérrez-Alejandre, A.; Gonzalez, H.; Ramirez Solis, J.; Busca, G. *Catal. Today* **2001**, *65*, 285.

- (209) Zecchina, A.; Marchese, L.; Bordiga, S.; Gianotti, E. *J. Phys. Chem. B* **1997**, *101*, 10128.
- (210) Sanchez Escribano, V.; Montanari T.; Busca, G. *Appl. Catal. B, Environ.* **2005**, *58*, 19.
- (211) Jobic, H.; Tuel, A.; Krossner, M.; Sauer, J. *J. Phys. Chem.* **1996**, *100*, 19545.
- (212) Jungsuttiwong, S.; Limtrakul, J.; Truong, T. N. *J. Phys. Chem. B* **2005**, *109*, 13342.
- (213) Bhan, A.; Joshi, Y. V.; Delgass, W. N.; Thomson, K. T. *J. Phys. Chem. B* **2003**, *107*, 10476.
- (214) Trombetta, M.; Busca, G.; Rossini, S. A.; Piccoli, V.; Cornaro, U. *J. Catal.* **1997**, *168*, 349.
- (215) Arstad, B.; Kolboe, S.; Swang, O. *J. Phys. Chem. B* **2004**, *108*, 2300.
- (216) Derouane, E. G.; Chang, C. D. *Micropor. Mesopor. Mater.* **2000**, *35–36*, 425.
- (217) Martucci, A.; Alberti, A.; Cruciani, G.; Radaelli, P.; Ciambelli, P.; Rapacciuolo, M. *Microporous Mesoporous Mater.* **1999**, *30*, 95.
- (218) Pazè, C.; Zecchina, A.; Spera, S.; Spano, G.; Rivetti, F. *Phys. Chem. Chem. Phys.* **2000**, *2*, 5756.
- (219) Grandvallet, P.; DeJong, K. P.; Mooiweer, H. H.; Kortbeek, A. G. T. G.; Krausaar- Czarnetki, B. EP Patent 501577, 1992.
- (220) Rossini, S. *Catal. Today* **2003**, *77*, 467.
- (221) http://www.cdtech.com/techProfilesPDF/IsoamylenesProduction_NormalPentenes-ISOMPLUS.pdf and <http://www.lyondell.com/html/products/Licensing/olefins.shtml>.
- (222) Houzvicka, J.; Ponec, V. *Catal. Rev. Sci. Eng.* **1997**, *39*, 319.
- (223) de Ménorval, B.; Ayrault, P.; Gnep, N. S.; Guisnet, M. *Appl. Catal. A: Gen.* **2006**, *304*, 1.
- (224) Millini, R.; Rossini, S. In *Progress in Zeolite and Microporous Materials*; Chon, H., Ihm, S. K., Uh, Y. S., Eds.; Elsevier: Amsterdam, The Netherlands, 1997; p 1389.
- (225) Armaroli, T.; Trombetta, M.; Gutiérrez Alejandre, A.; Ramirez Solis, J.; Busca, G. *Phys. Chem. Chem. Phys.* **2000**, *2*, 3341–3348.
- (226) Freude, D.; Ernst, H.; Wolf, I. *Solid State Nucl. Magn. Reson.* **1994**, *3*, 271.
- (227) Jänchen, J.; van Wolput, J. H. M. C.; van de Ven, L. J. M.; de Haan, J. W.; van Santen, R. A. *Catal. Lett.* **1996**, *39*, 147.
- (228) Baba, T.; Komatsu, N.; Ono, Y. *J. Phys. Chem. B* **1998**, *102*, 804.
- (229) Böhlmann, W.; Michel, D. *Top. Catal.* **2001**, *202*, 421.
- (230) Ramos Pinto, R.; Borges, P.; Lemos, M. A. N. D. A.; Lemos, F.; Védrine, J.; Derouane, E. G.; Ramôa Ribeiro, F. *Appl. Catal. A: Gen.* **2005**, *284*, 39.
- (231) Alario, F.; Guisnet, M. In *Zeolites for Cleaner Technologies*; Guisnet, M., Gilson, J. P., Eds.; Imperial College Press: London, U.K., 2002; p 189.
- (232) Degnan, T. F., Jr.; Morris Smith, C.; Venkat Chaya, R. *Appl. Catal. A: Gen.* **2001**, *221*, 283.
- (233) Beck, J. S.; Dandekar, A. B.; Degnan, T. F. In *Zeolites for Cleaner Technologies*; Guisnet, M., Gilson, J. P., Eds.; Imperial College Press: London, U.K., 2002; p 223–237.
- (234) Perego, C.; Ingallina, P. *Green Chem.* **2004**, *6*, 274.
- (235) Burgfels, G.; Kochloeff, K.; Ladebeck, J.; Schmidt, F.; Schneider, M.; Wernicke, H. J. (to Süd-Chemie). European Patent 0,369,364, 1989.
- (236) Keil, F. J. *Micropor. Mesopor. Mater.* **1999**, *29*, 49.
- (237) Tabak, S. A.; Krambeck, F. J.; Garwood, W. E. *AIChE J.* **1986**, *32*, 9.
- (238) Daage, M. In *Zeolites for Cleaner Technologies*; Guisnet, M., Gilson, J. P., Eds.; Imperial College Press: London, U.K., 2002; p 167–188.
- (239) Wallenstein, D.; Harding, R. H. *Appl. Catal. A: Gen.* **2001**, *214*, 11.
- (240) Okuhara, T. *Chem. Rev.* **2002**, *102*, 3641.
- (241) Ishida, H. *Catal. Surv. Jpn.* **1997**, *1*, 241.
- (242) Borade, R. B.; Clearfield, A. *Micropor. Mater.* **1996**, *5*, 289.
- (243) Mintova, S.; Valtchev, V.; Onfroy, T.; Marichal, C.; Knözinger, H.; Bein, T. *Micropor. Mesopor. Mater.* **2006**, *90*, 237.
- (244) Kunkeler, P. J.; Zuurdeeg, B. J.; van der Waal, J. C.; van Bockoven, J. A.; Koningsberger, D. C.; van Bekkum, H. *J. Catal.* **1998**, *180*, 234.
- (245) Marques, J. P.; Gener, I.; Ayrault, P.; Bordado, J. C.; Lopes, J. M.; Ramoa Ribeiro, F.; Guisnet, M. *Micropor. Mesopor. Mater.* **2003**, *60*, 251.
- (246) Jansen, J. C.; Creighton, E. J.; Njo, S. L.; van Koningsveld, H.; van Bekkum, H. *Catal. Today* **1997**, *38*, 205.
- (247) Jia, C.; Massani, P.; Barthomeuf, D. *J. Chem. Soc., Faraday Trans.* **1993**, *89*, 3659.
- (248) Casagrande, M.; Storaro, L.; Lenarda, M.; Ganzerla, R. *Appl. Catal. A: Gen.* **2000**, *20*, 263.
- (249) www.polimerieuropa.it.
- (250) Schmidt, R. *J. Appl. Catal. A: Gen.* **2005**, *280*, 89.
- (251) Perego, C.; Amarilli, S.; Villini, R.; Bellussi, G.; Girotti, G.; Terzoni, G. *Micropor. Mater.* **1996**, *6* 395.
- (252) Perego, C.; Ingallina, P. *Catal. Today* **2002**, *73*, 3.
- (253) Leonowicz, M. E.; Lawton, J. A.; Lawton, S. L.; Rubin, M. K. *Science* **1994**, *264*, 1910.
- (254) Lawton, S. L.; Leonowicz, M. E.; Partridge, R. D.; Chu, P.; Rubin, M. K. *Micropor. Mesopor. Mat.* **1998**, *23*, 109.
- (255) Zhou, D.; Baoa, Y.; Yang, M.; Hea, N.; Yang, G. *J. Mol. Catal. A: Chem.* **2006**, *244*, 11.
- (256) Onida, B.; Geobaldo, F.; Testa, F.; Crea, F.; Garrone, E. *Micropor. Mesopor. Mat.* **1999**, *30*, 119.
- (257) Onida, B.; Geobaldo, F.; Testa, F.; Aiello, R.; Garrone, E. *J. Phys. Chem. B* **2002**, *106*, 1684.
- (258) Ayrault, P.; Datka, J.; Laforge, S.; Martin, D.; Guisnet, M. *J. Phys. Chem. B* **2004**, *108*, 13755.
- (259) Corma, A.; Martinez Soria, V.; Schnoefeld, E. *J. Catal.* **2000**, *192*, 163.
- (260) Maache, M.; Janin, A.; Lavalley, J. C.; Benazzi, E. *Zeolites* **1995**, *15*, 507.
- (261) Bordiga, S.; Lamberti, C.; Geobaldo, F.; Zecchina, A.; Turnes Palomino, G.; Otero Arean, C. *Langmuir* **1995**, *11*, 527.
- (262) Datka, J.; Gil, B.; Weglarski, J. *Micropor. Mesopor. Mater.* **1998**, *21*, 75.
- (263) Martucci, A.; Cruciani, G.; Alberti, A.; Ritter, C.; Ciambelli, P.; Rapacciuolo, M. *Micropor. Mesopor. Mater.* **2000**, *35–36*, 405.
- (264) Bevilacqua, M.; Gutiérrez Alejandre, A.; Resini, C.; Casagrande, M.; Ramirez, J.; Busca, G. *Phys. Chem. Chem. Phys.* **2002**, *4*, 4575.
- (265) Ganapathy, S.; Kumar, R.; Delevoyle L.; Amoureux, J. P. *Chem. Commun.* **2003**, 2076.
- (266) Kao, H.-M.; Yu, C.-Y.; Yeh, M.-C. *Micropor. Mesopor. Mater.* **2002**, *53*, 1.
- (267) Montanari, T.; Bevilacqua, M.; Resini, C.; Busca, G. *J. Phys. Chem. B* **2004**, *108*, 2120.
- (268) Marie, O.; Massiani, P.; Thibault-Starzyk, F. *J. Phys. Chem. B* **2004**, *108*, 5073. Marie, O.; Thibault-Starzyk, F.; Massiani, P. *J. Catal.* **2005**, *230*, 28.
- (269) Alberti, A. *Zeolites* **1997**, *19*, 411.
- (270) Nesterenko, N. S.; Thibault-Starzyk, F.; Montouillout, V.; Yuschenko, V. V.; Fernandez, C.; Gilson, J.-P.; Famula, F.; Ivanova, I. I. *Micropor. Mesopor. Mater.* **2004**, *71*, 157.
- (271) van Bokhoven, J. A.; Tromp, M.; Koningsberger, D. C.; Miller, J. T.; Pieterse, J. A. Z.; Lercher, J. A.; Williams, B. A.; Kung, H. H. *J. Catal.* **2001**, *202*, 129.
- (272) Schmidt, F.; Köhler, E.; in Guisnet, M.; Gilson, J. P. Eds., *Zeolites for cleaner technologies*, Imperial College Press 2002, p.153–166.
- (273) Weyda, H.; Köhler, E. *Catal. Today* **2003**, *81*, 51.
- (274) Corma, A.; Martinez A.; in Guisnet, M.; Gilson, J. P., Eds., *Zeolites for cleaner technologies*, Imperial College Press 2002, p. 29–56.
- (275) Decroocq, D. *Revue de l'Institut Français du Pétrole* **1997**, *52*, 469.
- (276) Martucci, A.; Alberti, A.; Guzman-Castillo, M. L.; Di Renzo, F.; Fajula, F. *Micropor. Mesopor. Mater.* **2003**, *63*, 33.
- (277) Chen, J.; Chen, T.; Guan, N.; Wang, J. *Catal. Today* **2004**, *93–95*, 627.
- (278) McQueen, D.; Chiche, B. H.; Fajula, F.; Auroux, A.; Guimon, C.; Fitoussi, F.; Schulz, P. *J. Catal.* **1996**, *161*, 587.
- (279) Guisnet, M.; Ayrault, P.; Datka, J. *Micropor. Mesopor. Mater.* **1998**, *20*, 283.
- (280) Shigeishi, R. A.; Chiche, B. H.; Fajula, F. *Micropor. Mesopor. Mater.* **2001**, *43*, 211.
- (281) Anderson, M. W.; Klinowski, J. *Zeolites* **1986**, *6*, 455.
- (282) Sierka, M.; Eichler, U.; Datka, J.; Sauer, J. *J. Phys. Chem. B* **1998**, *102*, 6397.
- (283) Romero, S. F.; Marie, O.; Saussey, J.; Daturi, M. *J. Phys. Chem. B* **2005**, *109*, 1660.
- (284) Sarria, F. R.; Blasin-Aube, V.; Saussey, J.; Marie, O.; Daturi, M. *J. Phys. Chem. B* **2006**, *110*, 13130.
- (285) Cairon, O.; Chevreau, T.; Lavalley, J. C. *J. Chem. Soc., Faraday Trans.* **1998**, *94*, 3039.
- (286) Daniell, W.; Topsoe, N. Y.; Knozinger, H. *Langmuir* **2001**, *17*, 6233.
- (287) Niwa, M.; Suzuki, K.; Isamoto, K.; Katada, N. *J. Phys. Chem. B* **2006**, *110*, 264.
- (288) Navarro, U.; Trujillo, C. A.; Oviedo, A. *J. Catal.* **2002**, *211*, 64.
- (289) van Bokhoven, J. A.; Roest, A. L.; Koningsberger, D. C.; Miller, J. T.; Nachtegaal, G. H.; Kentgens, P. M. *J. Phys. Chem. B* **2000**, *104*, 6743.
- (290) Behring, D. L.; Ramirez-Solis, A.; Mota, C. J. A. *J. Phys. Chem. B* **2003**, *107*, 4342.
- (291) Omega, A.; Van Bokhoven, J. A.; Prins, R. *J. Phys. Chem. B* **2003**, *107*, 8854.
- (292) Omega, A.; Prins, R.; Van Bokhoven, J. A. *J. Phys. Chem. B* **2005**, *109*, 9280.
- (293) Menezes, S. M. C.; Camorim, V. L.; Lam, Y. L.; San Gil, R. A. S.; Bailly, A.; Amoureux, J. P. *Appl. Catal. A Gen.* **2001**, *207*, 367.
- (294) Xu, B.; Rotunno, F.; Bordiga, S.; Prins, R.; van Bokhoven, J. A. *J. Catal.* **2006**, *241*, 66.

- (295) Falabella Sousa-Aguiar, E.; Doria Camorim, V. L.; Zanon Zotin, F. M.; Correa dos Santos, R. L. *Micropor. Mesopor. Mater.* **1998**, *25*, 25.
- (296) Corma, A.; Lopez Nieto, J. M. in *Handbook on the Physics and Chemistry of Rare Earths*, Gschneidner, K. A.; Eyring, L. Eds., Vol. 29, 2000, Elsevier, Amsterdam.
- (297) Occelli M. L.; Ritz P. *Appl. Catal. A: Gen.* **1999**, *183*, 53.
- (298) Habib, E. T.; Zhao, X.; Yaluris, G.; Cheng, W. C.; Boock, L. T.; Gilson, J. P. in Guisnet, M.; Gilson, J. P., Eds., *Zeolites for cleaner technologies*, Imperial College Press 2002, p. 105.
- (299) Andersson, S. V.; Myrstad, T. *Appl. Catal. A Gen.* **1998**, *59*, 170.
- (300) O'Connor, P.; Verlaan, J. P. J.; Yanik, S. J. *Catal. Today* **1998**, *43*, 305.
- (301) Wallenstein, D.; Harding, R. H. *Appl. Catal. A Gen.* **2001**, *214*, 11.
- (302) Hernández-Beltrán, F.; Moreno-Mayorga, J. C.; Quintana-Solórzano, R.; Sánchez-Valente, J.; Pedraza-Archila, F.; Pérez-Luna, M. *Appl. Catal. B: Environ.* **2001**, *24*, 137.
- (303) Van Veen, J. A. R. Hydrocracking, in Guisnet, M.; Gilson, J. P., Eds., *Zeolites for cleaner technologies*, Imperial College Press 2002, p. 131.
- (304) AlkyClean – A true solid acid gasoline alkylation process, www.abb.com/lummus.
- (305) Dautzenberg, F. M.; Van der Pull, N. Advanced reactors and catalyst concepts, www.abb.com.
- (306) Ginosar, D. M.; Thompson, D. N.; Burch, K. C. *Ind. Eng. Chem. Res.* **2006**, *45*, 567.
- (307) Paillaud, J.-L.; Harbuzaru, B.; Patarin, J.; Bats, N. *Science* **2004**, *304*, 990.
- (308) Corma, A.; Diaz-Cabanas, M. J.; Jorda, J. L.; Martinez, C.; Moliner, M. *Nature* **2006**, *443*, 842.
- (309) Corma, A.; Fornés, V.; Guil, J. M.; Pergher, S.; Maesen, Th. L. M.; Buglass, J. G. *Micropor. Mesopor. Mater.* **2000**, *38*, 301.
- (310) Corma, A.; Diaz, U.; Domine, M. E.; Fornes, V. *J. Am. Chem. Soc.* **2000**, *122*, 2804.
- (311) Corma, A.; Martínez, A.; Martínez-Soria, V. *J. Catal.* **2001**, *200*, 259.
- (312) Tanabe, K.; Hölderich, W. F. *Appl. Catal. A: Gen.* **1999**, *181*, 399.
- (313) Kresge, C. T.; Leonowicz, M. E.; Roth, W. J.; Vartuli, J. C.; Beck, J. S. *Nature* **1992**, *359*, 710.
- (314) Yanagisawa, T.; Shimizu, T.; Kuroda, K.; Kato, C. *Bull. Chem. Soc. Jpn.* **1990**, *63*, 988.
- (315) Feng, X.; Lee, J. S.; Lee, J. W.; Lee, J. Y.; Wie, D.; Haller, G. L. *Chem. Eng. J.* **1996**, *64*, 255.
- (316) Kuroda, Y.; Mori, T.; Yoshikawa, Y. *Chem. Commun.* **2001**, 1006.
- (317) Bonelli, B.; Onida, B.; Chen, J. D.; Galarneau, A.; Di Renzo, F.; Fajula, F.; Garrone, E. *Micropor. Mesopor. Mater.* **2004**, *67*, 95.
- (318) Scokart, P. O.; Rouxhet, P. G. *J. Colloid Interface Sci.* **1982**, *86*, 96.
- (319) Boehm, H. P.; Knözinger, H. In *Catalysis, Science and Technology*; Anderson, J. R., Boudart, M., Eds.; Springer: Berlin, Germany, 1983; Vol. 4, p 39.
- (320) Cardona-Martínez, N.; Dumesic, J. A. *Adv. Catal.* **1992**, *38*, 149.
- (321) Morin, S.; Ayrault, P.; El Mouahid, S.; Gnep, N. S.; Guisnet, M. *Appl. Catal. A: Gen.* **1997**, *159*, 317.
- (322) Corma, A.; Grande, M. S.; Gonzalez-Alfonso, V.; Orchilles, A. V. *J. Catal.* **1996**, *159*, 375.
- (323) Di Renzo, F.; Chiche, B.; Fajula, F.; Viale, S.; Garrone, E. *Stud. Surf. Sci. Catal.* **1996**, *101*, 851–860.
- (324) Zamaraev, K. I.; Thomas, J. M. *Adv. Catal.* **1996**, *41*, 335.
- (325) Góra-Marek, K.; Derewiński, M.; Sarv, P.; Datka, J. *Catal. Today* **2005**, *101*, 131.
- (326) Góra-Marek, K.; Datka, J. *Appl. Catal. A: Gen.* **2006**, *302*, 104.
- (327) Crépeau, G.; Montouillout, V.; Vimont, A.; Mariey, L.; Cseri, T.; Maugé, F. *J. Phys. Chem. B* **2006**, *110*, 15172.
- (328) Luan, Z.; Fournier, J. A. *Micropor. Mesopor. Mater.* **2005**, *79*, 235.
- (329) Garrone, E.; Onida, B.; Bonelli, B.; Busco, C.; Ugliengo, P. *J. Phys. Chem. B* **2006**, *110*, 19087.
- (330) Brunner, E. *Catal. Today* **1997**, *38*, 361.
- (331) Heeribout, L.; Vincent, R.; Batamack, P.; Dorémieux-Morin, C.; Fraissard, J. *Catal. Lett.* **1998**, *53*, 23–31.
- (332) Luo, Q.; Deng, F.; Yuan, Z.; Yang, Y.; Zhang, M.; Yue, Y.; Ye, C. *J. Phys. Chem. B* **2003**, *107*, 2435.
- (333) Xu, M. C.; Wang, W.; Seiler, M.; Buchholz, A.; Hunger, M. *J. Phys. Chem. B* **2002**, *106*, 3202.
- (334) Chen, T. H.; Houthoofd, K.; Grobet, P. J. *Micropor. Mesopor. Mater.* **2005**, *86*, 31.
- (335) Shankland, R. V. *Adv. Catal. Relat. Subj.* **1954**, *6*, 271.
- (336) Pistarino, C.; Finocchio, E.; Larrubia, M. A.; Serra, B.; Braggio, S.; Busca, G.; Baldi, M. *Ind. Eng. Chem. Res.* **2001**, *40*, 3262.
- (337) Topsøe, H.; Clausen, B. S.; Massoth, F. E. In *Catalysis Science and Technology*; Anderson, J. R., Boudart, M., Eds.; Springer: Berlin, Germany, 1997; Vol. 11, p 1.
- (338) Du, H.; Fairbridge, C.; Yang, H.; Ring, Z. *Appl. Catal. A: Gen.* **2005**, *294*, 1.
- (339) Perego, C.; Amarilli, S.; Carati, A.; Flego, C.; Pazzucconi, G.; Risso, C.; Bellussi, G. *Micropor. Mesopor. Mater.* **1999**, *27*, 345.
- (340) Flego, C.; Peratello, S.; Perego, C.; Sabatino, L. M. F.; Bellussi, G.; Romano, U. *J. Mol. Catal. A: Chem.* **2003**, *204–205*, 581.
- (341) Pariente, S.; Trens, P.; Fajula, F.; Di Renzo, F.; Tanchoux, N. *Appl. Catal. A: Gen.* **2006**, *307*, 51.
- (342) Liu, Y.; Pinnavaia, P. J. *J. Am. Chem. Soc.* **2003**, *125*, 2376.
- (343) Wang, H.; Liu, Y.; Pinnavaia, P. J. *J. Phys. Chem. B* **2006**, *110*, 4524.
- (344) Trombetta, M.; Busca, G.; Willey, R. J. *J. Colloids Interface Sci.* **1997**, *190*, 416.
- (345) Daniell, W.; Schubert, U.; Glöckler, R.; Meyer, A.; Noweck, K.; Knözinger, H. *Appl. Catal. A: Gen.* **2000**, *196*, 247.
- (346) Yaripour, F.; Baghaei, F.; Schmidt, I.; Perregaard, J. *Catal. Commun.* **2005**, *6*, 147.
- (347) Buonomo, F.; Fattore, V.; Notari, B. U.S. Patent 4013589, 1977. Buonomo, F.; Fattore, V.; Notari, B. U.S. Patent 4013590, 1977. Manara, G.; Fattore, V.; Notari, B. U.S. Patent 4038337, 1977.
- (348) Butler, A. C.; Nicolaides, C. P. *Catal. Today* **1993**, *18*, 443.
- (349) Finocchio, E.; Busca, G.; Rossini, S.; Cornaro, U.; Piccoli, V.; Miglio, R. *Catal. Today* **1997**, *33*, 335.
- (350) Weissermel, K.; Arpe, H.-J. *Industrial Organic Chemistry*, 3rd ed.; VCH: Weinheim, Germany, 1997; p 70.
- (351) Trotta, R.; Miracca, I. *Catal. Today* **1997**, *34*, 447.
- (352) Bordiga, S.; Regli, L.; Cocina, D.; Lamberti, C.; Bjorgen, M.; Lillerud, K. P. *J. Phys. Chem. B* **2005**, *109*, 2779.
- (353) Wei, Y.; Zhang, D.; Liu, Z.; Su, B. L. *J. Catal.* **2006**, *238*, 46.
- (354) Liu, Z.; Liang, J. *Curr. Opin. Solid State Mater. Sci.* **1999**, *4*, 80.
- (355) Chen, J. Q.; Bozzano, A.; Glover, B.; Fuglerud, T.; Kvisle, S. *Catal. Today* **2005**, *106*, 103.
- (356) Dahl, I. M.; Mostad, H.; Akporiaye, D.; Wendelbo, R. *Micropor. Mesopor. Mater.* **1999**, *29*, 185.
- (357) U.S. Patent 6,903,240, ExxonMobil Chemical Patents Inc., Houston, TX, 2005. *Focus Catal.* **2006** (10), 7.
- (358) Liu, C.; Denga, Y.; Pan, Y.; Zheng, S.; Gao, X. *Appl. Catal. A: Gen.* **2004**, *257*, 145.
- (359) Mahgoub, K. A.; Al-Khattai, S. *Energy Fuels* **2005**, *19*, 329.
- (360) Flessner, U.; Jones, D. J.; Rozière, J.; Zajac, J.; Storaro, L.; Lenarda, M.; Pavan, M.; Jiménez-López, A.; Rodríguez-Castellón, E.; Trombetta, M.; Busca, G. *J. Mol. Catal. A: Chem.* **2001**, *168*, 247.
- (361) <http://www.sud-chemie.com>.
- (362) Hart, M. P.; Brown, D. R. *J. Mol. Catal. A: Chem.* **2004**, *212*, 315.
- (363) Chitnis, S. R.; Sharma, M. M. *React. Funct. Polym.* **1997**, *32*, 93.
- (364) Vaccari, A. *Appl. Clay Sci.* **1999**, *14*, 161.
- (365) Vogels, R. J. M. J.; Kloprogge, J. T.; Geus, J. W. *J. Catal.* **2005**, *231*, 443.
- (366) Yang, H.; Wilson, M.; Fairbridge, C.; Ring, Z. *Energy Fuels* **2002**, *16*, 855.
- (367) Yadav, G. D.; Salgaonkar, S. S. *Ind. Eng. Chem. Res.* **2005**, *44*, 1706.
- (368) Zebib, B.; Lambert, J.-F.; Blanchard, J.; Breyse, M. *Chem. Mater.* **2006**, *18*, 34.
- (369) Pinnavaia, T. J. *Science* **1983**, *220*, 365.
- (370) Figueras, F. *Catal. Rev. Sci. Eng.* **1998**, *30*, 457.
- (371) Trombetta, M.; Busca, G.; Lenarda, M.; Storaro, L.; Ganzerla, R.; Pievesan, L.; Jimenez, Lopez, A.; Alcantara-Rodríguez, M.; Rodríguez-Castellón, E. *Appl. Catal. A: Gen.* **2000**, *193*, 55.
- (372) Pruijsen, D. J.; Capková, P.; Driessen, R. A. J.; Schenk, H. *Appl. Catal. A: Gen.* **1997**, *165*, 481.
- (373) Occelli, M. L. *CHEMTECH* **1994**, 24.
- (374) Ding, Z.; Kloprogge, J. T.; Frost, R. L.; Lu, G. Q.; Zhu, H. Y. *J. Porous Mater.* **2001**, *8*, 273.
- (375) Albertazzi, S.; Baraldini, I.; Busca, G.; Finocchio, E.; Lenarda, M.; Storaro, L.; Talon, A.; Vaccari, A. *Appl. Clay Sci.* **2005**, *29*, 224.
- (376) Chauvel, A.; Delmon, B.; Holderich, W. *Appl. Catal. A: Gen.* **1994**, *115*, 173.
- (377) De Stefanis, A.; Tomlinson, A. A. G. *Catal. Today* **2006**, *114*, 126.
- (378) Ma, Y.; Tong, W.; Zhou, H.; Suib, S. L. *Micropor. Mesopor. Mater.* **2000**, *32*, 243.
- (379) Galarneau, A.; Borodawalla, A.; Pinnavaia, T. J. *Nature* **1995**, *374*, 529.
- (380) Polverejan, M.; Liu, Y.; Pinnavaia, T. J. *Chem. Mater.* **2002**, *14*, 2283.
- (381) Fernández López, E.; Sanchez Escribano, V.; Panizza, M.; Carnasciali, M. M.; Busca, G. *J. Mater. Chem.* **2001**, *11*, 1891.
- (382) Pokrovskii, K.; Jung, K. T.; Bell, A. T. *Langmuir* **2001**, *17*, 4297.
- (383) Busca, G.; Saussey, H.; Saur, O.; Lavalley, J. C.; Lorenzelli, V. *Appl. Catal.* **1985**, *14*, 245.
- (384) Ferretto, L.; Glisenti, A. *Chem. Mater.* **2003**, *15*, 1181.
- (385) Grzybowska-Swierkosz, B. *Appl. Catal. A: Gen.* **1997**, *157*, 263.
- (386) Busca, G.; Lietti, L.; Ramis, G.; Berti, F. *Appl. Catal. B: Environ.* **1998**, *18*, 1.
- (387) Svoronos, P. D. N.; Bruno, T. J. *Ind. Eng. Chem. Res.* **2002**, *41*, 5321.

- (388) Notari, B.; Willey, R. J.; Panizza, M.; Busca, G. *Catal. Today* **2006**, *116*, 99.
- (389) Gutierrez, A.; Trombetta, M.; Busca, G.; Ramirez, J. *Micropor. Mater.* **1997**, *12*, 79.
- (390) Gutierrez, A.; Gonzalez, M.; Trombetta, M.; Busca, G.; Ramirez, J. *Micropor. Mesopor. Mater.* **1998**, *23*, 265.
- (391) Daturi, M.; Cremona, A.; Milella, F.; Busca, G.; Vogna, E. *J. Eur. Ceram. Soc.* **1998**, *18*, 1079.
- (392) Ramirez, J.; Cedeño, L.; Busca, G. *J. Catal.* **1999**, *184*, 59.
- (393) Maity, S. K.; Ancheya, J.; Rana, M. S.; Rayo, P. *Energy Fuels* **2006**, *20*, 427.
- (394) Ramis, G.; Cristiani, C.; Elmi, A. S.; Villa, P. L.; Busca, G. *J. Mol. Catal.* **1990**, *61*, 319.
- (395) Chu, W.; Echizen, T.; Kamiya, Y.; Okuhara, T. *Appl. Catal. A: Gen.* **2004**, *259*, 199.
- (396) Murrell, L. L.; Dispenziere, N. C., Jr. *Catal. Lett.* **1990**, *4*, 235.
- (397) Wachs, I. E.; Kim, T.; Ross, E. I. *Catal. Today* **2006**, *116*, 162.
- (398) Scheithauer, M.; Cheung, T. K.; Jentoft, R. E.; Grasselli, R. K.; Gates, B. C. Knözinger, H. *J. Catal.* **1998**, *180*, 1.
- (399) Barton, D. G.; Soled, S. L.; Meitzer, G. D.; Fuentes, G. A.; Iglesia, E. *J. Catal.* **1999**, *181*, 57.
- (400) Vartuli, J. C.; Santiesteban, J. G.; Traverso, P.; Cardona Martinez, N.; Chang, C. D.; Stevenson, S. A. *J. Catal.* **1999**, *187*, 131.
- (401) Ramis, G.; Busca, G.; Lorenzelli, V. *Stud. Surf. Sci. Catal.* **1989**, *48*, 777.
- (402) Ramis, G.; Busca, G.; Cristiani, C.; Lietti, L.; Forzatti, P.; Bregani, F. *Langmuir* **1992**, *8*, 1744.
- (403) Gutierrez-Alejandre, A.; Castillo, P.; Ramirez, J.; Ramis, G.; Busca, G. *Appl. Catal. A: Gen.* **2001**, *216*, 181.
- (404) Calabro, D. C.; Vartuli, J. C.; Santiesteban, J. G. *Topics Catal.* **2002**, *18*, 231.
- (405) Busca, G.; Lavalley, J. C. *Spectrochim. Acta* **1986**, *42*, A 443.
- (406) Busca, G. *J. Raman Spectrosc.* **2002**, *33*, 348.
- (407) Scheithauer, M.; Grasselli, R. K.; Knözinger, H. *Langmuir* **1998**, *14*, 3019.
- (408) Barton, D. G.; Shtein, M.; Wilson, D.; R.; Soled, S. L.; Iglesia, E. *J. Phys. Chem.* **1999**, *103*, 630.
- (409) Haber, J.; Janas, J.; Schiavello, M.; Tilley, R. J. D. *J. Catal.* **1983**, *82*, 395.
- (410) Paganini, M. C.; Dell'Acqua, L.; Giamello, E.; Lietti, L.; Forzatti, P.; Busca, G. *J. Catal.* **1997**, *166*, 195.
- (411) Gutierrez-Alejandre, A.; Ramirez, J.; Busca, G. *Catal. Lett.* **1998**, *56*, 29.
- (412) Macht, J.; Baertsch, C. D.; May-Lozano, M.; Soled, S. L.; Wang, Y.; Iglesia, E. *J. Catal.* **2004**, *227*, 479.
- (413) Gallardo Amores, J. M.; Sanchez Escribano, V.; Busca, G. *J. Mater. Chem.* **1995**, *5*, 1245.
- (414) Baertsch, C. D.; Komala, K. T.; Chua, Y.-H.; Iglesia, E. *J. Catal.* **2002**, *205*, 44.
- (415) Kuba, S.; Che, M.; Grasselli, R. K.; Knözinger, H. *J. Phys. Chem. B* **2003**, *107*, 3459.
- (416) Hernández, M. L.; Montoya, J. A.; Del Angel, P.; Hernandez, I. Espinosa G.; Llanos, M. E. *Catal. Today* **2006**, *116*, 169.
- (417) http://www.exxonmobil.com/Refiningtechnologies/pdf/refin_EMICT_japan_beck110100.pdf
- (418) Fierro, J. L. G.; Mol, J. C. In *Metal Oxides: Chemistry and Applications*; Fierro, J. L. G., Ed.; CRC Press: Boca Raton, FL, 2005; p 517.
- (419) Macho, V.; Králik, M.; Jurecek, L.; Jurecekova, E.; Balazova, J. *Appl. Catal. A: Gen.* **2000**, *203*, 5.
- (420) Arata, K. *Adv. Catal.* **1990**, *37*, 165.
- (421) Saur, O.; Bensitel, M.; Mohammed Saad, A. B.; Lavalley, J. C.; Tripp, C. P.; Morrow, B. A. *J. Catal.* **1986**, *99*, 104.
- (422) Klose, B. S.; Jentoft, F. C.; Joshi, P.; Trunschke, A.; Schlögl, R.; Subbotina, I. R.; Kazansky, V. B. *Catal. Today* **2006**, *116*, 121.
- (423) Manoilova, O.; Olindo, R.; Otero Areán, C.; Lercher, J. A. *Catal. Commun.* **2007**, *8*, 865.
- (424) Ramis, G.; Busca, G.; Lorenzelli, V. *Stud. Surf. Sci. Catal.* **1989**, *48*, 777.
- (425) Semmer, V.; Batamack, P.; Doremieux-Morin, C.; Fraissard, J. *Topics Catal.* **1998**, *6*, 119.
- (426) Yaluris, G.; Larson, R. B.; Kobe, J. M.; Gonzales, M. R.; Fogash, K. B.; Dumesic, J. A. *J. Catal.* **1996**, *158*, 336.
- (427) Barthos, R.; Onyestyak, Gy.; Valyon, J. *J. Phys. Chem. B* **2000**, *104*, 7311.
- (428) Dijs, I. J.; Geus, J. W.; Jennessens, L. W. *J. Phys. Chem. B* **2003**, *107*, 13403.
- (429) Katada, N.; Endo, J.; Notsu, K.; Yasunobu, N.; Naito, N.; Niwa, M. *J. Phys. Chem. B* **2000**, *104*, 10321.
- (430) Bolis, V.; Magnacca, G.; Cerrato, G.; Morterra, C. *Topics Catal.* **2002**, *19*, 259.
- (431) Hammache, S.; Goodwin, J. G. *J. Catal.* **2003**, *218*, 258.
- (432) Lohitarn, N.; Lotero, E.; Goodwin, J. G. *J. Catal.* **2000**, *241*, 328.
- (433) Matasuhashi, H.; Miyazaki, H.; Kawamura, Y.; Nakamura, H.; Arata, K. *Chem. Mater.* **2001**, *13*, 3038.
- (434) Matasuhashi, H.; Tanaka, T.; Arata, K. *J. Phys. Chem. B* **2001**, *105*, 9669.
- (435) Charakraborty, A.; Sharma, M. M. *React. Polym.* **1993**, *20*, 1.
- (436) Harmer, M. A.; Sun, Q. *Appl. Catal. A: Gen.* **2001**, *221*, 45.
- (437) Di Girolamo, M.; Marchionna, M. *J. Mol. Catal. A: Chem.* **2001**, *177*, 33.
- (438) <http://www.rohmhaas.com/ionexchange>.
- (439) Thornton, R.; Gates, B. C. *J. Catal.* **1974**, *34*, 275.
- (440) Siril, P. F.; Brown, D. R. *J. Mol. Catal. A: Chem.* **2006**, *252*, 125.
- (441) Hutchings, G. J.; Nicolaidis, C. P.; Scurrell, M. S. *Catal. Today* **1992**, *15*, 23.
- (442) Miracca, I.; Tagliabue, L.; Trotta, R. *Chem. Eng. Sci.* **1996**, *51*, 2349.
- (443) http://www.cdtech.com/techProfilesPDF/MTBE_RefC4Feeds-CDMTBE.pdf.
- (444) Di Girolamo, M.; Tagliabue, L. *Catal. Today* **1999**, *52*, 307.
- (445) Marchionna, M.; Di Girolamo, M.; Patrini, R. *Catal. Today* **2001**, *65*, 397.
- (446) Honkela, M. L.; Krause, A. O. L. *Ind. Eng. Chem, Res.* **2005**, *44*, 5291.
- (447) Quiroga, M.; Capeletti, M. R.; Figoli, N.; Sedran, U. *Appl. Catal. A: Gen.* **1999**, *177*, 37.
- (448) Honkela, M. L.; Root, A.; Linblad, M.; Krause, A. O. I. *Appl. Catal. A: Gen.* **2005**, *295*, 216.
- (449) <http://www.fuelcells.dupont.com>.
- (450) Zecchina, A.; Spoto, G.; Bordiga, S. *Phys. Chem. Chem. Phys.* **2005**, *7*, 1627.
- (451) Kumar, P.; Vermeiren, W.; Dath, J.-P.; Hölderich, W. A. *Energy Fuels* **2006**, *20*, 481.
- (452) Mitsutani, A. *Catal. Today* **2002**, *73*, 57.
- (453) Ipatieff, V. N.; Corson B. B. *Ind. Eng. Chem.* **1938**, *30*, 1316.
- (454) Egloff, G. *Ind. Eng. Chem.* **1936**, *28*, 1461.
- (455) Krawietz, T. R.; Lin, P.; Lotterhos, K. E.; Torres, P. D.; Barich, D. W.; Clearfield, A.; Haw, J. F. *J. Am. Chem. Soc.* **1998**, *120*, 8502.
- (456) Cavani, F.; Girotti, G.; Terzoni, G. *Appl. Catal. A: Gen.* **1993**, *97*, 177.
- (457) Ramis, G.; Rossi, P. F.; Busca, G.; Lorenzelli, L.; La Ginestra, A.; Patrono, P. P. *Langmuir* **1989**, *5*, 917.
- (458) Busca, G.; Centi, G.; Trifiro, F. *J. Am. Chem. Soc.* **1985**, *107*, 7757.
- (459) Ramis, G.; Busca, G.; Lorenzelli, V.; La Ginestra, A.; Galli, P.; Massucci M. A. *J. Chem. Soc., Dalton Trans.* **1988**, 881.
- (460) Jones, E. K. *Adv. Catal. Relat. Subj.* **1958**, *10*, 165.
- (461) Chauvel, A.; Lefebvre, G. *Petrochemical Processes*; Technip: Paris, France, 1989; pp 185, 215.
- (462) de Klerk, A. *Ind. Eng. Chem. Res.* **2004**, *43*, 6325.
- (463) Prinsloo, N. M. *Fuel Process. Technol.* **2006**, *87*, 437.
- (464) Coetzee, J. H.; Mashapa, T. N.; Prinsloo, N. M.; Rademan, J. D. *Appl. Catal. A: Gen.* **2006**, *308*, 204.
- (465) Fougret, C. M.; Atkins, M. P.; Hölderich, W. F. *Appl. Catal. A: Gen.* **1999**, *181*, 145.
- (466) Chernyshkova, F. A. *Russ. Chem. Rev.* **1993**, *62*, 743.
- (467) Nowak, I.; Ziolk, M. *Chem. Rev.* **1999**, *99*, 3603.
- (468) Tanabe, K. *Catal. Today* **2003**, *78*, 65.
- (469) Ziolk, M. *Catal. Today* **2003**, *78*, 47.
- (470) Heeribout, L.; Semmer, V.; Batamack, P.; Doremieux-Morin, C.; Vincent, R.; Fraissard, J. *Stud. Surf. Sci. Catal.* **1996**, *101*, 831.
- (471) Martins, R. T. L.; Schitine, W. J.; Castro, F. R. *Catal. Today* **1989**, *5*, 483.
- (472) Armaroli, T.; Busca, G.; Carlini, C.; Giuttari, M.; Raspolli Galletti, A.; Sbrana, G. *J. Mol. Catal.* **2000**, *151*, 233.
- (473) Stoyanov, E. S.; Kim, K. C.; Reed, C. A. *J. Am. Chem. Soc.* **2006**, *128*, 1948.
- (474) Okazaki, S.; Kurosaki, A. *Catal. Today* **1990**, *8*, 113.
- (475) Faury, A.; Gaset, A.; Gorrion, J. P. *Inf. Chim.* **1981**, *214*, 203.
- (476) Carlini, C.; Giuttari, M.; Raspolli Galletti, A. M.; Sbrana, G.; Armaroli, T.; Busca, G. *Appl. Catal. A: Gen.* **1999**, *183*, 295.
- (477) Carniti, P.; Gervasini, A.; Biella, S.; Auroux, A. *Catal. Today* **2006**, *118*, 373.
- (478) Okuhara, T.; Mizuno, N.; Misono, M. *Adv. Catal.* **1996**, *41*, 113.
- (479) Hill, C. L., Ed. *Chem. Rev.* **1998**, *98* (1).
- (480) Kozhovnikov, I. V. *Chem. Rev.* **1998**, *98*, 171.
- (481) Timofeeva, M. N. *Appl. Catal. A: Gen.* **2003**, *256*, 19.
- (482) Misono, M. *Catal. Rev.—Sci. Eng.* **1987**, *30*, 269.
- (483) Bardin, B. B.; Bordawekar, S. V.; Neurock, M.; Davis, R. J. *J. Phys. Chem. B* **1998**, *102*, 10817.
- (484) Lefebvre, F.; Liu-Cai, F. X.; Auroux, A. *J. Mater. Chem.* **1994**, *4*, 125.
- (485) Essayem, N.; Coudurier, G.; Vedrine, J. C.; Habermacher, D.; Sommer, J. J. *Catal.* **1999**, *183*, 292.
- (486) Uchida, S.; Inumaru, K.; Misono, M. *J. Phys. Chem. B* **2000**, *104*, 8108.
- (487) Pazé, C.; Bordiga, S.; Zecchina, A. *Langmuir* **2000**, *16*, 8139.

- (488) Vimont, A.; Travert, A.; Binet, C.; Pichon, C.; Mialane, P.; Sécheresse, F.; Lavalley, J. C. *J. Catal.* **2006**, *241*, 221.
- (489) Mizuno, N.; Misono, M. *Chem. Rev.* **1998**, *98*, 199.
- (490) Janik, M. J.; Davis, R. J.; Neurock, M. *Catal. Today* **2006**, *116*, 90.
- (491) Kozhovnikov, I. V.; Holmes, S.; Siddiqui, M. R. H. *Appl. Catal. A: Gen.* **2001**, *214*, 47.
- (492) Sambeth, J. E.; Baronetti, G. T.; Thomas, H. J. *J. Mol. Catal. A: Chem.* **2003**, *191*, 35.
- (493) Briand, L. E.; Baronetti, G. T.; Thomas, H. J. *Appl. Catal. A: Gen.* **2003**, *256*, 37.
- (494) Baumgarten, E.; Weinstrauch, F. *Spectrochim. Acta* **1979**, *35A*, 1315.
- (495) Vigué, H.; Quintard, P.; Merle-Méjean, T.; Lorenzelli, V. *J. Eur. Ceram. Soc.* **1998**, *18*, 305.
- (496) Ayame, A.; Sawada, G.; Sato, H.; Zhang, G.; Ohta, T.; Izumizawa, T. *Appl. Catal.* **1989**, *48*, 25.
- (497) Clet, G.; Goupil, J.-M.; Szabo, G.; Cornet, D.; Clet, G. *Appl. Catal. A: Gen.* **2000**, *202*, 37.
- (498) Edgar, M. D. In *Applied Industrial Catalysis*; Leach, B. E., Ed.; Academic Press: New York, 1984; Vol. 3, p 124.
- (499) Villegas, L.; Guilhaume, N.; Provendier, H.; Daniel, C.; Masset, F.; Mirodatos, C. *Appl. Catal. A: Gen.* **2005**, *281*, 75.
- (500) Finocchio, E.; Sapienza, G.; Baldi, M.; Busca, G. *Appl. Catal. B: Environ.* **2004**, *51*, 143.
- (501) Khaleel, A.; Dellinger, B. *Environ. Sci. Technol.* **2002**, *36*, 1620.
- (502) http://www.uop.com/objects/Alkylene_final_2-15-05.pdf.
- (503) Chupas, P. J.; Corbin, D. R.; Rao, V. N. M.; Hanson, J. C.; Grey, C. P. *J. Phys. Chem. B* **2003**, *107*, 8327.
- (504) Scokart, O.; Selim, S. A.; Damon, J. P.; Rouxhet, P. G. *J. Colloid Interface Sci.* **1979**, *70*, 209.
- (505) Matulewicz, E. R. A.; Kerkhof, P. J. M.; Mooulijn, J. A.; Reitsma, H. J. *J. Colloid Interface Sci.* **1980**, *77*, 161.
- (506) Morterra, C.; Cerrato, G.; Cuzzato, P.; Masiero, A.; Padovan, M. *J. Chem. Soc., Faraday Trans.* **1992**, *88*, 2239.
- (507) Rodriguez, L. M.; Alcaraz, J.; Hernandez, M.; Dufaux, M.; Ben Taarit, Y.; Vrinat, M. *Appl. Catal. A: Gen.* **1999**, *189*, 53.
- (508) Corma, A.; Fornés, V.; Ortega, E. *J. Catal.* **1985**, *92*, 284.
- (509) Manzer, L. E.; Rao, V. N. M. *Adv. Catal.* **1993**, *39*, 329.
- (510) Cuevas, R.; Ramírez, J.; Busca, G. *J. Fluorine Chem.* **2003**, *122*, 151.
- (511) Olah, G. A.; Batamack, P.; Deffieux, D.; Török, B.; Wang, Qi.; Molnár, Á.; Surya Prakash, G. K. *Appl. Catal. A: Gen.* **1996**, *146*, 107–117.
- (512) Hommeloft, S. I.; Tøpsoe, H. F. A. U.S. Patent 5,245,100, 1993.
- (513) de Angelis, A.; Flego, C.; Ingallina, P.; Montanari, L.; Clerici, M. G.; Carati, C.; Perego, C. *Catal. Today* **2001**, *65*, 363.
- (514) Gladysz, J. A. *Chem. Rev.* **2002**, *102*, 3215.

CR068042E